The molecular mechanism of PARP1 activation and its downstream roles in ALC1-regulated transcription

München, Oktober 2014

Aus dem Adolf – Butenandt – Institut

Lehrstuhl Physiologische Chemie

der Ludwig – Maximilians – Universität München

Vorstand: Prof. Dr. Andreas G. Ladurner

The molecular mechanism of PARP1 activation and its downstream roles in ALC1-regulated transcription

Dissertation

zum Erwerb des Doktorgrades der Naturwissenschaften

an der Medizinischen Fakultät

der Ludwig – Maximilians – Universität

vorgelegt von

Marek Kozłowski

aus Ciechanów (Polen)

2014

Gedruckt mit Genehmigung der Medizinischen Fakultät

der Ludwig – Maximilians – Universität München

Betreuer: Prof. Dr. Andreas G. Ladurner

Zweitgutachter: Prof. Dr. rer. nat. Heiko Hermeking

Dekan: Prof. Dr. med. Dr. h. c. M. Reiser, FACR, FRCR

Tag der mündlichen Prüfung: 15.04.2015

Eidesstattliche Versicherung

Marek Kozłowski

Ich erkläre hiermit an Eides statt, dass ich die vorliegende Dissertation mit dem Thema

The molecular mechanism of PARP1 activation and its downstream roles in ALC1-regulated transcription

selbständig verfasst, mich außer der angegebenen keiner weiteren Hilfsmittel bedient und alle Erkenntnisse, die aus dem Schrifttum ganz oder annähernd übernommen sind, als solche kenntlich gemacht und nach ihrer Herkunft unter Bezeichnung der Fundstelle einzeln nachgewiesen habe.

Ort, Datum   Unterschrift Doktorand

Table of contents

1 Summary

Poly-ADP-ribose (PAR) is a post-translational modification (PTM), with widely recognized importance in regulating physiological homeostasis. Perturbed PAR signaling was linked to numerous human patho-physiologies like diabetes, neurodegeneration, cancer or ischemia. In a cell, PAR chains are synthesized in majority thanks to the enzymatic activity of poly-ADP-ribose polymerase 1 (PARP1). PARP1 is known as a "guardian of genome integrity" due to its involvement in regulation of multiple DNA repair mechanisms. More recently, PARP1 has been shown to function in DNA replication and transcription.

Key to PARP1 functions and activation is PARP1's interaction with DNA. Various distorted DNA structures activate PARP1 and it is known that PARP1 binds to DNA via its DNA binding domain (DBD). The functional importance of two zinc fingers within the DBD is however not clear and has been heavily disputed over the last 30 years. The molecular mechanism of PARP1's DNA target site selection and its ability to distinguish between DNA lesion and transcription sites has been never evaluated *in vivo*. In addition, PARP1 achieves majority of its nuclear functions via regulation of chromatin structure. For example, via PAR binding dependent recruitment of the ATP-utilizing chromatin remodeler called amplified in liver cancer (ALC1). The *in vivo* functions of ALC1 are not known.

In my Ph.D., I therefore aimed to evaluate the molecular mechanism of PARP1's DNA target site selection and activation, but also to study the *in vivo* role of ALC1 in transcription.

I tested PARP1's interactions with chromatin and analyzed in detail the roles of the DBD in binding to DNA *in vivo*. To do that, I used kinetic modelling of fluorescence microscopy data. I found that PARP1 recognizes target sites through free diffusion. PARP1 is highly mobile and constantly exchanges between genome sites with weak DNA binding. My data suggests that DNA breaks are key to PARP1`s immobilization *in vivo*. I found that both zinc fingers are essential and sufficient to promote PARP1 binding to DNA.

I also demonstrate that ALC1's role in transcription recapitulates PARP1 functions. My results suggest that ALC1 can both co-activate and co-repress transcription in a PAR-dependent manner. Nonetheless, the molecular details leading to this interesting double function await further experiments. My data also suggest that PARP1 and ALC1 are not essential for nuclear receptor-mediated transcription activation.

The novel insight into the mechanism of PARP1 binding DNA, which is the prerequisite to its activation, sheds new light on PARP1's roles in all DNA-related processes. My observation that ALC1 is involved in regulation of transcription is an important step forward in understanding the cancer origins that involve ALC1.

Poly-ADP-ribose (PAR) ist eine posttranslationale Modifikationen, die eine anerkannte große Bedeutung bei der Regulation der physiologischen Homöostase hat. Störungen im PAR Signalweg wurden mit zahlreichen menschlichen Pathophysiologien wie Diabetes, Neurodegeneration, Krebs oder Ischämie in Verbindung gebracht. In der eukaryotischen Zelle, die PAR Modifikation wird mehrheitlich durch das Enzym poly-ADP-ribose polymerase 1 (PARP1) katalysiert und aktiviert. Auf Grund der wichtigen Beteiligung von PARP1 bei DNA Reparaturmechanismen wird PARP1 klassischerweise betrachtet als ein "Hüter der Genom Integrität". In letzter Zeit, erlangte PARP1 auch wichtige Funktionen bei der DNA-Replikation und der Transkription. Der Schlüssel zu den Funktionen und der Aktivierung von PARP1 sind die Wechselwirkungen mit DNA. Verschiedene verzerrte DNA-Strukturen aktivieren PARP1 und es ist bekannt, dass PARP1 über dessen DNA-bindende Domäne (DBD) an DNA bindet. Die Bedeutung der beiden Zink-Finger innerhalb der DBD ist jedoch nicht klar und wurde in den vergangenen 30 Jahren intensiv diskutiert. Auch sind die molekularen Mechanismen der PARP1 Erkennung bestimmter der DNA-Zielsequenzen nicht bekannt. Sowohl die Auswahl, als auch die Spezifität der Erkennung von DNA-Läsionen wurde nie *in vivo* bisher noch nicht untersucht. Zum Beispiel, rekrutiert PARP1 über einen PAR-abhängigen Mechanismus den ATP-abhängigen „Chromatin Remodeler" amplified in liver cancer 1 (ALC1). Darüber hinaus sind die *in vivo* Funktionen von ALC1 nicht bekannt.

In meiner Doktorarbeit, habe ich somit gezielt die molekularen Mechanismen untersucht, die hinter der Auswahl und Erkennung von DNA-Zielseiten stehen. Auch habe ich die Funktion von PARP1 und ALC1 in Regulation der Transkription analysiert. Mittels kinetischer Modellierung von Fluoreszenz-Mikroskopie Daten habe ich *in vivo* die PARP1 Wechselwirkungen mit Chromatin, sowie die genaue Rolle der DBD getestet. Meine Daten zeigen, dass PARP1 Zielseiten durch freie Diffusion erkannt werden. PARP1 ist ein sehr mobiles Enzym das ständig im Austausch zwischen bestimmten Genom-Orten steht. Meine Daten lassen vermuten, dass *in vivo* DNA-Brüche der Schlüssel für die PARP1 Immobilisierung sind. Ich konnte auch zeigen, dass beide Zink-Finger notwendig und ausreichend für die PARP1 Bindung an DNA sind.

Meine Ergebnisse deuten auch darauf hin, dass ALC1 sowohl eine co-aktivierende, als auch co-reprimierende PAR-abhängige Rolle bei der Transkription ausüben kann. Es sind jedoch weitere Experimente nötig, um die molekularen Details dieser Doppelfunktion genau aufzuklären. Die neu gewonnenen Einblicke in den Mechanismus der PARP1 DNA-Bindung, eine Voraussetzung für Aktivierung von PARP1, werfen ein neues Licht auf PARP1's Beteiligung bei allen DNA-abhängigen Prozessen. Die Beobachtung, dass ALC1 direkt die Transkription regulieren könnte, ist ein wichtiger Schritt für das Verständnis über die Beteiligung von ALC1 bei der Entstehung bestimmter Tumore.

2 Introduction

The genome and epigenome integrity is critical to human health

Ongoing genome wide association studies (GWAS), epigenome wide association studies (EWAS) and epidemiologic studies constantly update our understanding on determinants of human health, aging and disease. Especially valuable is the progress concerning the identification of the genome alterations (e.g. Single Nucleotide Variation, Copy Number Variation), aberrant epigenomes (e.g. deregulated DNA methylation) and environmental risk factors (e.g. chemical hazards) causative to human disorders. The early detection of these pathological changes allow us to fulfill the promise of disease prevention and pave the way for the delivery of personalized medicine, accessible on the broad scale (Witte, 2010, Rakyan et al., 2011, Bakulski and Fallin, 2014). However, despite of the knowledge of frequently studied alterations within genomes and epigenomes of for example, one of the most frequently researched tumors, limitations still prevail. Specifically an identification of the exact molecular mechanisms that drive these alterations remains a challenge. Consequently, these unknown mechanisms prevent the development of the next generation therapies, urgently looked for in cancer treatment but also other human disorders. Importantly, the packaging of DNA into higher order chromatin structure is critical for genome and epigenome integrity. Aberrant chromatin structure (e.g. abnormal nucleosome positioning) could lead to regional increase of mutation rates, chromosomal translocations and aberrant gene expressions (Schuster-Böckler and Lehner, 2012, Roukos and Misteli, 2014). Thus, obtaining a complete understanding of unknown molecular mechanisms behind chromatin structure regulation by various nuclear proteins is of great significance. Poly-ADP-ribose polymerase 1 (PARP1) exemplifies this situation.

PARP1 is an abundant protein within the nucleus that directly and indirectly reorganizes chromatin structure, important in DNA repair, transcription and replication (Kraus and Hottiger et al., 2013). The focus of my Ph.D. was first, to investigate the details of the molecular mechanism of DNA-coupled PARP1 activation, which leads to synthesis of poly-ADP-ribose (PAR), a post-translational modification (PTM). The acceptor proteins of this PTM are in consequence regulated in their interactions with various proteins and functions on chromatin. For example, the PAR dependent chromatin remodeler called amplified in liver cancer (ALC1),

which *in vivo* functions are not known. My Ph.D. focued on evaluation of the basis of ALC1 functions in transcription, as well.

2.1 The PARP1 family regulates human physiology

2.1.1 Poly-ADP-ribose (PAR) originates from PARP activity

Poly-ADP-ribose (PAR) is an abundant post-translational modification. The beginning of studies over PAR took place already 51 years ago. All started with the report of the presence of an acid-insoluble fraction of poly(A)-containing products when liver nuclear extracts were incubated with nicotinamide adenine dinucleotide (NAD$^+$). The nuclear enzyme synthetizing PAR products, was named poly-ADP-ribose polymerase (PARP; Chambon et al., 1963). Soon after, the structure of PAR was reported and PARP was purified (Doly et al., 1967, Nishizuka et al., 1967, Reeder et al., 1967, Sugimura et al., 1967). Eventually the PARP gene (later named PARP1) was cloned and additional PARP genes were identified (Alkhatib et al., 1987, Kurosaki et al., 1987, Uchida et al., 1987). The PARP enzymes are conserved from prokaryotes to eukaryotes, with human orthologs identified e.g. in *Herpetosiphon aurantiacus, Neurosporra crassa, Aspergillus nidulans, Caenorhabditis elegans, Dictyostelium discoideum, Arabidopsis thaliana, Zea mays, Drosophila melanogaster, Danio rerio, Xenopus laevis, Gallus gallus, Canis familiaris* and others, except yeast (Hottiger et al., 2010).

The human PARP family consists of 17 members. Based on the presence of functionally characterized domains the human PARP proteins can be classified into: (i) DNA-binding PARPs, (ii) tankyrases with protein binding ankyrin repeats, (iii) PARPs that contain CCCH zinc finger domains shown to bind viral RNA, (iv) PARPs with macrodomains that bind PAR and ADP-ribose (see also 2.3.2), and (v) the remaining unclassified PARPs (Figure 2.1). Alternatively, the PARPs can be also classified into two groups: active and inactive enzymes. Active PARPs are further divided into PARPs synthesising PAR (PARP1-5), and PARPs catalyzing the mono-ADP-ribosylation of proteins (PARP6-8, 10-12, 14-16). Inactive enzymes, unable to bind NAD$^+$, are PARP9 and PARP13 (Kleine et al., 2008). Most human PARPs are present throughout the cell cycle in the cytoplasm with additional punctate or diffused enrichment at specific cellular sites for specific PARPs (centrosome, membranous organelles, nuclear envelope, Golgi, plasma

membrane, endoplasmic reticulum, mitotic spindle and spindle poles; Table 2.1; Vyas et al., 2013).
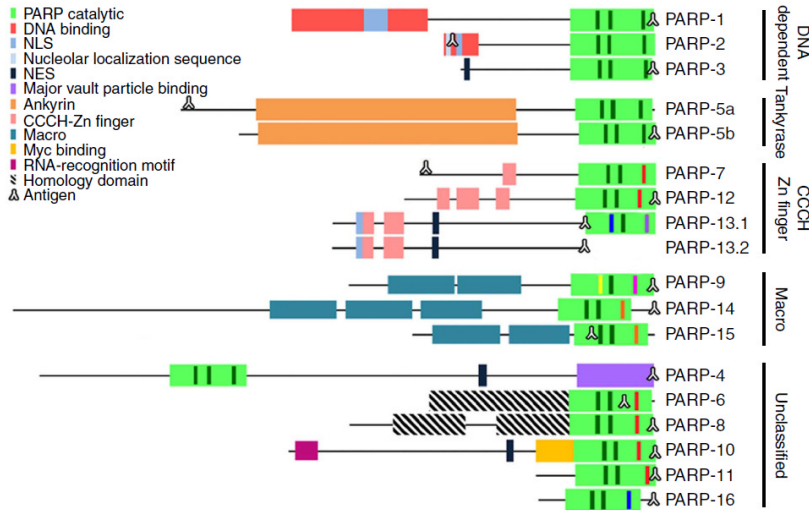
Figure 2.1 Human PARP proteins and their classification (from Vyas et al., 2013). Functional domains are indicated in colors, the green dashes within the catalytic domain indicate H-Y-E amino acids thought to be required for PAR synthesis activity. Dashes with different colors indicate the replacement of these amino acids with the following residues: I (red), Y (blue), V (purple), Q (yellow), T (pink) and L (orange) in PARP functional studies. **Antigen** – corresponds to the domain region, which served as antigen to generate antibodies specific to individual PARP, **NLS** - nuclear localization signal, **NES** - nuclear export signal. PARP13.1 and PARP13.2 are two isoforms originating from the same gene.

Table 2.1 The summary of PARP family member localization (from Vyas et al., 2013).

Subfamily	PARP	Other names	Localization		
			Interphase		Mitosis
			Cytoplasm	Nucleus	
DNA dependent	1	PARP, ARTD1		Diffuse	Chromatin
	2	ARTD2	Punctate	Punctate	Diffuse, cytoplasmic
	3	ARTD3	Punctate	Punctate	Punctate, cytoplasmic
Tankyrase	5a	TNKS1, ARTD5	Punctate, centrosome		Spindle pole
	5b	TNKS2, ARTD6	Punctate		Spindle
CCCH Zn finger	7	tiPARP, ARTD14	Punctate	Punctate	Diffuse, cytoplasmic
	12	ARTD12	Punctate, Golgi		Punctate, cytoplasmic
	13	ZAP, ARTD13	Punctate		Punctate, cytoplasmic
Macro	9	BAL1, ARTD9	Diffuse, plasma membrane	Diffuse	Diffuse, cytoplasmic
	14	BAL2, ARTD8	Punctate, focal adhesions	Punctate	Punctate, cytoplasmic
	15	BAL3, ARTD7	Not assayed	Not assayed	Not assayed
Unclassified	4	vPARP, ARTD4	Punctate	Diffuse	Diffuse, cytoplasmic
	6	ARTD17	Punctate		Punctate, cytoplasmic
	8	ARTD16	Punctate, centrosome, nuclear envelope		Spindle pole
	10	ARTD10	Punctate		Punctate, cytoplasmic
	11	ARTD11	Punctate	Punctate	Centriole
	16	ARTD15	Punctate, reticular		Punctate, cytoplasmic

Abbreviations: **PARP** – poly-ADP-ribose polymerase, **ARTD** – ADP ribosyl transferase with diphtheria toxin homology

According to the enzymatic reaction catalyzed by PARP proteins and to the rules for biochemical classifications from International Union of Biochemistry and Molecular Biology (IUBMB) ''transferase'' is an appropriate and accurate name for PARP enzymes (Hottiger et al., 2010). Some PARPs are also capable of only mono-ADP-ribosylation without poly-ADP-ribosylation activity. However all the PARP family members are referred to as poly-ADP-ribose polymerases, in a legacy of PARP1 discovery - the founder of the PARP family. Thus, majority of publications refers to these enzymes as PARPs.

PARP1 is the major enzyme responsible for synthesis of PAR, a key modification to PARP1 functions

The constitutive levels of PAR in unstimulated cells are usually very low (Ferro et al., 1978, Hilz et al., 1983, Kreimeyer et al., 1984). In contrast, upon mitogenic stimulus or genotoxic stress the PAR levels increase rapidly from 10 to 500 fold (see also 2.3.1). This transient PAR increase is in majority attributed to PARP1 activity, which alone produces up to 90 % of PAR levels within a cell (D'Amours et al., 1999). PARP1 is the most studied and thus the best characterized among the PARP family members. PARP1 modifies post-translationally various acceptor proteins, which could also contain a specific fold that recognizes exclusively PAR modification. Overall PAR can activate or inhibit activity of the acceptor molecule, impact its localization or complex formation with partner molecules (see also 2.3). PARP1, a highly abundant nuclear protein (up to 10^6 copies/cell) and functions across the genome: modulating DNA methylation, repair, transcription, chromatin structure and chromosome organization (Krishnakumar and Kraus, 2010, Kraus and Hottiger, 2013).

2.1.2 PARP1 regulates DNA based processes

PARP1 regulates the DNA damage response

Almost since its discovery, PARP1 has been linked to maintenance of genome integrity (Durkacz et al., 1980, De Lorenzo et al., 2013). PARP1 is essential for base excision repair (BER), where recruitment of the BER scaffold protein X-ray cross-complementing protein 1 (XRCC1) is dependent on its PARylation at DNA damage sites. XRCC1 binds to variety of BER proteins thereby facilitating efficient repair of damaged bases (Okano et al., 2000, Izumi et al., 2003, Horton et al., 2008, Curtin, 2012). PARP1 positively regulates recruitment of meiotic

recombination 11 (MRE11) and nijmegen breakage syndrome protein 1 (NBS1) to double strand DNA beaks, thus promoting homologous recombination (HR) (Haince et al., 2008). Simultaneously PARP1 inhibits non homologous end joining repair (NHEJ) an alternative to HR. NHEJ inhibition occurs subsequent to disassociation from DNA of Ku proteins due to their PARylation. Ku proteins provide a scaffold to NHEJ (Wang et al., 2006). Many proteins involved in DNA repair and stress response e.g. XRCC1, XRCC6, tumor suppressor p53, cyclin-dependent kinase inhibitor p21, mismatch-repair protein 6 (MSH6), nucleotide-excision repair protein (NER) xeroderma pigmentosum complementation group A (XPA) and type I topoisomerase (TOP1) share a specific motif called PAR binding motif (PB; Pleschke et al., 2000). Thanks to this motif PARP1 could regulate a recruitment of various proteins important for the DNA repair to occur (see also 2.3.2). It is also known that loosening of chromatin condensation facilitates DNA repair via providing an access to DNA damage sites for DNA repair proteins (Aubin et al., 1982, Poirier et al., 1982, Panzeter et al., 1992). PARP1 fosters reorganization of chromatin structure upon DNA damage. For example: via PARylation of histones, recruitment of histone chaperone with AP-endonuclease activity (APLF1) and the chromatin remodeler ALC1 functionally involved in DNA repair as well (Ahel et al., 2009, Gottschalk et al., 2009, Eustermann et al., 2010; Mehrotra et al., 2011).

PARP1 regulates transcription

Similarly to the functions in DNA repair, PARP1 was shown to possess dual (activator and repressive) roles in transcription control. In early studies PARP1 was found to co-immunoprecipitate with transcriptional factor TFIIC and PAR modify the TFIIC leading to repression of transcription (Slattery et al., 1983). Also, PARP1 was found to promote chromatin condensation *in vitro* thus inhibitory to transcription as well (Kim et al., 2004). This view of repressive PARP1 role in transcription predominated until PARP1 function in fly heat shock response was identified. Flies contain only one PARP protein, which corresponds to PARP1 (Tulin et al., 2002). *Drosophila melanogaster* PARP (dPARP) was found to increase spreading (puffs) of polytene chromosomes, that include heat shock protein 70 (*hsp70*) loci, upon heat shock (HS). The puffing and subsequent expression of proteins from the puff region required dPARP activation and presence of PAR modification (Figure 2.2; Tulin and Spradling, 2003).
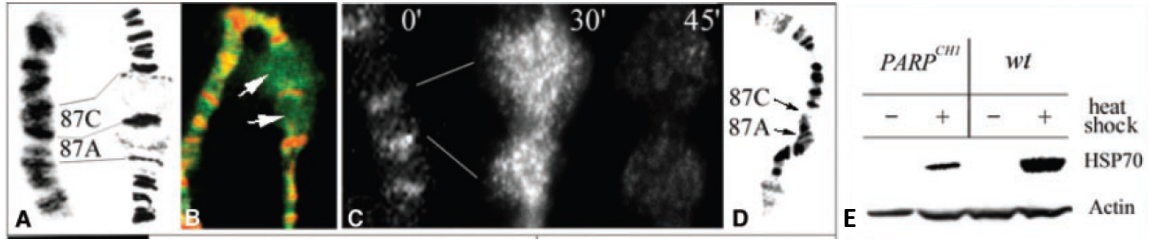
Figure 2.2 *Drosophila melanogaster* PARP is required for heat shock induced puffing and *hsp70* expression (modified from Tulin and Spradling, 2003). **A)** The 87A and 87C polytene chromosome region before (left) and after (right) a 30-min heat shock (37°C). **B)** PARP-GFP is widespread in the 87A and 87C puffs (arrows). **C)** No poly-ADP-ribose signal was detected before heat shock (0 minutes). PAR signal increased during heat shock (grey color; 30 minutes) and again decreased after heat shock (45 minutes). **D)** Puffing does not take place in larvae fed with the PARP inhibitor for 1 hour before heat shock. **E)** Levels of Hsp70 protein are reduced in flies with catalytically deficient PARP (ParpCH1), when compared to wild type (wt) flies; normalized to actin levels.

Similarly, like during the heat shock, PARP1 was found to enhance transcription of nuclear receptor target genes - progesterone receptor (PR) and estrogen receptor alpha (ERα). During the PR ligand addition (progesterone) PARP1 was found to be activated and cellular PAR levels increased (Figure 2.3; Wright et al., 2012). Strikingly, the ERα-regulated transcription of *pS2* gene (known also as trefoil factor 1, TFF1) was found to require an induction of a double DNA strand break at the *pS2* promoter. The presence of the break and its PARP1 binding were shown as essential in ERα-dependent transcription activation (Ju et al., 2006). ERα and PARP1 were found to co-immunoprecipitate and ERα was PARylated by PARP1 *in vitro* (Zhang et al., 2013a). The heat shock and nuclear receptor studies of PARP1 importance, presented PARP1 as a protein that plays a co-activation function in transcription initiation. However a PARP1 role more aligned with PARP1 DNA repair functions at these loci cannot be dismissed. For example, the heat shock loci upon heat shock, requires phosphorylation of H2A.V histone variant. This modification in flies is considered a DNA damage mark (Baldi and Becker, 2013).

PARP1 roles in transcription were evaluated in non-stressed cells as well (no ligand or heat shock treatment). Upon PARP1 stable knock-down in breast cancer cells (MCF-7), 204 genes out of 14500 genes (microarray tested) showed deregulation. Among these 204 genes: 115 genes were up-regulated and 89 were down-regulated, which was confirmed on selected genes via quantitative-PCR (Figure 2.4; Frizzell et al., 2009, Krishnakumar and Kraus, 2010).
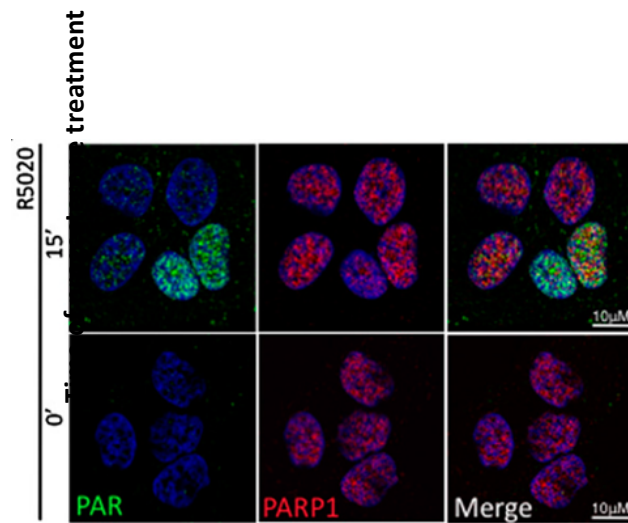
Figure 2.3 PAR rapidly accumulates following progesterone stimulation (from Wright et al., 2012). PAR levels (green) increase in breast cancer cells treated with R5020 (progesterone) for 15 min (first panel on the left). Levels of poly-ADP-ribose polymerase 1 (PARP-1) are shown in red (the middle panels). Merged PAR and PARP1 (the first panel on the right).

An investigation of the molecular mechanism, found PARP1 to reside and regulate the chromatin structure at the transcriptional start site (TSS) of positively regulated genes. A regulation of chromatin structure by PARP1 was linked to PARylation and subsequent removal of the lysine specific demethylase 5B (KDM5B) from the regulated genes. In consequence a histone 3 lysine 4 trimethylation (H3K4me3) favoring open chromatin was maintained. No PARP1 role in chromatin reorganization of the negatively regulated genes was observed (Krishnakmar and Kraus, 2010).
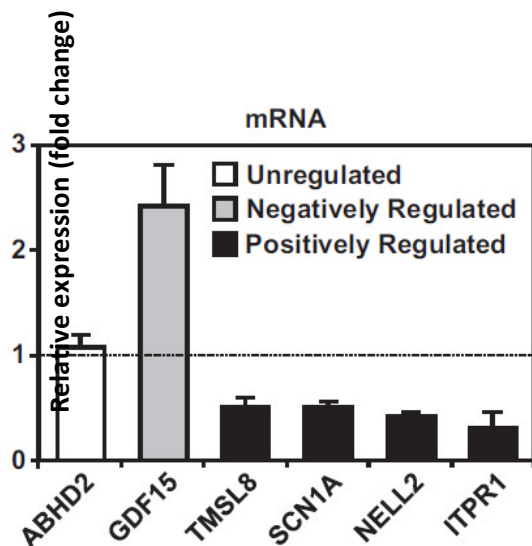
Figure 2.4 RT-qPCR analysis of mRNA expression for six genes in MCF-7 cells with PARP-1 knockdown (from Krishnakumar and Kraus, 2010). Each bar represents the mean plus the SEM, n=3. The differences observed for all genes except *ABHD2* are significant (Student's t-test, $p\text{-value} < 0.05$). The tested genes are: ***ABHD2*** - abhydrolase domain-containing 2, ***GDF15*** - growth differentiation factor 15, ***TMSL8*** - thymosin-Like 8, ***SCN1A*** - sodium channel type I alpha subunit, ***NELL2*** - NEL-like 2, ***ITPR1*** - inositol 1,4,5-trisphosphate receptor 1.

2.1.3 Deregulation of PAR metabolism leads to human pathophysiology

The associations between deregulated PAR metabolism and human pathophysiology are on the rise. Among them, the most extensively studied are the PARP family functions in carcinogenesis. If tumor origin comprises of 6 hallmarks (Figure 2.5), deregulated PAR metabolism and PARP family members were shown to impact all of them (Masutani et al., 2005, Hanahan and Weinberg, 2013).
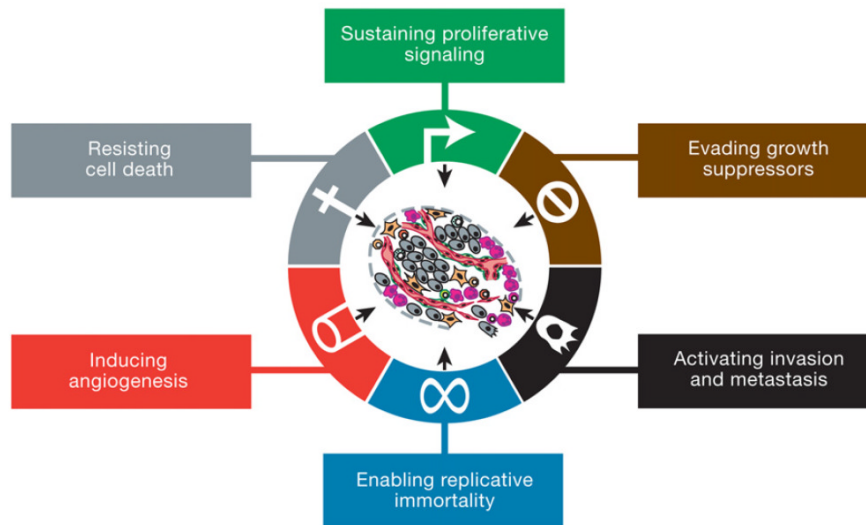
Figure 2.5 The hallmarks of cancer (from Hanahan and Weinberg, 2013).

In an early discovery the occurrence of pancreatic cancer increased after DNA damage induced with streptozotocin, while PARP1 was inhibited with benzamides (Yamagami et al., 1985). Since then PARP1 was suggested to act as a tumor suppressor. These findings were further confirmed and expanded in mouse models with individually knocked out *PARP1, PARP2, PARP4 or poly-ADP-ribose glycohydrolase (*PARG; see also 2.3.3). As summarized in Table 2.2 incidence of tumors across various tissues and across various genetic backgrounds (p53$^{-/-}$, Ku80$^{-/-}$) increased upon deregulation of PAR metabolism.

Table 2.2 The summary of susceptibility to carcinogenesis in mouse models of deregulated PAR metabolism (from Masutani and Fujimori, 2013).

Molecule	Spontaneous/induced	Outcome	Tissue or tumor type
$Parp\text{-}1^{-/-}$ (ex2)	Spontaneous (18–24 months)	Increased	Hepatocellular carcinoma
$Parp\text{-}1^{-/-}$ (ex1)	Spontaneous (7 months)	No change	Various tissues
	Spontaneous (15 months)	No change	Various tissues
$Parp\text{-}1^{-/-}$ (ex2)	Spontaneous	Increased	Uterine, lungs, hepatocellular carcinoma
$Parp\text{-}1^{-/-}$ (ex2)	Spontaneous	Increased	Breast
$Parp\text{-}1^{-/-}$ (ex1)	BHP	Increased	Hemangioma, hemangiosarcoma
$Parp\text{-}1^{-/-}$ (ex1)	Azoxymethane	Increased	Colon, liver (nodule)
$Parp\text{-}1^{-/-}$ (ex2)	Diethylnitrosamine	Increased	Hepatocellular carcinoma
$Parp\text{-}1^{-/-}$ (ex1)	4-Nitroquinoline 1-oxide	No change	Oral cavity, esophagus
$Parp\text{-}1^{-/-}$ (ex1)	IQ	No change	Liver, forestomach
$Parp\text{-}1^{-/-}$ (ex2)	$p53^{-/-}$	Increased	Colon, breast, brain
$Parp\text{-}1^{-/-}$ (ex4)	$p53^{-/-}$	Decreased	Thymic lymphoma
$Parp\text{-}1^{-/-}$ (ex2)	$Ku80^{-/-}$	Increased	Liver
$Parp\text{-}1^{-/-}$ (ex2)	$SCID$	Increased	Thymus
$Parp\text{-}1^{-/-}$ (ex2)	$Ptc^{-/-}$	Increased	Medulloblastoma, basal cell carcinoma
$Parp\text{-}1^{-/-}$ (ex2)	$Wrn^{Dhel/Dhel}$	Increased	Various tissues
$Parp\text{-}2^{-/-}\ p53^{-/-}$		Increased	T-cell lymphoma
$Parp\text{-}4^{-/-}$	Diethylnitrosamine	Increased	Colon
$Parp\text{-}4^{-/-}$	Urethane	Increased	Lungs
$Parg^{-/-}$ (110 kD)	Diethylnitrosamine	Increased	Liver
$Arh1^{-/-}$	Spontaneous	Increased	Lymphoma, adenocarcinoma

Currently 94 mutations of PARP1 are reported in the Catalog of Somatic Mutations in Cancer (COSMIC). The precise function in tumor development for the majority of these mutations was not confirmed yet. However a few mutations, like PARP1 single nucleotide polymorphism (SNP) Val762Ala (valine to alanine) were investigated in detail. This SNP decreases PARP1 activity (Wang et al., 2007) and was linked to a higher risk of prostate cancers in Caucasians (Lockett et al., 2004) but also esophageal and lung cancers in Chinese populations (Hao et al., 2004, Zhang et al., 2005). The same SNP was associated with decreased risk for glioma in Caucasians (Liu et al., 2009). Importantly not only mutations but also PAR metabolism and PARP1 protein levels can be considered as a tumor biomarker. For example, PARylation of proteins in peripheral blood leukocytes decrease more than 50 % in head, neck, breast and cervical cancers (Lakadong et al., 2010). PARP1 high expression levels were linked to poor clinical outcome of oral squamous cell carcinomas (Mascolo et al., 2012).

The mechanisms of pathophysiology

Carcinogenesis involving PARPs stem from deregulated DNA repair and transcription. PARP1, PARP2 and PARP3 are directly linked to participation in DNA repair. PARP1 especially was shown to control multiple DNA repair mechanisms. Lack of correct PAR metabolism temporally

and spatially leads to loss of heterozygosity (LOH) or chromosome translocations, which are aberrations often observed in carcinogenesis. These abnormalities are especially increased when *PARP1/2* knock-out mice are challenged with DNA damage inducing agents like alkylating agents. Similar chromosome alterations and increased tumor rate are observed upon deletion or amplification of proteins downstream from PAR e.g. checkpoint with fork head associated (FHA) and RING domain (CHFR; Yu et al., 2005) or the chromatin remodeler ALC1 (Cheng et al., 2013; see also 2.4). Inadequate PAR degradation due to lack of PARG or ADP-ribosylarginine hydrolase (ARH1), also leads to increased incidence of hepatocellular carcinoma and adenocarcinoma with increased metastases, respectively (Min et al., 2010, Kato et al., 2011).

PARP1 was shown to co-regulate transcription of genes important for carcinogenesis upon retinoic acid or progesterone stimuli (Pavri et al., 2005, Wright et al., 2012). PARP1 acts as a co-activator of the cellular oncogene c-FOS and the nuclear factor kappa-light-chain-enhancer of activated B cells (NF-κB), a transcription factor regulating inflammation (Hassa et al., 2005). Inflammation is observed during various human diseases including cancer. NF-κB transcription regulation is compromised upon PARP1 deletion and results in reduced levels of pro-inflammatory cytokines in lipopolysaccharide (LPS) treated animals (Hassa and Hottiger, 1999, Oliver et al., 1999). Inflammation related animal models with genetically depleted or chemically inhibited PARP1 exhibit resistance to tissue injury, lower organ inflammation rate and higher survival rate (Shall and de Murcia, 2000, Kraus and Hottiger, 2013). Levels of tumor necrosis factor alpha (TNFα), interleukin 6 (IL-6) and interleukin 10 (IL-10) are reduced in a *Parp1*^{-/-} mice upon for example induction of polymicrobial sepsis with cecal ligation and puncture (Soriano et al., 2002). Both, the prolonged presence of DNA lesions and chronic inflammation are considered as important stages in cancer development (Davalos et al., 2010). Inflammation can stimulate epithelial-mesenchymal transition (EMT), leading to cancerous stem-cell development (Heldin, 2012). In cells undergoing anti-cancer drug treatment PARP1 inhibition reduces inflammatory damage (Mukhopadhyay et al., 2011).

In addition, PARP family members were shown to be implicated in cancer metastasis (PARP1), angiogenesis (the PARP family, PARG; Pyriochou et al., 2008, Tentori et al., 2007, Lacal et al., 2009, Pan et al., 2012), inhibition of apoptosis (PARP9/14/15) or induction of cell death via NAD$^+$ depletion or PAR stimulation of apoptosis inducing factor (AIF; Yu et al., 2006),

induction of autophagy (PARP1; Munoz-Gamez et al., 2009; Rodriguez-Vargas et al., 2012, Kleine et al., 2012).

PARP inhibitors reached clinical trials to treat cancer

Functions of PARP family members have been recognized as an opportunity for targeted sensitization of tumor cells to genotoxic agents and radiotherapy. Although *PARP1* knock-out mice are viable they are hypersensitive to ionizing radiation and to alkylating agents, both broadly used to treat cancer. Thus, it was considered that PARP1 inhibition could lead to specific tumor cell death (Soldatenkov and Smulson, 2000). Indeed, the breast and ovarian cancer susceptibility protein 1 (*BRCA1)* – and breast cancer susceptibility protein 2 (*BRCA2)*- mutant cells were 1000-fold more sensitive to PARP inhibitors, when compared to *BRCA1/2*- competent cells (Bryant et al., 2005, Farmer et al., 2005, McCabe et al., 2005).

Normally *BRCA1/2* mutations are acquired during tumor formation, leading to risk increase for breast (45-65 % risk) and ovarian cancers (11-39 % risk; Mackay and Szecsei, 2010). The non-transformed cells possess a wild type, functional BRCA1/2. The absence of BRCA1/2 leads to absence of classic homologous recombination (HR) DNA repair pathway. Upon chemo- or radio-therapies, cancer cells with BRCA1/2 mutations presumably switch to alternative homologous recombination, while PARP1 primarily inhibits the error prone non-homologous end joining (NHEJ). In contrast, upon administration of PARP inhibitors, the NHEJ becomes predominant resulting in decreased stability and tumor cell death (Figure 2.6).

This concept was followed by several pharmaceutical companies with various PARP inhibitors tested already in clinical trials. None of the inhibitors was approved by the Food and Drug Administration (FDA) until now. Clinical trials (phase I and II) suggest that PARP inhibitor treatment prolongs, to a variable degree, tumor progression free survival in *BRCA1/2* mutant patients. Only subgroup of patients bearing *BRCA1/2* mutations (4-74 %) responds to PARP inhibition, thus a long term benefit of the treatment remains to be determined. A concern is present regarding emergence of clones resistant to PARP inhibition therapy e.g. via reverse mutations mechanisms (Ashworth, 2008). During PARP inhibition, *BRCA2* can further acquire mutations, which are able to restore BRCA2 function (Edwards et al., 2008, Barber et al., 2013).
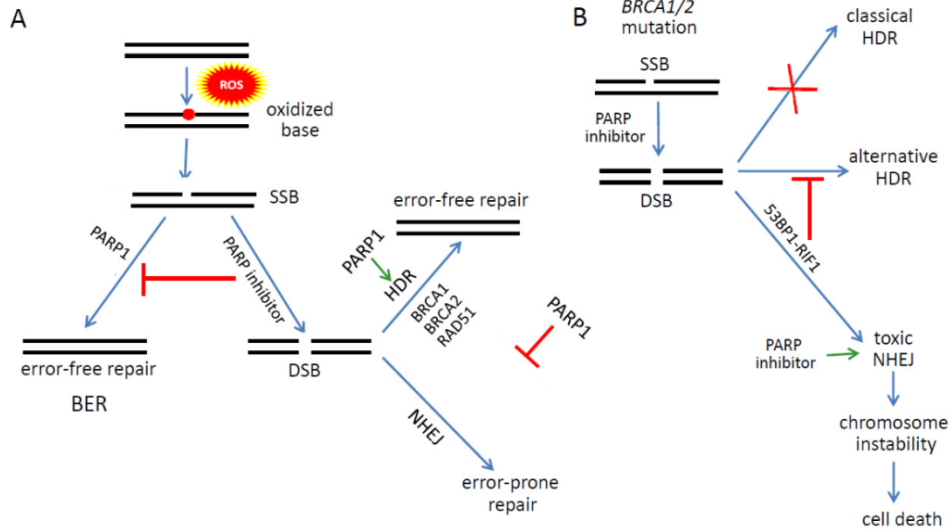
Figure 2.6 Consequences of poly-ADP-ribose polymerase (PARP1) inhibition in (A) ***BRCA1/2*-competent and (B) *BRCA1/2*-mutant cells** (from Rosen and Pishvaian, 2014). **A)** Reactive oxygen species (**ROS**) cause DNA base lesions, normally repaired by the base excision repair (**BER**) pathway. The site of the damaged base is converted to a single-strand break (**SSB**) by one of several BER enzymes depending upon the lesion type. PARP1 then recognizes SSB and regulates assembly of a repair complex. In the presence of a PARP inhibitor, the SSB cannot be repaired and eventually becomes a double-strand break (**DSB**) or a collapsed replication fork during S-phase. In homology directed repair (**HDR**) competent cells, the DSB or collapsed replication fork is repaired in an error free manner by HDR. **B)** In *BRCA1* or *BRCA2* mutant cells, the classical HDR pathway is defective and cannot be utilized to repair DSBs or collapsed replication forks. Instead, the cells enter into a "toxic" deregulated non homologous end joining (**NHEJ**) pathway, leading to chromosomal instability, cell cycle arrest, and apoptosis. However, if the NHEJ pathway is blocked, the cells can repair the damage through an alternative HDR mechanism that is not well understood.

2.2 The molecular mechanism behind PARP1 functions

There are three major and interdependent PARP1 characteristics, which are key to understand the molecular mechanism of PARP1 activation and deactivation and thus, PARP1 physiological functions. These three characteristics encompass: (i) PARP1 domain composition and inter-domain communication regulating PARP1 chromatin associations and activation in space and time; (ii) specific PARP1 interactions with various proteins in a cell; and (iii) external and internal stimuli triggering PARP1 signaling.

2.2.1 PARP1 contains six globular domains

Since the PARP1's purification from calf thymus in the late 70s (Mandel et al., 1977) multiple studies aimed to decipher the structural composition of PARP1, which has a molecular-weight of 116 kilodaltons (kDa). The very first study reported a presence of only two PARP1 fragments. The first fragment was found to mediate DNA binding and the second fragment contained multiple sites for PAR modification (Nishikimi et al., 1982). Next, an additional segment of PARP1 – a domain responsible for NAD^+ binding (PARP1 substrate) - was identified (Kameshita et al., 1984). This characterization of distinct PARP1 domains is valid until today. In summary, the three main functional PARP1 fragments are: an amino-terminal DNA binding domain (DBD), a central automodification domain (AMD) and a carboxy-terminal catalytic domain (CD). Over the past years the fragment composition of PARP1 was further redefined (Figure 2.7; de Murcia, 1999).
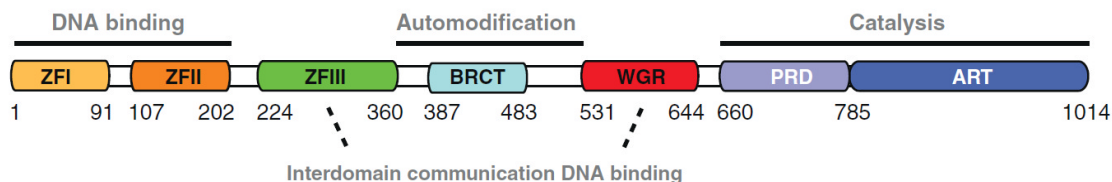
Figure 2.7 Schematic representation of human PARP1 domain composition (from Hassler and Ladurner, 2012). Zinc-finger 1 (**ZFI**) and zinc-finger 2 (**ZFII**) form the DNA binding domain (DBD), zinc-finger 3 (**ZFIII**), BRCA1 carboxy-terminal domain (**BRCT**), BRCT and flanking loop regions form the automodification domain (AMD), named after a conserved central motif (**WGR**), PARP regulatory domain (**PRD**), PARP family defining catalytic core required for basal activity ADP-ribosyl transferase (**ART**), PRD and ART form the catalytic domain.

As shown on Figure 2.7 the DBD is composed of two zinc finger domains (ZFI/ZF1 and ZFII/ZF2) which contain the characteristic Cys(Cysteine)-Cys-His(Histidine)-Cys zinc finger motif (Uchida et al., 1987, Lamarre et al., 1988, Gradwohl et al., 1990). The DBD is followed by an additional zinc finger fold (ZFIII/ZF3), which was found to mediate inter-domain contacts crucial in PARP1 activation (Langelier et al., 2008 and 2010). The third zinc finger does not bind to DNA alone *in vitro* (Tao et al., 2008) and does not reduce, when mutated, the binding to DNA of the full length PARP1 (Langelier et al., 2010). Between DBD and ZF3 resides a bipartite nuclear localization signal (NLS) and a caspase-3-cleavage site (Schreiber at el., 1992, Tewari et al., 1995). The AMD fragment contains the BRCA1 carboxy-terminal domain (BRCT), found to mediate protein-protein interactions for example of PARP1 with XRCC1 during DNA repair.

19

The carboxy-terminal CD contains the PARP signature motif, which binds NAD$^+$ (Simonin et al., 1990). This is the most conserved region across PARP family members across all species. Next to the CD, on the left, resides WGR motif, named after the conserved amino acid sequence in the motif (Tryptophan, Glycine, Arginine). WGR functions in DNA binding and inter domain contacts mediating PARP1 activation (Langelier et al., 2012). The structures of all individual domains or fragments of PARP1 are available (Figure 2.8). The nearly the full length X-ray structure of PARP1 (missing ZF2 and BRCT) bound to double strand break on DNA is known as well (Langelier et al., 2012).

2.2.2 The DBD is important for DNA binding and PARP1 activation

Already the early experiments have demonstrated the importance of damaged DNA as a co-factor for PARP1 activity (Benjamin, 1980; Ohgushi, 1980). The DNA breaks were found to be exclusively recognized by DBD via ZF1 and ZF2 (Zahradka & Ebisuzaki, 1984, Uchida et al.,1987, Lamarre et al., 1988, Mazen et al., 1989). Over the years a contribution of each zinc finger to DNA break recognition and subsequent PARP1 activation became extensively studied, although with partially contrasting results. For example one study where binding of zinc (Zn2$^+$) was abolished via mutagenesis, reported that ZF2 is a major part of the DBD involved in a specific recognition of a nick on a single stranded DNA. Lack of functional ZF1 resulted in only a minor reduction in DNA binding (Gradwohl at el., 1990). Another study found however that ZF1, next to ZF2, is actually important for a detection of a nick or a break on single stranded DNA (ssDNA) and subsequent PARP1 activation. In addition the importance of functional ZF2 in recognition of a nick on double stranded DNA (dsDNA) was diminished (Ikejima et al., 1990).

Various residues between ZF1 and ZF2, but also residues within N-terminal part of the central automodification domain (AMD) were suggested to mediate PARP1 activation upon DNA binding. These residues, when mutated, however did not compromise DNA binding (Trucco et al., 1996). Such inter-domain interactions were further confirmed with the identification and crystallization of the third zinc finger (ZF3), which is important for transmission of a DNA bound state to the catalytic domain (Langelier et al., 2008 and 2010). The transmission of DNA bound state to the molecule's activation, was suggested to be facilitated via dimerization of PARP1 molecules (Mendoza-Alvarez et al., 1993, Pion et al., 2005). At first, the identified ZF3 was claimed to be important in PARP1 dimerization (Langelier at al., 2008).
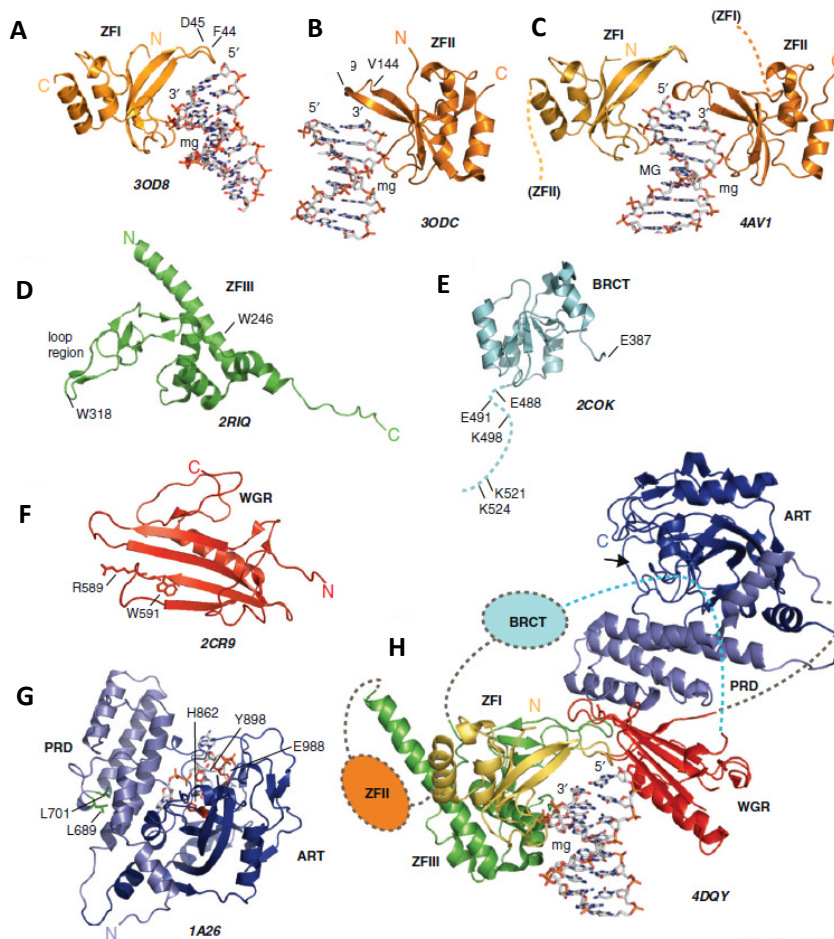
Figure 2.8 The structures of human PARP1 protein (from Hassler and Ladurner, 2012). **A)** Zinc finger I (**ZFI**) in complex with blunt-ended DNA. ZFI binds the minor groove side. Important loop residues for DNA recognition (F44) and WGR interaction (D45) are indicated. **B)** Zinc finger II (**ZFII**) in complex with blunt ended DNA. ZFII binds also from the minor groove side. Important loop residues for interaction with ZFI (V144, P149) are indicated. **C)** hetero-dimeric complex between ZFI and ZFII from 2 different PARP1 molecules and a 3 prime recessed DNA. Note that ZFI binds the major groove of the DNA in the complex. **D**) Zinc finger III (**ZFIII**) domain. Important residues are highlighted. **E)** NMR structure of the BRCA1 carboxy-terminal domain (**BRCT**) domain. The location of the flanking flexible automodification region including experimentally verified sites of ADP-ribosylation are indicated. **F**) NMR structure of the WGR domain, named after the defining W and R residues. These residues mediate DNA contacts (W) and interaction with ZFI and PRD (R). **G**) X-ray structure of the catalytic domain consisting of PARP regulatory domain (**PRD**) and ADP-ribosyl transferase (**ART**) domain of PARP1 in complex with a nonhydrolyzable NAD$^+$ analogue. The NAD$^+$ analogue is bound at the PAR binding site and an additional NAD$^+$ molecule is modeled into the catalytic site. Catalytic triad residues (red, HYE) and PRD residues mediating catalytic activation (green) are highlighted. **H**) X-ray structure of a near full-length PARP1 (lacking ZFII domain and automodification region, dotted grey) in complex with blunt-ended DNA. The DNA binding mode shown here is mutually exclusive with the one in C.

However, a subsequent nuclear magnetic resonance (NMR) spectroscopy study by the same authors ruled out the possibility of dimerization (Langelier et al., 2010). In contrast, studies favoring monomerization of PARP1 were reported as well. For example, based on measurements of PARP1 catalysis rate, it was concluded that PARP1 is most likely monomeric (Ikejima et al., 1987). Other studies left the question of PARP1 dimerization unsolved, concluding that, if the enzyme auto-modifies itself, kinetic analysis as a function of protein concentration cannot discriminate between monomolecular or bimolecular mechanism (Honegger et al., 1989).

### 2.2.3 Structural insights into zinc finger interactions with DNA

ZF1 and ZF2 bind the DNA break differently

The work over the molecular mechanism of PARP1 binding to DNA and PARP1's subsequent activation, was facilitated by the X-ray determination of the crystal structure of PARP1-DBD bound to DNA break (Ali et al., 2012).

The N-terminal segment of human PARP1 encompassing both zinc fingers (residues 5–202) was crystallized as bound to 11 base pair long duplex DNA with single-base 5′ overhang on each end. The PARP1-DBD structure, bound to the each end of the single DNA duplex was refined at 3.1 Å resolution. Both zinc fingers interact with DNA via sugar-phosphate backbone grip and the base stacking loop. Majority of the contacts with the DNA phosphodiester backbone are formed by the residues 15-22 and 119-126 for ZF1 (residues 6-91) and ZF2 respectively (residues 107-122). In ZF1, residues 16-Ser-Gly-Arg-Ala-19 project into the major groove, with Arg18 contacting the edges of the base pairs. In ZF2, residues 120-Ser-Asn-Arg-Ser-123 project to minor groove with Arg122 making interactions with base pairs like Arg 18 of ZF1 (Figure 2.9).

The interface between ZFs suggests PARP1 dimerization

Despite similarity of architecture between the zinc fingers, they interact with DNA differently. The major difference is the loop between β-strands 2 and 3. In case of ZF2 the loop (Leu 151, Ile 154) projects into DNA, over the 3 prime end (Figure 2.10 A). The same loop region in ZF1 does not make contact with DNA, however overlies the projecting loop of ZF2, which results in a hydrophobic interface between ZF1 and ZF2. The interface is made between residues Met43,
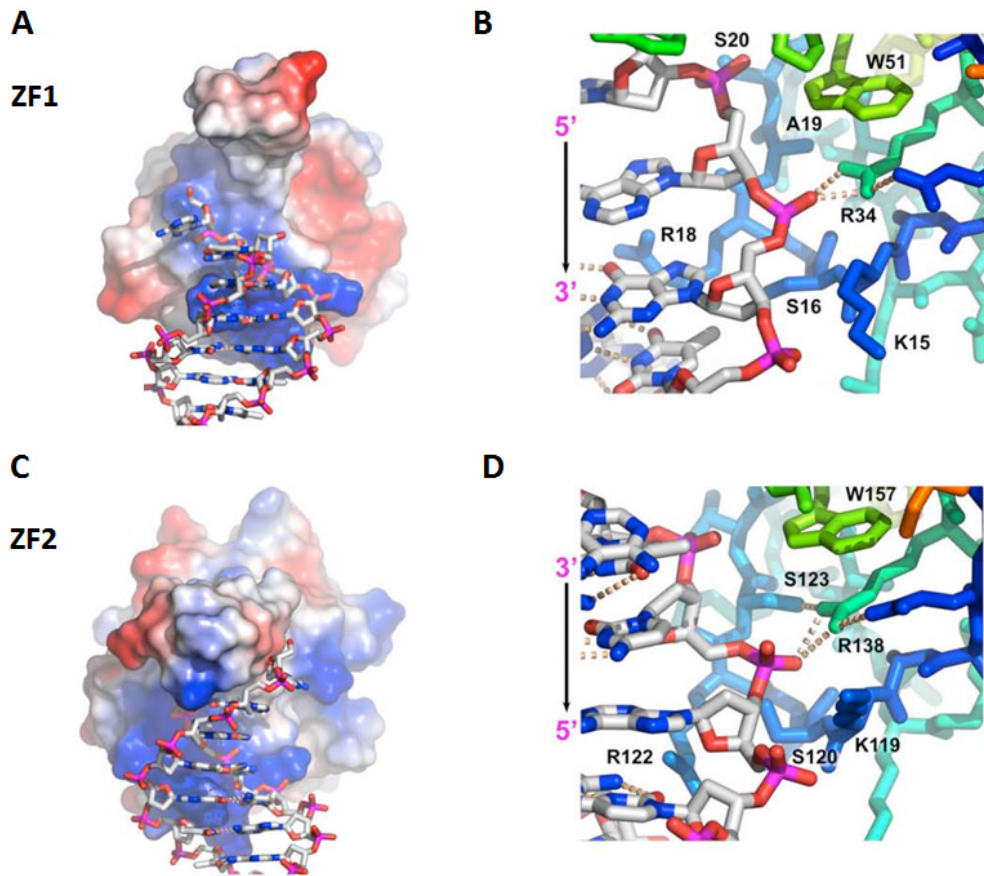
Figure 2.9 PARP1-DBD interactions with DNA (from Ali et al., 2012). The interactions are based on the X-ray structure of DNA Binding Domain (DBD) bound to DNA with a single base 5′ overhang **A)** Zinc finger 1 (ZF1) DNA-interacting surface (colored by electrostatic potential, with positive in blue and negative in red) interacts with the sugar-phosphate backbone of the overhanging strand and the major groove. **B)** Details of ZF1 and DNA interactions, centered on the polar interaction of Arg34 (R34) and a DNA phosphate group. **C)** Zinc finger 2 (ZF2) DNA-interacting surface (colored by electrostatic potential, with positive in blue and negative in red) interacts with the sugar-phosphate backbone of the recessed strand and the minor groove. **D)** Details of ZF2 and DNA interactions, centered on the polar interaction of Arg138 (R138) and a DNA phosphate group.

Phe44, Val48 of ZF1 against Val144, Pro149, Gln150, Gly152 and Met153 (Figure 2.10 B). Interestingly, the complex of DBD with DNA suggested that both zinc fingers must come from two PARP1 molecules, because the linker connecting two zinc fingers on the same molecule is too short to span the distance and interactions observed in the crystal. This result suggests that PARP1 dimerizes via N-terminal on DNA substrate. The dimerization was tested and indeed confirmed experimentally using the linker deletion approach and the UV-laser cutting array

evaluating the recruitment of DBD wild type and mutants to the sights of DNA damage (Ali et al., 2012).
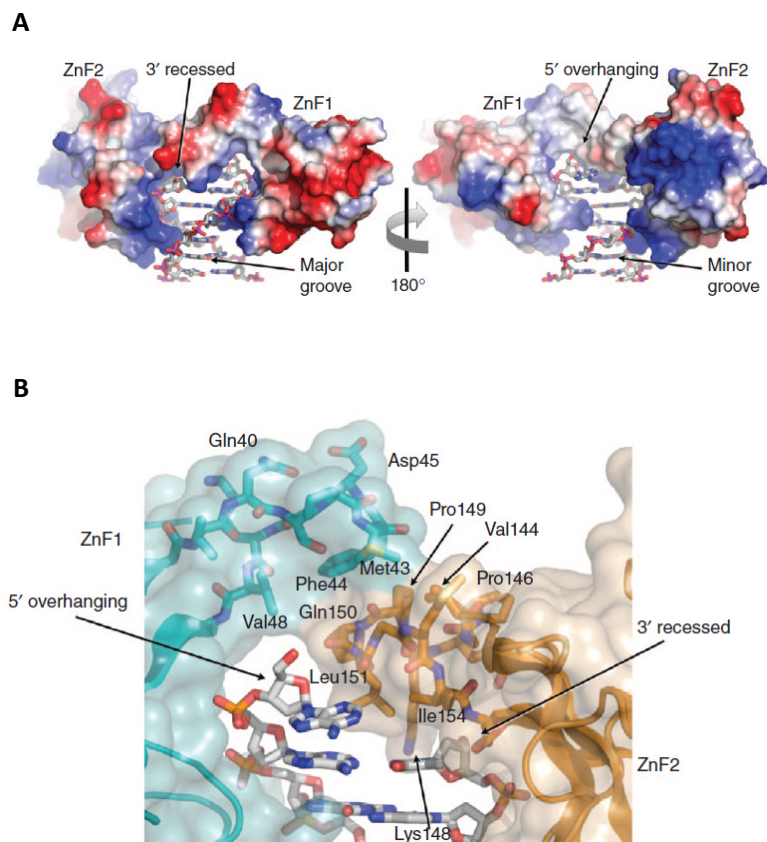
Figure 2.10 DNA-end binding by the ZnF1-ZnF2 complex (from Ali et al., 2012). **A)** Molecular surface of the DNA-end binding structure formed by PARP1 ZnF1 and ZnF2 domains extending across the surface of the DNA end and interacting with both grooves of the duplex. The 3′ recessed end of one strand is on the left, and the 5′ overhanging end of the other strand is on the right. **B)** Detail of the interface between the tips of the β-2–3 connecting loops of ZnF1 and ZnF2, which form the bridge overlying the terminal base pair of the duplex. Transparent molecular surface and carbon atoms are colored by domain, with ZnF1 in cyan and ZnF2 in gold.

There are two opposing models for DNA break binding by PARP1

In addition to the structure of DBD bound to DNA (Figure 2.9), two different structures were reported: (i) two zinc fingers, each bound alone to blunt ended duplex DNA (Figure 2.8 A and B; Langelier et al., 2011), and (ii) nearly full length PARP1 bound to blunt ended DNA (Figure 2.8 H; Langelier et al., 2012). ZF2 in both structures (single ZF and DBD; Langelier et al., 2011, Ali et al., 2012) interacts with DNA in the same manner. Significant differences occur in the case of

ZF1 which binds to DNA with opposite polarities in both structures. In both structures the backbone grip uses the same conserved arginine (Arg34) residue to bind to the phosphate backbone, but the entire domain is flipped such that arginine (Arg18) is directed into the DNA major groove (the Ali structure) rather than the minor groove (the Langelier structure). Moreover β-2–3 loop (the Ali structure) engages in a stacking interaction with the corresponding loop in ZFII (Figure 2.10) which is not at all observed in the Langelier structure.

The third structure, the nearly full length PARP1 structure (missing ZF2 and BRCT domains) sheds light on cooperative interactions between PARP1 domains outside of the DBD. This structure reveals that interface of PARP1 molecule with broken DNA is distributed over ZF1, ZF3 and WGR (Langelier et al., 2012). Mainly ZF1 binds DNA via ribose-phosphate backbone grip and the base stacking loop in sequence-independent manner. The N-terminal region of ZF3 domain binds to the DNA on the same side as ZF1. The WGR domain binds to the 5 prime-terminus of the break, with the DNA backbone held between the central β-sheet of WGR and the α-helix that runs parallel to the β-sheet. WGR contacts with DNA extend the contacts made by the ZF1 base stacking loop which rests on the nucleotide bases at the end of the DNA. The mutagenesis of residues of ZF1, ZF3 and WGR which mediate DNA contact reduce PARP1 activity. Moreover binding to DNA of ZF1, ZF3 and WGR promotes allosteric distortion of the PRD, suggesting the CD activation (Figure 2.8 H). None of the Langelier structures supports dimerization of PARP1 over the DNA. The Langelier structures favor monomerization of PARP1.

ZF2 was eliminated from the almost full length PARP1 study, because ZF2 was assumed to be not essential in studies over PARP1 activity. This conclusion was based on the findings were PARP1 missing ZF1 or ZF2 was evaluated for its automodification capability by SDS-PAGE. The results found ZF1 to be essential for PARP1 automodification, whereas ZF2 was obsolete. A similar outcome was detected in fibroblasts transiently transfected with PARP1 missing ZF1 or ZF2. Upon DNA damage induction with hydrogen peroxide only PARP1 missing ZF1 did not show PAR staining in the nucleus. However when it comes to DNA binding *in vitro*, the importance of zinc fingers changed. ZF2 as individual domain had 100-fold higher affinity to DNA, in comparison to ZF1 alone. A deletion of ZF2 from full length PARP1 reduced DNA affinity 3-fold, whereas deletion of ZF1 almost not at all (Langelier, et al., 2011). Various DNA

structures –duplex DNA containing an overhang or a nick or blunt were evaluated in this activity study of zinc fingers. In summary, these are major differences which needed to be experimentally addressed especially via *in vivo* approaches.

## 2.2.4 The mechanism of DNA target site selection by, and activation of PARP1

PARP1 binds to distorted DNA *in vitro* and *in vivo*

In the aftermath of the report, that broken DNA stimulates the enzymatic activity of PARP1 the molecular and functional characteristics of the interactions between PARP1 and DNA became extensively studied *in vitro* (Benjamin, 1980, Ohgushi, 1980). PARP1 was found to bind various forms of broken and closed circular DNA (Menissier-de Murcia et al., 1989). In addition to the DBD, the automodification domain of PARP1 (without the DBD) was shown to weakly interact with unbroken and 222 base pair long DNA fragment. However this interaction did not lead to the enzymatic activation (Uchida et al., 1987, Buki et al., 1989, Mazen et al., 1989). The catalytic domain alone does not bind to DNA (Thibodeau et al., 1993). In addition to broken DNA, other distorted DNA structures like hairpins, cruciforms, loops and AATT rich sequences positively correlated with PARP1 binding and stimulation (Lonskaya et al., 2005).

Recently, the interaction of PARP1 and DNA were again reevaluated. PARP1 full length and N-terminal fragment (residues 1-486, from ZF1 to BRCT domain) shown preference for free DNA with bent or curved conformations induced by a nick or an AATT insert over a blunt or DNA with overhangs. PARP1 full length exhibited between 1.4 - 3 fold, higher affinity (for tested DNA fragments) when compared to N-terminal fragment. Both of the PARP1 constructs (N-terminal and full length) bound stronger to nucleosomes than to free DNA. Importantly, PARP1 bound to nucleosomes only in presence of DNA arms (linker DNA). PARP1 full length bound significantly stronger to tested DNA fragments (up to 50 fold) in comparison to N-terminal PARP1 fragment. PARP1 binding to DNA/nucleosome did not correlate strongly with PARP1 activity (Clark et al., 2012).

Of course, it is of high interest if these *in vitro* PARP1 associations with DNA/nucleosomes have the same character *in vivo*. Accordingly, PARP1 full length and its product PAR were visualized

via immunofluorescence to be enriched over DNA breaks introduced with a 780 nm long wavelength laser in a cell (Haince et al., 2008; Figure 2.11).
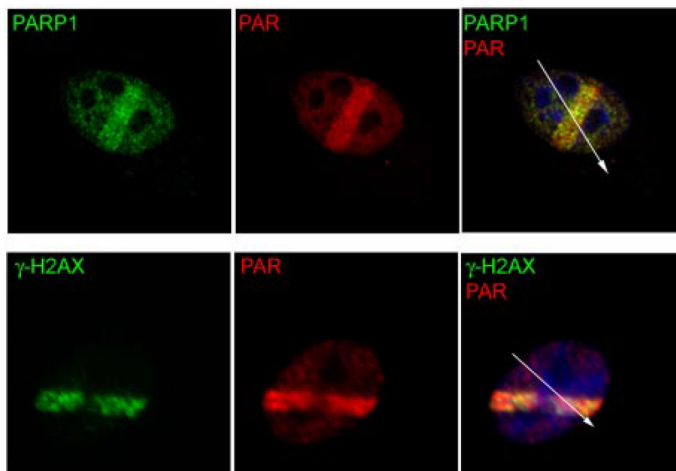
Figure 2.11 Sites of DNA damage marked with phosphorylated H2A.X showed high concentration of poly-ADP-ribose polymerase 1 (PARP1) enzyme and a product of its activity, poly-ADP-ribose (PAR) (from Haince et al., 2007).

From genome wide PARP1 enrichment data analysis (in no DNA damage conditions) it was found that PARP1 resides at 758 promoters (1517 tested genes). These PARP1 associations with chromatin were shown to be specific only to transcription start sites (TSS) with weak ChIP-chip (chromatin immunoprecipitation coupled with DNA microarray) signal proceeding into the gene body, and no detectable enrichment upstream from the TSS. The presence of PARP1 at these sites correlated with depletion of histone 1 (H1; Figure 2.12). The exact mechanism behind specific enrichment of PARP1 over TSS was not tested (Krishnakumar et al., 2008). Unfortunately none of the *in vivo* studies evaluated the importance of zinc fingers directly for association with chromatin.
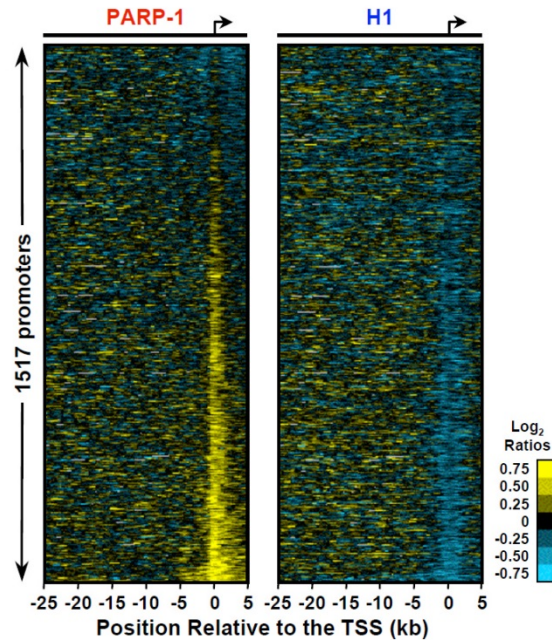
Figure 2.12 Distinct patterns of genomic localization for H1 and PARP-1 (from Krishnakumar et al., 2008). Heat maps of H1 and PARP-1 ChIP-chip data for 1517 promoters tiled from -25 kb to +5 kb (kilobase) relative to the transcription start site (TSS). The promoters are ordered top to bottom based on increasing intensity of the PARP-1 signal in a 10 kb window surrounding the TSS. PARP1 signal is centered over TSS (0 kb), whereas H1 signal is around TSS (upstream and downstream from TSS).

The histone code regulates PARP1 association at the heat shock loci

Already the early *in vitro* studies showed that PARP1 does not bind directly core histones: H2A, H2B, H3 or H4 (Buki et al., 1995). However these histones, when embedded into a nucleosome *in vitro,* are readily associated with PARP1 (Kim et al., 2004). *In vivo,* PARP1 and nucleosome associations were nicely illustrated by studies over mammalian, heat shock inducible human *Hsp70.1* promoter. This promoter contains nucleosomes with incorporated macroH2A1.1 histone variant, which contains a macrodomain tail. The macrodomain recognizes chains of PAR, and was shown to be important for PARP1 associations with this *Hsp70.1* promoter. When macroH2A.1.1 was mutated and thus unable to bind PAR, PARP1 did not show association with the *Hsp70.1* promoter (Figure 2.13). This work showed an importance of PARylation mediated PARP1 association to *Hsp70* promoter.
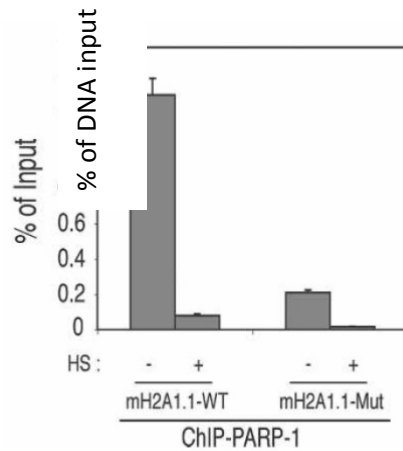
Figure 2.13 PARP1 levels at *Hsp70.1* promoter (from Ouararhni et al., 2006). The amount of PARP-1 associated *in vivo* with the *Hsp70.1* promoter in the stable cell lines expressing mutated mH2A1.1 is much lower compared with PARP1 association with the *Hsp70.1* promoter in the stable cell lines expressing WT-mH2A1.1. WT - wild type, (HS; −) non heat-shocked and (HS; +) heat-shocked (30 minutes at 42°C).

Upon heat shock the PARP1 bound fraction to the *Hsp70* promoter increased at 5 minutes post stimuli. With time: 10, 20 and 30 minutes both PARP1 and macroH2A1.1 showed gradual displacement from the promoter (Ouararhni et al., 2006). Investigation of *in vivo* associations of PARP1 with chromatin revealed that among proteins co-immunoprecipitated with PARP1 are: histones H4, H3, H2A, and H2B (Pinnola et al., 2007). Histone 1 (H1) was shown to be an antagonist of PARP1 binding *in vitro and in vivo* (Kim et al., 2004, Krinskakumar et al., 2008). When PARP1 was immobilized on the beads and incubated *in vitro* with reconstituted histone octamers, H3 and H4 were found to interact with PARP1 the strongest. In addition, the N-terminal tail of H4 was found to be a more potent PARP1 activator that broken DNA. However, PARP1 missed its DBD in this experiment, suggesting overactive PARP1 in the reaction (Pinnola et al., 2007). Thus, the interaction with histones of PARP1 was probably PAR mediated. When H4 was assembled together with other histones into an octamer the H4 role in PARP1 activation was lost, due to potential inhibitory effect of H2A (Pinnola et al., 2007). Importantly, mass spectrometry identified that many lysines and glycines of all of the histones are actually *in vivo* PARylated by PARP1 (Zhang et al., 2013b).

After the discovery of *Drosophila melanogaster* PARP (dPARP) activity requirement for the heat-shock-induced puffing and transcription of *hsp70* in Drosophila larvae (Tulin and Spradling

2003), subsequent studies investigating PARP1 chromatin association and the histone code at *Drosophila melanogaster* heat shock loci followed. The H2A.V (H2A.X/H2A.Z variant in mammals) acts as the negative regulator of PARP1 association to chromatin. Upon depletion of H2A.V from *hsp70* promoter, PARP1 residency over the loci increases (Figure 2.14). Whereas in *wild type* flies, H2A.V is phosphorylated by Jil1 kinase, which leads to activation of PARP1, then removal of H2A.V resulting in correct *hsp70* transcription (Kotova et al., 2011, Thomas et al., 2014). Fly PARP was found as necessary for both transcription-independent and -dependent nucleosome loss during HS (Pet   ad Lis, 2008).
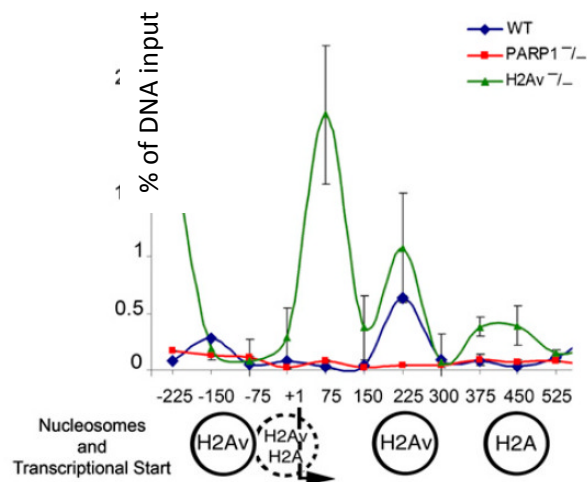
Figure 2.14 PARP1 occupancy at the *hsp70* promoter (from Kotova et al., 2011). Chromatin immunoprecipitation (ChIP) profiles of PARP1 at *hsp70* loci in flies with wild type (WT) levels of H2A.V (blue), depleted H2A.V (green) and depleted PARP1 (red).

Inactive dPARP resides at *hsp70* loci prior to heat shock at TSS exclusively. Upon HS, dPARP moves into the gene body and PAR levels become detectable. The association of dPARP with *hsp70* loci seems to be controlled by at least two mechanisms. Prior HS dPARP association is PAR independent thus, probably zinc finger mediated. During HS dPARP association is PAR dependent. As shown by loss of dPARP from *hsp70* loci upon chemical inhibition of dPARP or PAR degradation via treatment with enzyme degrading PAR – PARG (Petesch and Lis, 2012). The association of dPARP at hsp70 loci was found to be modulated by Tip60 mediated

acetylation of H2A and H4. The acetylation led to dPARP activation. The knock down of dPARP did not affect levels of acetylation upon HS (Petesch and Lis, 2012).

An evaluation of dynamicity of dPARP interactions with chromatin *in vivo* found that dPARP exchanges between chromatin domains faster than a canonical histone H2A. This study was conducted in the fly salivary glands via fluorescence recovery after photobleaching (FRAP). The fluorescence intensity recovery rate depended on the chromatin domain: euchromatin and heterochromatin. On average, the half time recovery (representing 50 % recovery of the bleached spot) was 100 seconds (Figure 2.15).

It is known that PARP1`s DNA binding to the target sites will be affected by histone modification and the chromatin structure. However more studies deciphering these determinants are needed.
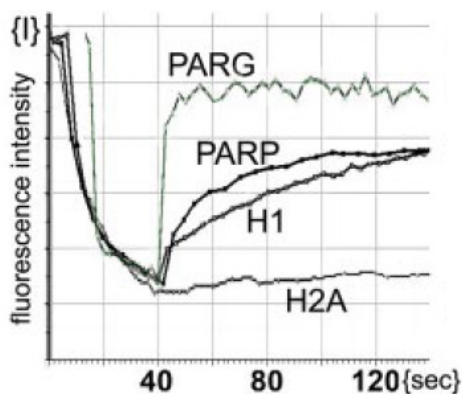
Figure 2.15 Comparative FRAP analysis of dPARP protein dynamics *in vivo* (from Pinnola et al., 2007). Comparative analysis of the recovery after photobleaching for recombinant protein is shown, including **PARP-EGFP** – poly-ADP-ribose polymerase labelled with enhanced Green Fluorescent Protein. **PARG-EGFP** – poly-ADP-Ribose glycohydrolase labelled with enhanced Green Fluorescent Protein, **H1-EYFP** – histone 1 labelled with enhanced Yellow Fluorescent Protein, **H2A-ECFP** – histone H2A labelled with enhanced Cyan Fluorescent Protein.

2.2.5 Posttranslational modifications modulate PARP1 activity

The cellular signaling, during DNA repair or transcription, encloses dynamic and regulatory interplay between various posttranslational modifications. It is known that in addition to automodification with PAR moieties, PARP1 becomes post-translationaly modified and regulated by various PTMs.

Phosphorylation activates PARP1

Phosphorylation was the first PTM of PARP1 identified. Initially the phosphorylation was considered as a negative modification to PARP1's activity, based on *in vitro* PARP1 modifications by protein kinase C (PKC; Tanaka et al., 1987, Bauer et al., 1992). However, the subsequent studies found links to PARP1 phosphorylation as stimulatory. For example, extracellular-signal-regulated kinases 1 and 2 (ERK1/2) were shown to stimulate PARP1 activity up to 75 % *in vitro*. However, only ERK2 regulated PAR levels *in vivo* (Kauppinen et al., 2006). Both, AMP-activated protein kinase (AMP-K) and c-Jun-N-terminal kinase 1 (JNK1), upon hydrogen peroxide- induced cell death, activated PARP1 (Walker et al., 2006, Zhang et al., 2007). Recently, a comprehensive study predicted over 20 phosphorylation sites across the whole PARP1 molecule with NetPhosK and Phoscan algorithms. Next the predications were compared with results from subsequent mass spectrometry analysis of the recombinant PARP1 that has been incubated with PKC, ERK1/2, Ca2$^+$/calmodulin-dependent protein kinase II (CaMK-II), JNK1 and cyclin dependent kinase 5 (CDK5). This analysis identified most the known phosphorylation sites today (Gagne et al., 2009). The mutagenesis of some of the phosphorylated residues proved their physiological importance. For example, mutagenesis of serines (S) residing in zinc finger 1 (ZF1) abolished the recruitment of PARP1 molecule to DNA damage sites induced with a laser (Figure 2.16; Gagne et al., 2009). The evaluated serines reside in vicinity of residues involved in DNA break recognition and interface contact between ZF1 and ZF2, thus phosphorylation presence or absence may alter zinc finger ability to engage with DNA.

Acetylation activates PARP1

Acetylation of PARP1 is studied as comprehensively as phosphorylation. PARP1 was found to be acetylated at lysines: Lys-498, Lys-505, Lys-508, Lys-521 and Lys-524 upon activation of nuclear factor kappa-light-chain-enhancer of activated B cells (NF-kB) dependent transcription *in vivo*. The transcription was induced with bacterial lipopolysaccharides (LPS) or tumor necrosis factor alpha (TNFα). The PARP1 acetylation was found to be p300/CBP dependent and was detectable only in presence of deacetylase inhibitors. The acetylation strengthened the interactions between PARP1 and transcription factor p50 *in vivo* (Hassa et al., 2003 and 2005). The co-incubation of PARP1 with p300/CBP-associated factor (PCAF) acetyltransferase resulted

in enhanced PARP1 activity *in vitro*. *In vivo,* acetylation of PARP1 decreased and increased upon PCAF *knock down* and overexpression respectively. Sirtuin 1 (SIRT1) and histone deacetylase 1 (HDAC1) were found to deacetylate PARP1 *in vivo* and to decrease PARP1 activity upon deacetylation *in vitro*. Moreover, cardiomyocytes under mechanical stress where shown to contain more PAR in mice lacking SIRT (SIRT$^{-/-}$) when compared to WT mice (Rajamohan et al., 2009).
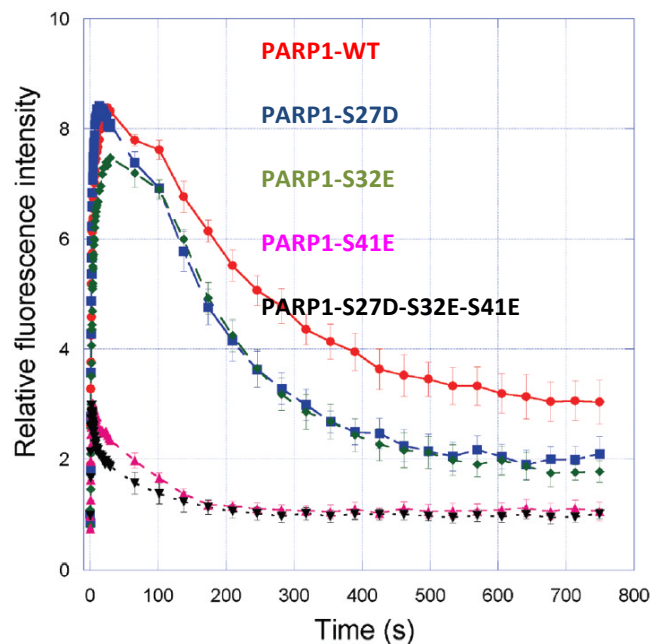
Figure 2.16 Evaluation of PARP1 phosphorylation importance on recruitment to DNA breaks (from Gagne et al., 2009). S41 Erk-1 phosphorylation site located in the first zinc finger motif of PARP-1 reveals altered recruitment kinetics at sites of DNA damage following laser microirradiation. The spatial dynamics of GFP-tagged single and triple glutamate- and aspartate-substituted derivatives that mimic a permanently phosphorylated protein (S27D-S32E-S41E) were investigated by microirradiation-induced DNA damage using a 750-nm laser. The relative fluorescence intensity at the microirradiated region of HeLa cells was normalized and plotted as a function of time after integrating data from at least five low-expressing cells. The error bars represent the standard error.

SUMOylation and ubiquitination deactivate PARP1

Similarly to many other proteins, PARP1 becomes SUMOylated as well (Vertegaal et al., 2004, Rosas-Acosta et al., 2005, Blomster et al., 2009). PARP1 was found to be modified

predominantly by small ubiquitin-related modifier 3 (SUMO3). The SUMO modification can be reversed by SUMO1/sentrin specific peptidase 1 and 3 (SENP1 and SENP3), which knock down contributes to elevated levels of sumoylated PARP1 in HEK293T cells. The specific acceptor residue of PARP1 molecules was predicted by the SUMOsp analysis program to be lysine 486. This residue indeed when mutated abrogates SUMO signal from PARP1 *in vitro* and *in vivo*. PARP1 with or without the SUMO modification (introduced by SUMO3) shows the same mono- and poly-ADP-ribosylation activity *in vitro*. PAR levels were found to be comparable in cell with damaged DNA, regardless of endogenous or overexpressed levels of SUMO3. SUMOylation was however found to prevent p300 mediated acetylation of PARP1. Correspondingly, a sumoylation-deficient PARP1 mutant has a higher acetylation status than wild-type PARP1 (Messner et al., 2009). Additional PARP1 SUMOylation sites were identified to be K203 and K512 (Martin et al., 2009, Zilio et al., 2013).

SUMO2 mediated SUMOylation of PARP1 can lead to enhanced ubiquitination by Ub E3 Ring Finger Protein 4 (RNF4) ligase and subsequent degradation of PARP1. Such regulation was found to take place during transcription burst at the heat shock loci (Martin et al., 2009). Lack of SUMOylation reduces mRNA levels from the heat shock loci. Similarly, Ub E3 RNF198 ligase checkpoint with forkhead and ring finger domains (CHFR) was found to be rapidly recruited to the sites of DNA damage site, thanks to the PAR-binding zinc finger (PBZ) motif. This ligase recognizes specifically auto-PAR-modified PARP1 molecules and ubiquitinates them at least at K68 and K63 residues. The ubiquitination of PARP1 leads to proteasome mediated PARP1 degradation. Lack of CHFR leads to delay of DNA damage site repair (Liu et al., 2013). Interestingly, poly-ubiquitination of PARP1 *in vitro* did not inhibit its ADP-ribose activity (Wang et al., 2008).

Mono-ADP-ribosylation activates PARP1

DNA breaks are perceived as major inducers of PARP1 activity. Interestingly PARP1 was shown to be activated thanks to mono-ADP-ribosylation, introduced by poly-ADP-ribose polymerase 3 (PARP3) *in vitro* in absence of DNA (Loseva et al., 2010). In addition, *in vivo* mono-ADP-ribosylation by sirtuin 6 (SIRT6) appears to enhance PARP1 activity as well (Mao et al., 2011). Currently it is assumed that mono-ADP-ribosylation could serve as a base for further extension

of PAR chain and/or triggers certain conformational change within PARP1 molecules fostering PARP1 activation.

Methylation activates PARP1

Methylation is the most recent PTM of PARP1 identified. The modification is introduced *in vitro* and *in vivo* by SET and MYND domain containing histone methyltransferase (SMYD2) on lysine 528 of PARP1 and leads to increased PARP1 activity. HeLa cells with induced oxidative DNA damage due to hydrogen peroxide treatment show reduced or elevated levels of PAR depending on SMYD2 reduction via knock down or overexpression, respectively (Piao et al., 2014).

2.2.6 Open questions

The variety of cellular functions regulated by PARP1 is on the rise. The interdependence of these processes can be especially difficult to interpret in human patho-physiology, where PAR metabolism plays a significant role. Despite the recent progress regarding the molecular mechanism of PARP1 activation via identification of the X-ray PARP1 structures bound to DNA more studies are needed (see also 2.2.3). To truly decipher PARP1's physiological functions it is important to gain a full spatiotemporal understanding of PARP1's *in vivo* interactions with DNA as a major PARP1 inducer (see also 2.2.2). The predominant view is that PARP1, in its dormant state, is constantly associated with chromatin. At the same time, upon variety of stimuli, a conformational change within PARP1 molecule triggers its activation. But, if PARP1 was associated across the genome, how does it specifically recognize its target sites and specifically become activated at these sites? This question is especially valid in the context of non-stress conditions (no DNA damage, no heat shock and no hormone treatment). In transcription PARP1 can function as co-activator or co-repressor. How, are these two contrasting outcomes (co–activation or co-repression) spatially and temporally resolved? Further, what are the regulatory steps in PAR mediated chromatin reorganization? Both, condensation and de-condensation are possible (Wacker et al., 2007, Tallis et al., 2014). Clues to answer these questions exist, but limitations and shortage of information as well. Pivotal to answer these questions is an exact mechanism of DNA target selection and PARP1 activation in detail. It is clear that upon presence of DNA breaks, PARP1 binds to the breaks via the DBD. What is less clear is the role each zinc

finger plays in DNA break recognition and transmission of DNA bound state to the catalytic domain. The current structural models are incompatible (see also 2.2.3). It is not clear how PARP1 becomes enriched at gene promoters. The studies over heat shock gene containing macroH2A1.1 suggest a PAR-dependent immobilization of PARP1 (see also 2.2.4). Its appears that *in vivo* analysis of PARP1's chromatin association via fluorescence microscopy, genome wide studies can advance and answer some of these confusions. Finally, after PARP1 becomes associated with chromatin, what immediate role will it play in chromatin structure organization? A depletion of ISWI chromatin remodeler, but recruitment at the same time of ALC1 chromatin remodeler seems to trigger a specific cellular program upon localized PAR signaling. Moreover, a relatively new is an aspect of PAR importance in triggering phosphorylation and ubiquitination cascades at sites of PARP1 activity. The crosstalk between these three regulatory PTMs is of high importance in disease diagnosis and treatment.
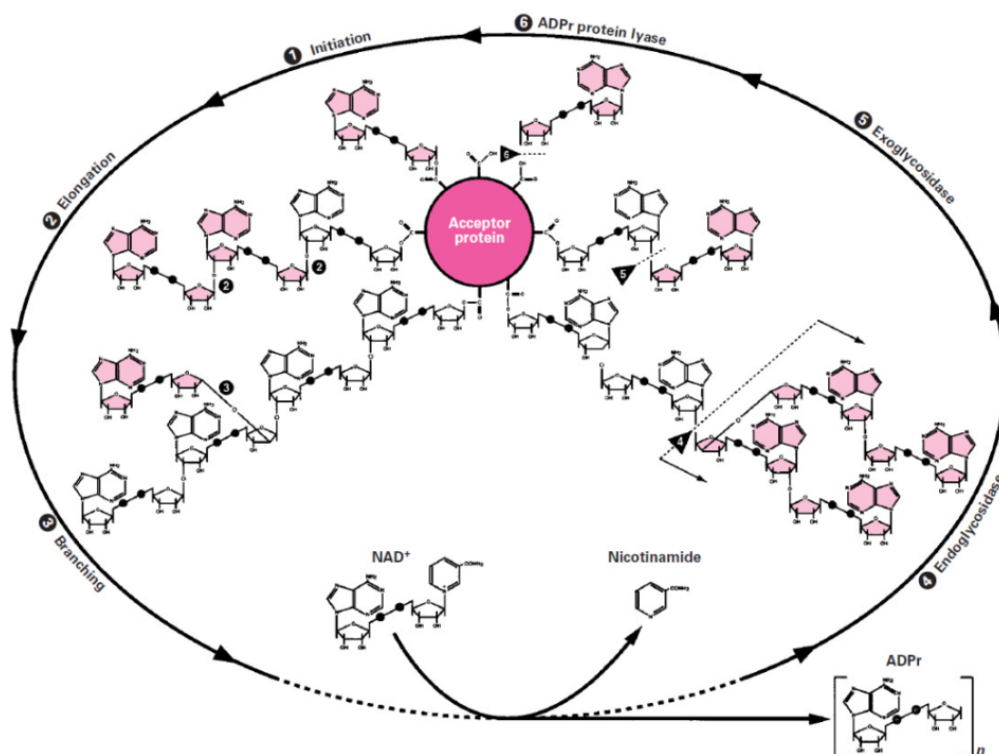
2.3 Life of poly-ADP-ribose (PAR)

2.3.1 Insights into PAR synthesis

Despite the high abundance of the enzymes capable of PAR synthesis (see also 2.1.1), the usual cellular levels of PAR are very low, unless a cell counteracts the DNA damage with mechanisms involving PARP1 activity. In result PAR levels increase transiently. Majority of PAR within the cell is synthesised by PARP1. In detail, activated PARP1 catalyzes transfer of the ADP-ribose moiety from NAD^+ substrate (with release of nicotinamide) to specific amino acid residues on itself or acceptor proteins. At first is introduced a single unit of mono-ADP-ribose, which is further elongated (up to 200 units) and branched (every 20-50 units). ADP-ribose units are linked by glycosidic ribose-ribose 1 -> 2 bonds (O-glycosidic ribose–ribose). Poly-ADP-ribose is negatively charged due to presence of two negatively charged phosphate groups per ADP-ribose (Tanaka et al., 1977, Alvarez-Gonzalez and Jacobson, 1987, D'Amours et al., 1999, Hottiger et al., 2010, Barkauskaite et al., 2013; Figure 2.17).

The heterogeneity of PAR polymers in size and structure allows for flexible contacts with the target proteins and assembly of multi protein complexes, underlying the diversity of PAR functionality as a PTM. Residues that become ADP-ribosylated were found to be aspartic acid, glutamic acid, lysine, arginine, cysteine and asparagine (Hassa et al., 2006). PARP1 auto-

modifies itself with PAR, as well. The mass spectrometry study which favored identification of ADP-ribosylation on aspartic acid (Asp) and glutamic acid (Glu) residues, pinpointed 37 sites which become ADP ribosylated upon activation of PARP1 (Figure 2.18; Zhang et al., 2013b)

Figure 2.17 The cycle represent the anabolic and catabolic reactions in the metabolism of poly-ADP-ribose (from D'Amours et al., 1999). The PAR cycle proceeds counterclockwise. The pink circle in the middle of the scheme represents a hypothetical protein acceptor modified on a glutamic acid residue (c-COOH group shown).

In addition to PARP1 auto-modification sites, the mass spectrometry study identified PAR Asp and Glu modifications representing in total 340 proteins. Gene Ontolgy analysis of PARylated peptides revealed that the modified proteins are important for chromosmome organization, DNA repair, transcription and RNA splicing (Zhang et al., 2013b). Majority of these modifications were absent in the samples pretreated with two recent PARP inhibitors (olaparib and AG14361; Zhang et al., 2013b).
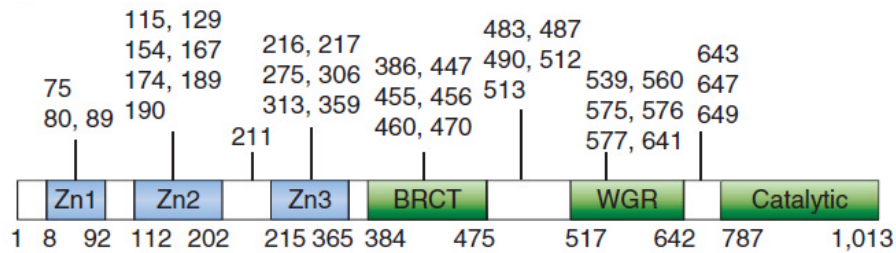
Figure 2.18 The aspartic acid (Asp) and glutamic acid (Glu) sites on PARP1 molecule which become ADP-ribosylated (from Zhang et al., 2013c).

PARP1 is a protein that predominantly acts on the chromatin fiber via PAR modification of itself and acceptor proteins regulating positively or negatively processes occurring on chromatin. This regulation can encompass at least one of the following mechanisms: (i) recruitment or depletion of certain proteins, (ii) regulation of complex formation and activity via regulation of protein – protein interactions, or (iii) regulation of protein activity including target recognition (Althaus et al., 1999). Importantly poly and mono–ADP-ribose are reversible modifications with half time in order of minutes (see also, 2.3.3; Alvarez-Gonzalez and Althaus, 1989).

2.3.2 Specific recognition of PAR

Poly-ADP-ribose binding motif (PBM)

Majority of PARylated proteins share the poly-ADP-ribose binding motif (PBM) shown on Figure 2.19 (Pleschke et al., 2000, Gagne et al., 2008). The PBM is composed of hydrophobic and basic residues downstream from positively charged residues. This motif is not only present in DNA repair associated proteins, but also proteins involved in chromatin structure reorganization, transcription, replication, apoptosis or cell cycle checkpoint. The PBM often overlaps with important regulatory protein domains, thus addition of PAR to the PBM can modulate folding of the domain, protein-protein or protein-ligand interactions.
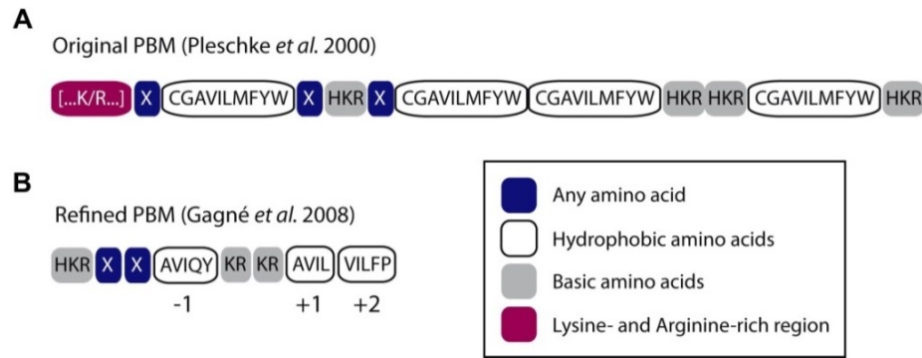
Figure 2.19 Scheme of Poly-ADP-ribose Motif, PBM (from Krietsch et al., 2013). **A**) The motif is primarily composed of a hydrophobic and basic amino acid core flanked by a cluster of positively charged residues [. . .K/R. . .]. Each box represents one amino acid position. **B**) The refined poly-ADP-ribose (PAR) binding signature confirmed the overall basic nature of the PBM but represents a minimal stand-alone version of the motif, the K/R-rich N-terminal cluster being dispensable for efficient binding. Outside the dual [KR][KR] site, there are additional preferences for hydrophobic amino acids (positions 1, +1 and +2), mostly those with alkyl side chains. The basic [KR][KR] doublet is an important requirement for the PBM since most substitutions in this region result in a substantially reduced binding affinity for PAR.

Macrodomains recognize ADP-ribose

Already the early reports found poly-ADP-ribose glycohydrolase (PARG) as a major enzyme regulating the turnover of PAR (Miwa and Sugimura, 1971). However an exact domain responsible for PAR recognition and hydrolysis remained unknown until 2005. The macrodomain was identified in the core histone variant macroH2A, as an unusually long C-terminal tail (Pehrson et al., 1992). Subsequently the ability of the macrodomain to selectively recognize ADP-ribose was determined via isothermal titration calorimetry (ITC) studies of the macrodomain with ADP-ribose and related nucleotides. Moreover a crystal structure of Afl1521 macrodomain (Archaeoglobus fulgidus) bound to ADP and ADP-ribose was determined (Figure 2.20; Karras et al., 2005). Similarly to the PARP catalytic domain, the macrodomains are evolutionary conserved and thus found, not only in vertebrates but also, in genomes of plants (Arabidopsis thaliana), viruses (Rubella and Hepatitis E), bacteria (Salmonella typhimurium, Listeria; Till and Ladurner, 2009). In humans, so far, 12 macrodomain containg proteins were identified.
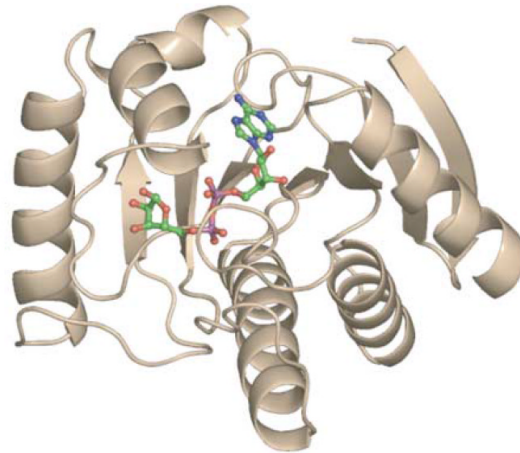
Figure 2.20 Structure of the complex formed between Af1521 and ADP-ribose (from Karras et al., 2005). The ADP-ribose molecule is bound by the Af1521 (Archaeoglobus fulgidus) macrodomain in an L-shaped cleft. The ADP-ribose ligand is shown as a ball-and-stick model.

The macrodomains are not identical. Their structural differences predetermine macrodomain containing protein to act solely as a reader of mono-ADP-ribose or poly-ADP-ribose, or to act as a reader and eraser of the modification as well. A globular macrodomain comprises of six-stranded mixed β-sheet and five α-helices, which form a cleft for the ligand. The binding occurs via stacking interaction with the adenine ring, strengthened via the interactions with the pyrophosphate of ADP-ribose, and with specificity provided by hydrogen bonding with the distal ribose (Karras et al., 2005, Till and Ladurner, 2009, Han et al., 2011). Sequence differences among macrodomains determine specificity for various NAD^+ metabolites: O-acetyl-ADP-ribose, ADP-ribose, poly-ADP-ribose. For example the macrodomain containing ALC1 binds exclusively PAR.

Poly-(ADP-ribose)-binding zinc finger (PBZ)

Classically zinc fingers are viewed as DNA and RNA binding domains. It turned out that C2H2 zinc fingers can mediate protein-protein interactions via PAR binding, thanks to 6-8 amino acid spacer with the following consensus [K/R]xxCx[F/Y]GxxCxbbxxxxHxxx[F/Y]xH (b = basic residue, x = any residue; Ahel et a., 2008). Poly-ADP-ribose binding zinc finger (PBZ) is conserved across eukaryotes with an exception of yeast. For example, one and two PBZ domains

are present in checkpoint with forkhead and ring finger domains (E3 ubiquitin protein ligase) (CHFR) and aprataxin and PNKP like factor (APLF) proteins, respectively.

Alternatives to the PBM

An additional PAR binding fold is the GAR domain, named after a high content of glycine and arginine residues. The GAR domain motif lacks hydrophobic residues like the PBM motif, and is found mostly in proteins involved in RNA metabolism or proteins which are associated with chromatin. One of the proteins that are regulated by PAR and contain GAR is meiotic recombination 11 homolog A (MRE11) part of the MRN complex protein which mediates DNA break end resection, facilitating DNA repair (Haince et al., 2008, Ying et al., 2012). Additional motifs to GAR are the following: the RNA recognition motif (RRM; Clery et al., 2008) and Serine/Arginine repeats (SR; Long and Caceres, 2009). RRMs are found in proteins that bind to RNA and ssDNA. These motifs can be found in combination on one protein. For example, alternative splicing factor 1 (ASF) contains on N-terminal RPM and on C-terminal SR domain (Malanga et al., 2008) or heterogeneous nuclear ribonucleoproteins (hnRNPs) contain RPM and GAR (Han et al., 2010). Proteins that bear these motifs are involved in control of mRNA stability and splicing, DNA replication, chromatin remodeling, telomere maintenance, DNA repair and genome stability (Gagne et al., 2003).

WWE domain

The recently discovered WWE domain is shared across 12 proteins in humans. The motifs name is attributed to highly conserved amino acids: W (tryptophan) and E (glutamate), flanked by non-conserved residues (Wang et al., 2012). Interestingly proteins containing WWE domain, bear either E3 ligase domain or PAR catalytic domain.

PAR binding regulatory motif and oligonucleotide/oligosaccharide binding fold

The identification of motifs that specifically recognize PAR seems to be continuous. The recent additions encompass PAR-binding regulatory (PbR) motif, which is critical to the recruitment and full activation of checkpoint kinase 1 (CHK1; Min et al., 2013). The oligonucleotide/oligosaccharide-binding (OB) fold is classically known for ssDNA or RNA binding. Unexpectedly the OB fold of human ssDNA-binding protein 1 (hSSB1) was found to

bind PAR and to be recruited to the sites of DNA damage thank to the OB-fold (Zhang et al., 2014).

2.3.3 Macrodomains remove PAR

The extent of ADP-ribosylation of proteins within a cell depends greatly on the enzymes producing this modification, but also on the activity of enzymes responsible for removal of ADP-ribose. Similarly to its rapid synthesis, PAR chains are as well rapidly removed, in order of minutes (Wielckens et al., 1983 and 1984, Alvarez-Gonzalez et al., 1989). The first PAR degrading enzyme, poly-ADP-ribose glycohydrolase (PARG) was found early on (Miwa and Sugimura, 1971), however the mechanistic insights into PAR binding and hydrolysis came only recently (Slade et al., 2011, Dunstan et al., 2012). To a surprise at first, the X-ray structure of bacterial PARG (derived from Thermomonospora curvata), revealed that the catalytic center is essentially a macrodomain with a loop region that contains the PARG signature sequence (GGG-X6 − 8-QEE).

The PARG signature motif is shared among PARG proteins from protozoa to humans. The bacterial PARG is exo-glycohydrolase, which means that the protein binds the terminal ADP-ribose unit of PAR. The canonical PARG structures suggested that it is possible that PARG can bind not only terminal ADP of PAR, but also intra ADP units of the chain, which accounts for additional endo-glycohydrolitic activity of PARG activity (Kim et al., 2012, Tucker et al., 2012). PARG cleaves the O-glycosidic ribose–ribose bonds between ADP-ribose units, which are originally introduced by PARP1 and any other PARP polymerase. Upon cleavage free ADP ribose is released (Ueda et al., 1972, Slade et al., 2011). Recent reports also suggest that a second hydrolase, ARH3, exhibits the analogous activity to PARG predominantly removing PAR in mitochondria (Niere et al. 2012). More studies are however needed, because ARH3 was mostly reported to cleave OAADPR, a product of NAD^+ - dependent protein deacetylases of the sirtuin family (Ono et al., 2006, Mueller-Dieckmann et al. 2006). Importantly ARH3 does not contain the macrodomain fold.

PARG is unable to cleave the ester bond between the terminal ADP-ribose unit and the ADP-ribosylated glutamate (Slade et al, 2011), thus not capable of the complete removal of PAR from the acceptor protein. This function is carried on by three enzymes: terminal ADP-ribose protein

glycohydrolase (TARG1/C6orf130; Sharifi et al. 2013), MacroD1 and MacroD2 (Jankevicius et al. 2013, Rosenthal et al., 2013, Barkauskaite et al., 2013). All three enzymes reverse mono-ADP-ribosylation. In addition, C6orf130 can release PAR chains from the PAR modified molecule, acting specifically at the glutamate-ADP-ribose ester bonds. PARP1 can be directed for proteasome degradation thanks to ubiquitination, thus further generation of PAR is prevented (for details see 2.2.5, SUMOylation and ubiquitination deactivate PARP1).

2.4 ALC1 in PAR biology

The analysis of the genetic basis of hepatocellular carcinoma (HCC) as a major cause of primary liver cancers revealed an amplification of region 21 on the long arm of chromosome 1 (ch1q21) in over 50 % of patients (Marchio et al., 1997, Wong et al., 1999, Qin et al., 1999, Guan et al., 2000). Further investigation of this region (ch1q21) led to an identification of *ALC1* loci (amplified in liver cancer 1) as a potential oncogene, which when overexpressed in nude mice indeed led to increased tumorigenicity and metastasis (Ma et al., 2008). Sequence analysis of ALC1 showed that the protein contains N-terminaly placed SNF2 domain (ATPase domain) and interestingly a macrodomain fold placed on C-terminus (see also 2.3.2). Due to 45 % sequence identity between SNF2 domains between ALC1 and CHD1 (chromodomain-helicase DNA binding protein 1) chromatin remodeler, ALC1 was named as well chromodomain-helicase DNA binding protein 1-like (CHD1L).

2.4.1 ALC1 is PAR dependent

The C-terminal macrodomain of ALC1 binds PAR *in vitro.* Importantly PAR binding by the macrodomain is indispensable for ATPase activity of ALC1, but not sufficient. In addition, it appears that ALC1 needs to be modified by PAR in order to stimulate ATPase domain activity. Thus, ALC1 with two functional domains, in presence of PARP1, NAD^+ and DNA is able to hydrolyse ATP and remodel a mono nucleosome *in vitro* (Figure 2.21 A and B; Gottschalk et al., 2009). Upon ALC1 mediated sliding of a mono-nucleosome, the accessibility of HhaI cutting site increases, otherwise protected by the nucleosome. At the same time, normally unprotected XhoI site becomes protected by a nucleosome. In presence of PARP1 inhibitor, ALC1 loses its nucleosome remodeling functions (Figure 2.21 C; Gottschalk et al., 2009).
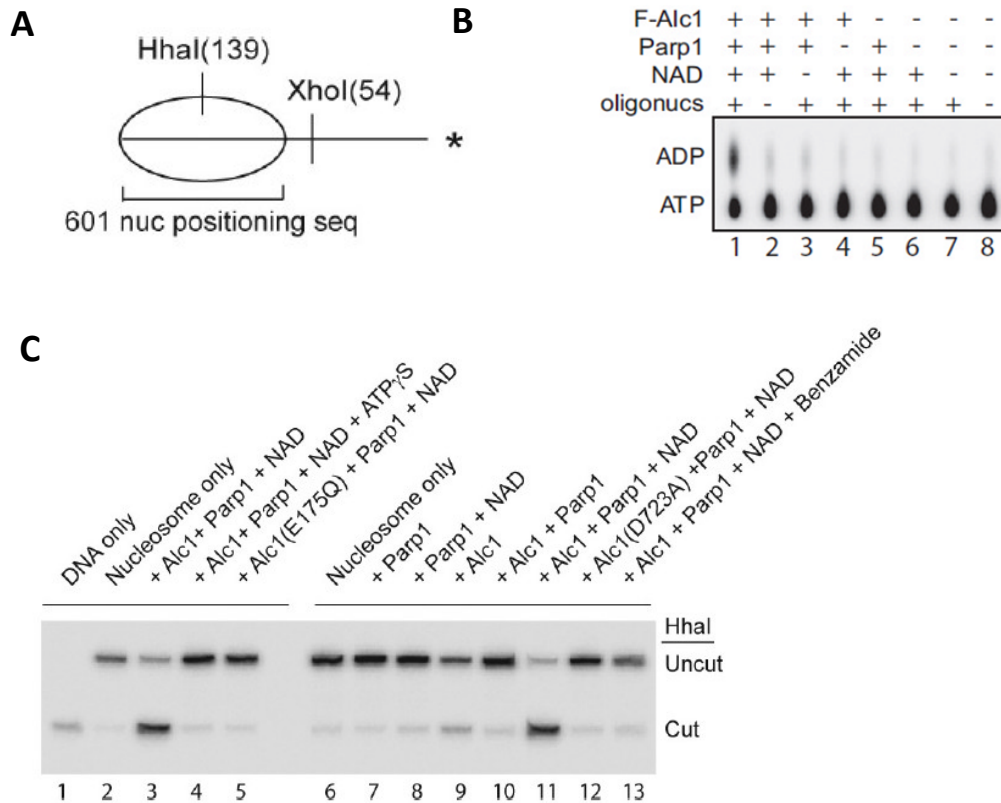
Figure 2.21 ALC1 has PARP1 and NAD$^+$ dependent nucleosome remodeling and binding activities (from Gottschalk et al., 2009). **A**) Scheme of a positioned nucleosome (nuc) and length of HhaI and XhoI cleavage products. **B**) ATPase assays were performed with the indicated combinations of recombinant F-Alc1, Parp1, NAD$^+$, and oligonucleosomes. **C**) DNA or reconstituted nucleosomes were monitored for restriction enzyme accessibility after incubation with ATP (lanes 3, 5, 7–13) or ATPS (lane 4) and wild-type or mutant Alc1, Parp1, NAD, or 2 mM benzamide.

Similarly like *in vitro*, the functional macrodomain is essential for ALC1's interactions with PARP1 *in vivo*. ALC1 deficient in PAR binding (D723A) is not enriched over the laser induced DNA damage sites, known to undergo increase of PARP1 and PAR levels (see also 2.2.4). The recruitment of ALC1 to the damage sites is exclusively dependent on active PARP1. Upon siRNA mediated depletion of PARP1 the recruitment of ALC1 is lost (Figure 2.22; Gottschalk et al., 2009).
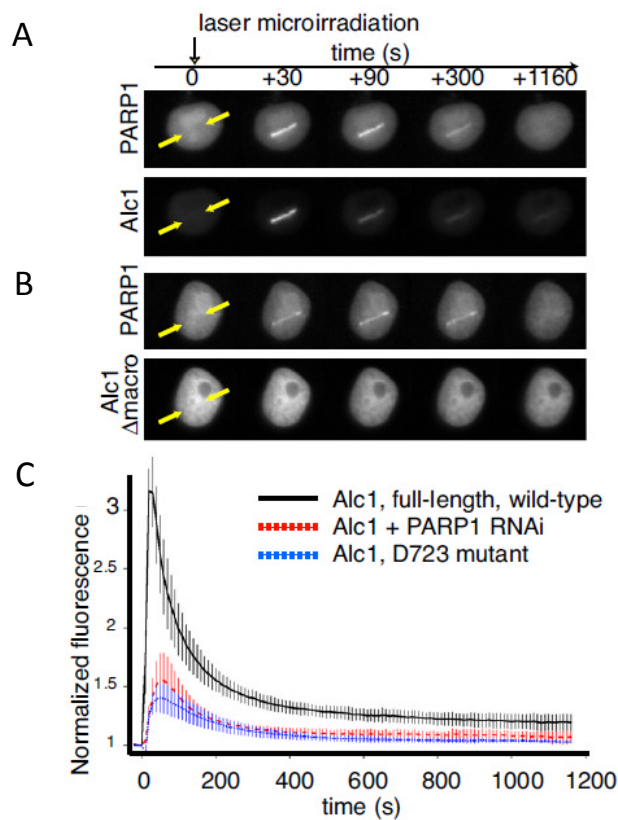
Figure 2.22 ALC1's recruitment after microirradiation depends on its macrodomain and on PARP1 activity (from Gottschalk et al., 2009). **A)** Recruitment of EYFP-ALC1 and PARP1-mCherry to the site of microirradiation (between arrows). **B)** Loss of ALC1's macrodomain abrogates PARylation-induced recruitment of ALC1 to chromatin. **C)** Kinetics of recruitment (n = 6) to microirradiated sites of wild-type (black) and D723A macrodomain mutant (blue) ALC1, or recruitment of wild-type ALC1 after PARP1 knockdown (red).

A more detailed investigation of ALC1's dependence on active PARP1, revealed that both proteins cooperatively bind to DNA or nucleosomes *in vitro*. In result, formed PARP1-ALC1-DNA/nucleosome complex is stable and prevents release of PARP1 from the complex, despite addition of DNA substrate normally readily bound by PARP1 (Figure 2.23). The PARP1-ALC1-nucleosome complex *in vitro* protects PAR degradation by PARG (Figure 2.24; Gottschalk et al., 2012).
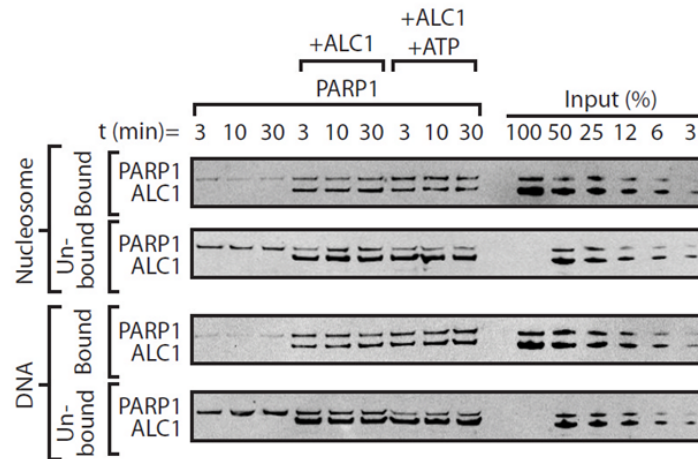
Figure 2.23 Cooperative binding of PARP1 and ALC1 to nucleosomes (from Gottschalk et al., 2012). Biotinylated DNA or mononucleosomes reconstituted with HeLa cell histones were immobilized on streptavidin beads and incubated for 5 minutes with PARP1 and NAD$^+$, with or without ALC1 and ATP. After addition of competitor DNA, reactions were incubated for the indicated times (3, 10 or 30 minutes). PARP1 and ALC1 in bound and unbound fractions were detected via western blotting.
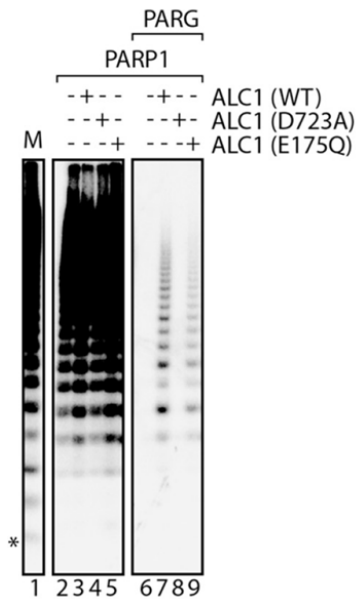
Figure 2.24 The ALC1 macrodomain protects PAR chains from PARG digestion (from Gottschalk et al., 2012). Reactions performed contained PARP1 and wild type or mutant ALC1, without or with 5 ng PARG. Marker lanes (M) show the total reaction products synthesized in a reaction containing nucleosomes and PARP1. Free ATP runs at the position indicated by the asterisk

2.4.2 Nuclear functions of ALC1 and their physiological consequences

In addition to hepatocellular carcinoma (HCC), the analysis of ALC1 overexpression in colorectal carcinoma, ovarian and bladder cancers suggested that ALC1 can serve as biomarker of tumor progression and survival prognosis in patients (He at al., 2012, Ji et al., 2013, Tian et al., 2013, Hyeon et al., 2013). The disease free survival (DFS) time of patients overexpressing ALC1 was around 6 months shorter, when compared to patients with negative ALC1 levels (Figure 2.25). Over 30 mutations within cDNA of ALC1, spanning both the domains and the linker region, were reported in the catalogue of somatic mutations in cancer (COSMIC). The precise function for the majority of these mutations in tumor development was not evaluated yet.
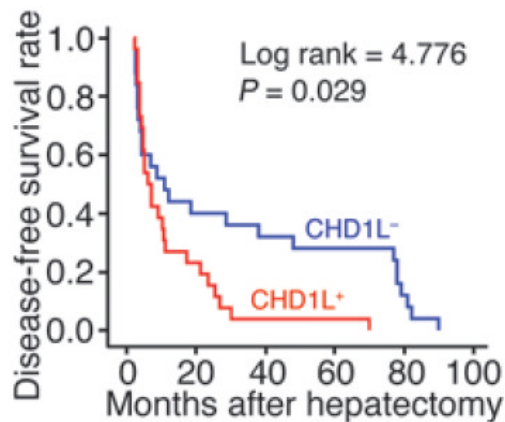
Figure 2.25 Kaplan-Meier disease free survival (DFS) curve of HCC patients in correlation with CHD1L (ALC1) expression (from Chen et al., 2010). The median disease free survival (DFS) time in the CHD1L-negative (ALC1 negative) HCC patients was 11.8 months (95 % confidence interval, 4.4–19.2 months; n = 24, blue line), whereas the median DFS in CHD1L-positive (ALC1 positive) patients was only 6 months (95 % confidence interval, 3.1–8.9 months, n = 29, red line).

ALC1 has six mRNA isoforms, from which 5 encode a protein. The overexpression of human ALC1 in mice, in addition to endogenous Alc1, leads to development of spontaneous tumors (including HCC) in the offspring of these transgenic mice (n=10/41, 24.4 %). Tumor formation was not observed in wild-type littermates (n=39; Chen at el., 2010). Functional studies showed that overexpression of ALC1 in transgenic mice fosters cell proliferation, acceleration of G1/S phase transition and inhibition of apoptosis, which was linked to RNA up-regulation of cyclins

(A, D1 and E), cyclin-dependent kinases 2 and 4 (CDK2 and 4) and down-regulation of retinoblastoma protein (Rb), cyclin-dependent kinase inhibitor 1B (p27Kip1) and tumor suppressor p53 (Chen et al., 2009). Similarly to PARP1, ALC1 was linked to functions in DNA repair and transcription, however with little molecular mechanistic details. So far, it is known that ALC1 overexpression leads to elevated levels of H2A.X phosphorylation (a marker of DNA damage) 1 hour post DNA damage induction with phleomycin (Figure 2.26). The same effect was, however not observed when DNA damage was induced with hydrogen peroxide or gamma radiation.
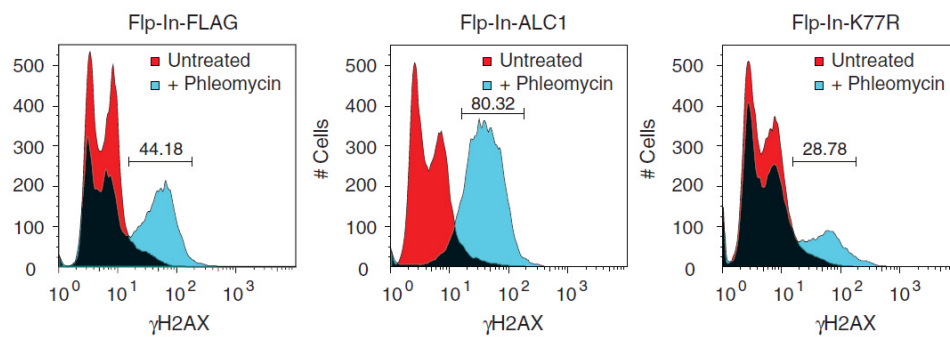
Figure 2.26 Phosphorylated H2A.X levels assessed by fluorescence-activated cell sorting analysis in cell lines of the indicated genotype, 1 hour after 300 mM phleomycin treatment (from Ahel et al., 2009).

Overexpression of ALC1 was linked to transcriptional control of two genes namely: Rho guanine nucleotide exchange factor 9 (ARHGEF9) and testican-1 (SPOCK1; Figure 2.27 A and B). ALC1 was found via ChIP-PCR to reside upstream of TSS of these genes. For ARHGEF9 no specific localization of ALC1 was reported, whereas ALC1 at SPOCK1 was found between - 0.2kb to (-) 1.5kb in comparison to TSS. Importantly, both of the genes are highly expressed in HCC and promote tumorigenicity (Chen et al., 2010, Li et al., 2013).
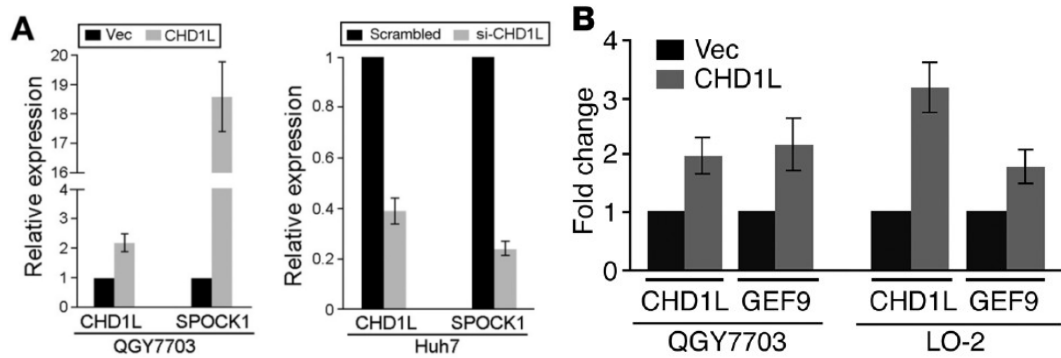
Figure 2.28 ALC1 regulates transcription of two genes linked to tumorigenicity (from Chen et al., 2010 and Li et al., 2013). mRNA levels of **A**) SPOCK1 and **B**) ARHGEF9 increase and decrease upon ALC1 overexpression or knock-down, respectively.

In addition to ALC1 roles in tumor formation, ALC1`s missense mutations in vicinity to the macrodomain, were linked to congenital anomalies of the kidneys and urinary tract (CAKUT). CAKUT comprise ~15 % of all congenital anomalies detected prenatally and found in more than 250 syndromes and in more than one-third of chromosome aberrations. Thus functions of ALC1 for cellular homeostasis are of great importance (Brockschmidt et al., 2012).

2.4.3 Open questions

Chromatin structure affects all processes requiring DNA template. Among many chromatin state modifiers, so called chromatin remodelers play a primary role in: movement, eviction and reorganization of nucleosomes, which directly regulate accessibility of DNA regulatory elements (Clapier and Cairns, 2009). Thus, a specificity and control of DNA use can be achieved through an activation or inhibition of a particular chromatin remodeler. ALC1, specifically regulated by PAR modification was linked to DNA repair and transcription. The molecular details of ALC1 functionality are however missing. Reported so far, a critical to cancer genesis, deregulation of transcription by ALC1 lacks convincing basis. The effect of ALC1 overexpression as a chromatin remodeler linked to transcription regulation of two genes (ARHGEF9 and SPOCK1) may be simply a secondary effect of a global chromatin structure alteration. No negative controls were reported neither. Moreover, especially interesting would be to determine the PARP1 importance in ALC1`s recruitment to DNA transcription sites. Moreover, a precise identification of ALC1 enrichment sites genome wide (promoters, gene body, enhancers and etc.) would help to further evaluate an importance of ALC1 role on regulation of histone variant incorporation or eviction and nucleosome position.

In addition, the findings that PARP1`s association with chromatin is regulated *in vitro* via ALC1 is intriguing (Figure 2.23). PARP1`s association with chromatin is crucial to its activity, thus time of   Taking into account that PARP1 can be removed from chromatin via caspase 7 cleavage (Erener et al., 2012) or ubiquitin mediated degradation (Liu et al., 2013) it is possible that PAR readers like ALC1 actively regulate PARP1`s binding to chromatin as well. Therefore it is of high interest, if a stable complex (PARP1-ALC1-nucleosome) forms *in vivo* as well, and what consequences the PARP1-ALC1-nucleosome complex bears on regulation of PARP1 association with a DNA break, PAR levels and eventually DNA repair mechanism regulation.

2.5 Aims of this Ph.D. thesis

After a few decades of research concerning poly-ADP-ribose (PAR) and poly-ADP-ribose polymerase 1 (PARP1), the exact mechanisms that govern PARP1 genome integrity and transcription functions are far from being completely understood. Despite these limitations, the significance of PARP1 regulatory functions in human physiology regulation is already recognized. For example, chemical compounds that inhibit PARP1 activity are currently evaluated in clinical trials as inducers of synthetic lethality of BRCA1/2-deficient tumor cells. However, precautions must be taken. PARP1 impacts human physiology homeostasis and is considered e.g. a tumor suppressor (for details see 2.1.3). Thus inhibition of PARP1 activity may lead to undesirable and currently unknown off-target effects.

Therefore, a detailed understanding of the PARP1 functional roles in regulation of chromatin-associated processes like DNA repair, replication and transcription must be carefully obtained. Among many chromatin state modifiers, ATP-dependent chromatin remodelers play a crucial role in movement, eviction and reorganization of nucleosomes, which directly regulate accessibility of DNA regulatory elements. Thus, specificity and control of access to distinct DNA loci can be achieved through the activation or inhibition of a particular chromatin remodeler, like the PAR-regulated remodeller <u>a</u>mplified in <u>l</u>iver <u>c</u>ancer ALC1.

The first goal of this Ph.D. thesis answers a long-standing call to advance the PARP1 field. I aimed to gain insights into the PARP1 molecular mechanism of activation, which is a cornerstone to all chromatin-based PARP1 functions. I aimed to identify the *in vivo* mechanism of PARP1's recognition and binding to DNA lesions and promoters, including the specific roles of the DNA Binding Domain in this process. For detailed aims, please see **4.1 section** (**pages 69-70**).

The second goal of this Ph.D. thesis was to get detailed mechanistic insights into the roles of the PAR-dependent ATP-utilizing remodeller ALC1 in the regulation of transcription. For detailed aims, please see **5.1 section** (**pages 99-100**).

3 Materials and methods

3.1 General materials

Table 3.1 provides an overview of general materials used in this study.

Table 3.1 Materials used in the study.

Name	Manufacturer
Acetone	Fisher Scientific
Acrylamide	Bio-Rad
Agarose	Denville Agarose HS
Ammonium chloride (H_4ClN)	Fluka
Amonium sulfate ($(NH_4)_2SO_4$)	Fluka
Ampicilin	Sigma
β-mercapto-ethanol	Fluka
Bromophenol blue	Sigma
Bovine Serum Albumine (BSA)	Sigma
Chloramphenicol	Sigma
Coverslips	Thermo Scientific
Cryo Tubes TM Vials	Nunc
Dithiothreitol (DTT)	Biomol
dNTPs PCR Nucleotide Mix	Roche
Ethylendiamine tetra acetate (EDTA)	Sigma
Ethanol (EtOH; molecular grade)	Pharmaco-AAPER, Sigma
Ethidium Bromide (EtBr)	Bio-Rad
Salmon sperm DNA	Sigma
Formaldehyde (35 %)	Merck
Glycerol	Fisher Scientific
Glycine	Sigma
HEPES	Sigma
Isopropanol	Sigma (molecular grade)
Kanamycin	Sigma
Methanol (MeOH)	Pharmco-AAPER
Milk powder	Frema Reform
Multiwell dishes: 6-well, 12well and 24-well	Nunc
Nonident P-40 (NP40)	Fluka
Object slides 76 x 26 mm	Thermo Scientific
Petri dishes (different sizes)	Nunc
Poly-L-lysine	Sigma
Ponceau S	AppliChem
Sodiumdodecylsulfate (SDS)	Sigma
Sodium chloride (NaCl)	Sigma
Sodium hydrogen carbonate $NaHCO_3$	Merck
Tetramethylethylenediamine (TEMED)	Sigma
TRIS Base	Sigma
Triton X-100	Fisher Scientific
Trypsin EDTA	Sigma
Tween20	Sigma

Table 3.2 The cell lines used in this work and cell culture media requirements.

No.	Cell line	Media composition
1	HeLa-Kyoto *wild type* (cervical carcinoma)	DMEM (Life Technologies, no. 11880-028), 10 % FBS
2	HeLa-Kyoto-*PARP1* knock-down (cervical carcinoma) (previously generated in Ladurner laboratory; Ali et al., 2012)	DMEM (Life Technologies, no. 11880-028), 10 % FBS, puromycin (1:200, Gibco)
3	*Michigan Cancer Foundation-7 cells (MCF-7) (adenocarcinoma)	DMEM (Life Technologies, no. 11880-028 or no. 21063-029),10 % FBS
4	*MCF-7-human-*ERα*-GFP (provided by Dr. Huet from Univ. of Rennes, Reid et al., 2003)	DMEM (Life Technologies, no. 11880-028 or no. 21063-029), 10 % FBS, hygromycin (1:200, Gibco)
5	*M.D. Anderson - metastatic breast cancer cells MDA-MB231-human-*ERα* (provided by Dr. Reid from IMB Mainz, Reid et al., 2003)	DMEM (Life Technologies, no. 11880-028 or no. 21063-029), 10 % FBS
6	*MDA-MB231-human-*ERα*-GFP (provided by Dr. Reid from IMB Mainz, Reid et al., 2003)	DMEM (Life Technologies, no. 11880-028 and no. 21063-029), 10 % FBS
7	*T47D (ductal carcinoma) (provided by Dr. Reid from IMB Mainz)	RPMI (Life Technologies, no. 11835-063 or no. 116967), 10 % FBS
8	U2OS-*wild type* (osteosarcoma)	DMEM (Life Technologies, no. 11880-028),10 % FBS
9	U2OS-*ALC1*-YFP (osteosarcoma) (previously generated in Ladurner laboratory)	DMEM (Life Technologies, no. 11880-028), 10 % FBS, hygromycin (1:200, Gibco)
10	U2OS-*HP1alpha*-YFP (osteosarcoma) (provided by Dr. Ellenberg from EMBL)	DMEM (Life Technologies, no. 11880-028), 10 % FBS, Geneticin (G418; 1:100, Gibco)

*Prior to hormone treatment the cells were washed once with PBS (RT) and kept for 48 hours in regular media where standard fetal bovine serum (Invitrogen, heat inactivated) was replaced with charcoal stripped FBS (Life Technologies, no. 12676029), DMEM or RPMI lacked phenol red.

3.2 Cell Culture and Cell Lines

The cell lines used in this work and particular cell line media requirements are listed in Table 3.2. The cells were grown in 37°C with 5 % CO2 level. All the media were supplemented with 50 U/ml penicillin and 50 mg/ml streptomycin (Sigma). Prior to hormone treatment the cells were washed once with PBS and kept for 48 hours in regular media where standard fetal bovine serum (FBS, Invitrogen, heat inactivated) was replaced with charcoal stripped FBS (Life Technologies, no. 12676029) and Dulbecco's Modified Eagle Medium (DMEM) or Roswell Park Memorial Institute (RPMI) 1640 with no phenol red. The hormone treatment was one of the following: (i) 10 nM or 100 nM estradiol (Sigma, no. 8750), (ii) 10 nM or 100 nM progesterone (promegestone, R5020, Perkin Elmer no. NLP004005), (iii) 10 μM all trans retinoic acid (Sigma, no. R2625). Depending on the assay the cells were treated with the hormone for 20 minutes, 30 minutes or 3 hours. When indicated the cells were treated with PARP1 chemical inhibitor (one of the following): 1 μM, 5 μM and 15 μM AG14361 (Selleckchem, no. S2178), or 1 μM and 5 μM olaparib (Selleckchem, no. S1060). The inhibitors were added 40 minutes before the hormone stimulation, and kept within media upon treatment with hormones. The experiments were conducted on cells with low passage number. For long term storage the cells were first suspended in freezing media (FBS with 10 % DMSO), transferred to Cryo-Tubes and stored in liquid nitrogen.

3.3 Chromatin immuno-precipitation (ChIP)

The following is the modified ChIP protocol originally from Krishnakumar et al., 2008. The cells (MCF-7 *wild type*, U2OS *wild type*, U2OS-*ALC1*-YFP) were always collected from 90 % confluent 10 cm dish plate. The cells were rinsed once with room temperature (RT) PBS (Sigma, no. 8537). Next, the crosslinking fixative was added (1 % formaldehyde in PBS, RT) and kept for 10 minutes. The cells were treated with 2.5 M glycine for 5 minutes (4°C). All the buffers and PBS contained protease inhibitors (Complete EDTA-free Protease Inhibitor Cocktail Roche, no. 11873580001). After quenching with glycine the cells were rinsed three times with ice cold PBS and collected with the cell scraper. The cells were centrifuged for 5 minutes at 3000 rpm (4°C). The excess of PBS was removed and the cell pellet was snap frozen in liquid nitrogen and stored at -80°C before use (no longer than 2 months). When further processed, the cells were suspended in the lysis buffer (1 % SDS, 10 mM EDTA, 50 mM Tris-HCl pH 7.9) and incubated

on ice for 10 minutes. Next, the DNA was sheared to desirable size (200 base pairs or 500 base pairs) with use of Covaris S220 (sonication in 1ml tube with and without the fiber and the Covaris settings: Peak Incident Power 105 Watt, Duty Factor 25 %, Cycle Burst 200 counts, time 10 minutes or 18 minutes). The sheared DNA was span for 10 minutes at 14000 rpm at 10°C. The supernatant was kept and diluted 10 times in the dilution buffer (0.5 % Triton-X100, 2 mM EDTA, 150 mM NaCl, 20 mM Tris-HCl pH 7.9). Next, protein sepharose A or G from GE Healthcare (50 % slurry in 10 mM Tris-HCl pH 8.1 and 1 mM EDTA) was added to the supernatant for 2 hours at 4°C (with constant rotation). Next the beads (sepharose) were removed following the 1 minute spin at 3000 rpm at 4°C. The supernatant was incubated with specific antibodies over-night (o/N), including the constant rotation at 4°C (see 3.4 for details regarding the used antibodies). Next, protein A or G sepharose was added and incubated for no longer than 2.5 hours at 4°C. The agarose beads were washed four times for 3 minutes each wash in wash buffer (0.25 % NP-40, 0.05 % SDS, 2 mM EDTA, 20 mM Tris pH 7.9, 250 mM NaCl). The beads were rinsed only briefly in Tris-EDTA buffer. Finally, the protein-DNA complexes were eluted with elution buffer (50 mM, Tris pH 8.0, 1 mM EDTA and 1 % SDS). To reverse crosslinking the samples were kept at 65°C O/N followed by addition of proteinase K for 1 hour at 55°C. Digestion of RNA (RnaseA 10 mg/ml at 37°C for 30 minutes) was followed by DNA purification with MiniElute columns (Qiagen). The presence of specific DNA was evaluated via quantitative PCR (see 3.11 section for details). Data was analyzed as usual by taking the cycle threshold (Ct) values. The signal for all samples was adjusted relative to the total input fraction. The following primers were used for the target genes. Primers were designed with Primer3Plus software and analyzed with BLAST (Basic Local Alignment Search Tool) not to match other sequence than the targeted gene.

ABHD2_upstream_0.5kb_forward AGGCCCTAGTTCCAAGGCTA

ABHD2_upstream_0.5kb_reverse ACCCGAAGGAGAGGAAAAGA

ABHD2_upstream_1kb_forward AGCCCACTGTTCCTTGTCAC

ABHD2_upstream_1kb_reverese GAGCCTGAAACTGCTTTTGC

ABHD2_downstream_0.5kb_forward GCTCACTCCTGGGTCTTCAG

ABHD2_downstream_0.5kb_reverse CCGAACTCGGTAAATGTGCT

ABHD2_TSS_forward GCCTCCACTCTGAGGAACAG

ABHD2_TSS_reverse TTGTTCATTGGGCAGTTCAG

GDF15_upstream_0.65kb_forward AGGGGCTTTTTGCGTAGAGT

GDF15_upstream_0.65kb_reverse AAGGGCAACCTTGATGTGTC

GDF15_downstream_0.5kb_forward AATATCCTGGATCCCCTTGG

GDF15_downstream_0.5kb_reverse CACACCCCCATTGTTTCTCT

GDF15_TSS_forward CTCAGATGCTCCTGGTGTTG

GDF15_TSS_reverse CTCGGAATCTGGAGTCTTCG

ITPR1_upstream_0.5kb_forward CAGAGGCTGCTCCTAAATGG

ITPR1_upstream_0.5kb_reverse CAGGGCTCAGAGAAATCAGG

ITPR1_downstream_0.5kb_forward AGGGCGGAGCAGATTAAATA

ITPR1_downstream_05kb_reverse GGCTAGGAGCTCGGATTTCT

ITPR1_TSS_forward GAGCCCTAAGCAGCGTGTAG

ITPR1_TSS_reverse CTCTCCAAGAGCTCCGAATG

RAPGEF4_upstream_forward CCTAAGCCAGTTGACCCAGA (negative control)

RAPGEF4_upstream_reverse AAATGAAGCCGCTAGGAACA (negative control)

RAPGEF4_TSS_forward GTAACTCCCGACGACAGCTC (negative control)

RAPGEF4_TSS_reverse CTGTCACAGCCTGGAAACAA (negative control)

3.4 Immuno-precipitation (IP)

The cells were washed once with PBS (RT) and: (i) not crosslinked (ii) crosslinked, or (iii) crosslinked and Covaris sonicated. All the steps were conducted the same as described in the ChIP section (see 3.3 for details). Instead of DNA, the proteins were eluted via treatment of the beads with SDS-loading buffer for 10 minutes at 95°C. The IP efficiency was evaluated via Western Blot. The following antibodies were used anti-GFP (Ladurner laboratory, own stock), serum-ALC1 (serum from rabbits immunized with ALC1 peptide as an antigen, for details see 3.7). The most suitable concentration of the antibodies (in each case) was determined via titration experiment.

3.5 Determination of protein concentration

Protein concentration was determined using the Bradford assay. The protein sample (1–10 µl) was added to 1 ml of 5-fold diluted Protein Assay reagent (Bio-Rad) and incubated for 10 minutes at RT. The absorbance of the samples was measured at 595 nm in 1 cm path – length cuvette. The concentration of the protein sample was determined based on the standard curve prepared with a solution of known protein concentrations (Bio-Rad).

3.6 Protein separation and Western Blot

Proteins were separated according to their size via standard sodium dodecyl sulfate polyacrylamide gel electrophoresis (SDS-PAGE) system. Prior to loading on the gel, the protein samples were mixed with SDS loading buffer and incubated at 95°C for 5 minutes. After the separation on the gel the proteins were transferred to nitrocellulose (Protran Whatman) or polyvinylidene fluoride (PVDF) membrane (Millipore) in transfer buffer at 60 V for 60 minutes at 4°C. After 1 hour blocking in 5 % milk in PBST (PBS buffer, 0.05 % Tween 20) at RT proteins were incubated with protein specific primary antibody in PBST O/N at 4°C. Next, the excess of the primary antibody was washed away via three washes with PBST at RT for 10 minutes (each wash). The horseradish peroxidase (HRP) coupled secondary antibody was kept in PBST for 1 hour at RT, followed by 3 washes in PBST at RT for 10 minutes. The secondary antibodies were used in 1:10000 ratio: anti-rabbit-HRP (Bio-Rad, no. 172-1019) and anti-mouse-HRP (Bio-Rad, no. 170-6516). The membrane was developed with Immobilon Western Chemiluminescent HRP Substrate (Millipore, WBKLS0050) and Fuji medical X-ray films

(Super RX). When necessary the membranes where stripped from antibodies in order to reuse the membrane. The membranes were incubated in Western blot stripping buffer for 15 minutes at RT. Subsequently the buffer solution was discarded and the membrane was washed for 1 hour with PBST and again blocked with 5 % milk in PBST as before. Typically the membranes were stripped and reused to evaluate the protein loading with antibody against α-Tubulin (1:10.000, 1 hour at RT). The incubation with the primary antibody and the steps afterwards were conducted, as just described.

SDS protein sample loading buffer

125 mM Tris-HCl pH 6.8

10 % β-mercaptoethanol

4 % SDS

20 % glycerol

0.004 % Bromophenol Blue

Stacking gel

5 % weight per volume (w/v) acrylamide

0.1 % (w/v) bis-acrylamide

60 mM TRIS-HCl pH 6.8

0.1 % (w/v) SDS

0.05 % (w/v) APS

0.05 % (v/v) TEMED

Separating gel

8–16 % (w/v) acrylamide

0.16–0.33 % (w/v) bis-acrylamide

375 mM TRIS-HCl pH 8.8

0.1 % (w/v) SDS

0.05 % (w/v) APS

0.05 % (v/v) TEMED

Laemmli running buffer

63 mM Tris HCl

10 % glycerol

2 % SDS

0.0025 % Bromophenol Blue pH 6.8

Western Blot transfer buffer

3.1 g/l Tris base

14.4 g/l glycine

10 % MeOH

Western blot stripping buffer

SDS 10%

Tris HCl pH 6.8 (0.5 Molar)

0.8 % ß-mercaptoethanol

3.7 Generation of antibodies

The peptides corresponding to PARP1 individual zinc fingers (ZF1 and ZF2), and ALC1 individual domains (ATPase and macrodomain) were recombinantly expressed and purified via affinity chromatography by Dr. Markus Hassler (Ladurner laboratory). The individual zinc fingers corresponding to 1-111 amino acids (ZF1) and 112-214 amino acids (ZF2) of PARP1 were mixed in a 1:1 ratio with an adjuvant. The *Titer Max Gold* was used for the first injection and *Freund`s Adjuvant Incomplete* for the following injections. Before the start of immunization, the blood was collected (pre-immune serum) and tested for reactivity against the recombinant antigen. Two rabbits were injected with 100 µg of the antigen (50 µg of each zinc finger were

mixed) per each injection. In total, five immunizations every 6 weeks followed. Starting from the second immunization, ten days after the injection 20 ml of blood was collected. The collected blood was kept for 2 hours at RT. Next, the blood was centrifuged for 10 minutes at 4000 rpm at RT. The supernatant was transferred to a new tube and centrifuged again for 15 minutes at 15000 rpms at 4°C. Collected supernatant was heat inactivated for 30 minutes at 56°C. The collected serum was stored at -20°C. The generated antibodies were evaluated via the Western blot. The antibody against PARP1 was generated at LMU Adolf-Butenandt-Institute Animal Facility.

The ALC1 antibodies corresponding to ATPase domain (31-556 amino acids) and macrodomain (615-878 amino acids) were generated at Eurogentec (Belgium) according to the company`s protocol. Blood from four rabbit bleeds was provided, including pre-immune serum. The specificity of generated antibody was tested via the Western blot and immuneprecipitation.

3.8 Small interfering RNA (siRNA) mediated gene knock-down

Prior to the transfection, the cells were seeded in 6 well plates (10^5 cells/well) in the standard media. The following day the cells were washed once with PBS and treated with respective siRNA mixed with oligofectamine (Life Technologies, no. 12252-011) according to the manufactures guidelines. Prior to addition to the cells, the Opti-MEM, siRNA and oligofectamine mixture was incubated for 20 minutes at RT. The cells were kept for 12 hours in the solution containing siRNA (ALC1, Dharmacon, no. M014368-01 or PARP1 from Ambion no. 4390824 and Dharmacon, no. L006656-03), Opti-MEM (Life Technologies, no. 31985-070) and standard DMEM or RPMI media deprived of serum. Next, the cells were washed once with PBS and kept for 48 hours in the standard media, including serum till the follow up experiments were conducted and total RNA was extracted. The siRNA from Dharmacon are composed of highly specific four siRNA targeting various exons of the targeted gene.

3.9 Total RNA extraction

Before the total RNA extraction the cells were washed once with PBS. Total RNA was extracted as follows, 0.5 ml of Trizol (Life Technologies, no. T9424) was added per 90 % cell confluent 10 cm dish. Cells were collected with the cell scraper and homogenized via pipetting. The samples were centrifuged for 10 minutes at 14000 rpm at 4°C. Supernatant was collected and left

for 5 minutes at RT, before mixing it with 0.1 ml chloroform (Sigma, the molecular grade) and roughly vortex mixed (15 seconds). Next, the samples were left for 15 minute incubation in RT, followed by spinning for 15 minutes at 12000 rpm at 4°C. The upper layer was collected and mixed with 0.25 ml of isopropanol (Sigma, the molecular grade) and let it stand for 10 minutes at RT. Next, the samples were centrifuged for 10 minutes at 12000 rpm at 4°C. The resulted pellet was washed with 0.5 ml of 75 % EtOH via short vortexing and centrifugation for 5 minutes at 7500 rpm at 4°C. Pellet was air dried for 5-10 minutes and dissolved in nuclease free water. The extracted RNA concentration and purity were tested with NanoDrop 1000 Spectrophotometer. In case the RNA purity was low, based on the ratio of absorbance at 260:280 nm (ca. 2.0) and 260:230 nm (ca. 2.0-2.2), the RNA was further purified with use of RNeasy Mini Kit (Qiagen, no. 74104). The extracted RNA was stored at -80°C till further use (no longer than 1 month).

3.10 Synthesis of complementary DNA

The extracted total RNA was thawed on ice and the RNA concentration was again tested using the NanoDrop 1000 Spectrophotometer. Total RNA (500 ng) was used for cDNA synthesis with SuperScript II Reverse Transcriptase kit (Invitrogen, no. 18064-014) according to the standard protocol with use of random primers (Invitrogen, no. 48190-011).

3.11 Quantitative PCR (qPCR)

qPCR was conducted on the Applied Biosystems 7500 Fast Real-Time PCR system using fast SYBR green master mix (Applied Biosystems). In order to quantify mRNA levels of tested genes the detected Ct values were normalized to Ct values of the control gene GAPDH. The sequences (5` > 3`) of the primers for the tested genes are below. Primers specificity was analyzed with BLAST not to match other sequence than the targeted gene. The sequences of primers come from Hah et al., 2011 for estrogen receptor alpha (ERα) regulated genes, from Le May et al., 2012 for retinoic acid receptor (RAR) regulated genes and Wright et al., 2012 for progesterone receptor (PR) regulated genes.

CASP7_forward CTGGGTGGGTACTTCCTTCA

CASP7_reverse TGTGGTCTCCTAGACGTTGC

C-FOS_forward CCGGGGATAGCCTCTCTTAC

C-FOS_reverse GTGGGAATGAAGTTGGCACT

DUSP1_forward CAGCTGCTGCAGTTTGAGTC

DUSP1_reverse AGAGGTCGTAATGGGGCTCT

EGFR_forward GGCAGGTCTTGACGCAGTGG

EGFR_reverse TGTTTGGGACCTCCGGTCAG

FAM117B_forward ATTCTACCCAGGCCTCCAGT

FAM117B_reverse CAGAGGAGATTGGCATGTGA

GAPDH_forward AGCTCACTGGCATGGCCTTC

GAPDH_reverse ACGCCTGCTTCACCACCTTC

GDF15_forward CTACAATCCCATGGTGCTCA

GDF15_reverse TATGCAGTGGCAGTCTTTGG

GFRA1_forward GCCATATTTGGCTGTGGTCT

GFRA1_reverse CGGAGGACAATCAGCTCTTC

GREB1_forward GACCTGCCAAATGGAAGAAG

GREB1_reverse AAAGCCATGTCCTTCCACAC

ITPR1_forward TGCCTCCACAATTCTACG

ITPR1_reverse TGAATGTCCCACAGTTGC

PDK4_forward ACCCAAGCCAGATTGGAAGCA

PDK4_reverse AACTGTTGCCCGCATTGCATT

SMAD3_forward TTGTCCAGTCCCAACTGTAAC

SMAD3_reverse GTCAACTGGTAGACAGCCTCAAA

TFF1_forward GGAGCAGAGAGGAGGCAAT

TFF1_reverse GGCGCAGATCACCTTGTT

TGM2_forward CGAGCCCTGGTAGATAAA

TGM2_reverse TAAGAGATGCTGTGGAGGAG

3.12 Generation of PARP1 and ALC1 fluorescently tagged constructs and mutagenesis

Zinc finger 1 (residues 1–111), Zinc finger 2 (residues 112–214), DNA binding domain (DBD, 1-214 amino acids), full length Δ zinc finger 1 (112-1014), full length Δ zinc finger 2 (Δ112-214), full length Δ catalytic domain (Δ660-1014) and full length (FL, 1-1014 amino acids) PARP1 constructs and PARP2 were PCR amplified from cDNA and introduced into pmEGFP-N1 plasmid (Clontech) via NheI and SmaI restriction sites (the restriction enzymes from New England Biolabs). Single residue mutants of PARP1 DBD and FL were generated using QuikChange site-directed mutagenesis (Stratagene). For expression of PARP1-mCherry, PARP1 was PCR amplified from cDNA and introduced into pmCherry-N1 plasmid (Clontech) via NheI and SmaI sites. For expression of EYFP-ALC1 and mCherry-ALC1, ALC1 was PCR amplified from cDNA and introduced into pEYFP-C1 and mCherry-C1 (Clontech) via BglII and EcoRI restriction sites (the restriction enzymes from New England Biolabs) respectively. All constructs were sequence verified via use of primer sequences spanning the both sides of the insert (GATC Biotech Sequencing service). Constructs expressing monomeric (1x) and triple (3x) EGFP were kindly provided from Dr. Ellenberg`s laboratory (Bancaud et al., 2009). Plasmids were amplified in *Escherichia coli* (DH5α) and purified with Plasmid Midi Kit (Qiagen).

3.13 Plasmid DNA transfection

A day before a transfection, the cells were seeded in 8-well Lab-Tek chambered coverglass (3 x 10^4 cells/well) from Nunc (no. 155411). The transfections of plasmids were carried with Effectene Transfection Reagent (Qiagen, no. 301425) in case of FCS, FRAP and FLIP experiments. For the remaining experiments (live cell imaging) the transfection reagent XFECT (Clontech, no. 631317) was used. Both reagents were used according to the manufactures guidelines with usual amount of plasmid DNA no higher than 1 µg per well. Transfected cells were analyzed the next day.

3.14 Fluorescence Correlation Spectroscopy (FCS)

FCS experiments were performed on Leica TCS SP2 AOBS FCS2 system. The confocal microscope was equipped with a diode laser (405 nm wavelength) with maximum output of 50 mW, an argon laser (488 nm) with maximum output of 50 mW and 63×/1.4–numerical objective water-immersion. The typical acquisition time was 60 seconds (3 times for 20 seconds) and the

same laser intensities were used for all the conditions and constructs (488 nm laser set to 11 %). Data was acquired with Vista 3.6.22 program. The autocorrelation function was calculated with Fluctuation Analyzer software (version 1.2, developed by Dr. Malte Wachsmuth at EMBL). The autocorrelation function, ACF = $G(\tau)$ was fitted to the formula (equation 1) for anomalous diffusion allowing detection of one or two components (with use of OriginPro software)

$$ACF = \frac{1}{N} * \left(1 - \Theta1 + \Theta1 * \exp\left(-\frac{x}{\tau T1}\right) - \Theta2 + \Theta2 * \exp\left(-\frac{x}{\tau T2}\right)\right)$$

$$* \left(\frac{\dfrac{f1}{1 + \left(\frac{x}{\tau D1}\right)^{\alpha1}}}{\mathrm{sqrt}\left(1 + \dfrac{\left(\frac{x}{\tau D1}\right)^{\alpha1}}{\kappa^2}\right)}\right) + \left(\frac{\dfrac{1 - f1}{1 + \left(\frac{x}{\tau D2}\right)^{\alpha2}}}{\mathrm{sqrt}\left(1 + \dfrac{\left(\frac{x}{\tau D2}\right)^{\alpha2}}{\kappa^2}\right)}\right)$$

(Equation 1)

Here, **N** denotes the number of particles, **f1** - the percentile of the first component, **τD1** and **τD2** are diffusion times for the first and the second component respectively, **κ** (kappa) is the structure parameter of the microscopes focal volume (the ratio of the axial and lateral focus radius), **α_1** and **α_2** are anomaly parameters for the first and the second component respectively. Additional parameters for fitting the FCS curve consider the EGFP photophysical dynamics, like triplet state, which probability is given by **Θ** and relaxation time (**τT**). Each component was considered separately, thus **τT1** correspond to component one, and **τT2** correspond to component two (Müller et al., 2009). Typical fits had the coefficient of determination (R^2) values above 0.95 (0 means a poor fit, 1 means a very good fit).

The lateral radius of the confocal volume (**ω_0**) in used experimental setting has been determined by FCS measurements of Alexa Fluor 488 C5 maleimide (Invitrogen, Molecular Probes) dissolved in water at RT, which diffusion coefficient (**D**) is well known (Müller et al., 2009). Thus the **ω_0** was calculated according to the equation 2.

$$\omega_o^2 = 4D\tau$$

(Equation 2)

Once ω_o was calculated it was possible to calculate the diffusion coefficient (*D*) for all FCS measured PARP1, HP1α and EGFP constructs, according to the equation (3). Time of diffusion (**τ**) was calculated with equation (1).

$$D = \frac{w_0^2}{4\tau_{diff}}$$

(Equation 3)

The accuracy of the equation was consulted with Dr. Malte Wachsmuth (Cell Biology and Biophysics, EMBL, Heidelberg). Results shown in the results section combine the measurement from at least 10 cells per each condition tested. In addition there were at least three measurements taken in each cell to eliminate not representative cells. The measurement spot was chosen randomly, however the nucleoli and nuclear periphery were avoided. Only cells with very similar levels of GFP signal were chosen for the measurements. During imaging the cells were kept in CO_2-independent imaging medium (Gibco) supplemented with 10 % (v/v) FBS (Gibco), 1 mM sodium pyruvate (Sigma) and 2 mM L-glutamine (Sigma), 100 U/ml penicillin and 100 μg/ml streptomycin (Sigma).

3.15 Fluorescence Recovery After Photobleaching (FRAP)

FRAP experiments were performed on a Leica SP2-AOBS confocal microscope or a PerkinElmer UltraView Vox spinning-disk microscope. Both systems were equipped with a diode laser (405 nm wavelength) with maximum output of 50 mW and an argon laser (488 nm) with maximum output of 50 mW or 75 mW, and 63×/1.4–numerical objective water-immersion and 63×/1.4–numerical objective oil-immersion objectives for Leica SP2 and PerkinElmer Vox, respectively. In all experiments the photobleached region corresponds to a 3 μm wide square. For bleaching, the argon laser was set to 100 % transmission (Leica) and 80 % transmission (PerkinElmer). Fluorescence recovery quantification was performed with freely available ImageJ

(http://fiji.sc/Fiji). Fluorescence of a bleached region was background subtracted and normalized to the total intensity, also background subtracted. FRAP was conducted in no–DNA-damage and DNA-damage conditions. DNA damage across the whole nucleus was induced with the 405-nm-wavelength diode laser set to 60–80 % transmission for 0.8 s. Before DNA damage induction, cells were sensitized with Hoechst 33285 dye (0.5 mg/ml) for at least 10 minutes. The FRAP curves were fitted with use of OriginPro software to the following equation (number 4), according to the two dimensional (2D) diffusion model (Im et al., 2014). Diffusion coefficient for unbound molecules was determined in no DNA damage conditions.

$$
y = y0 - A1
$$
$$
* \left(\mathrm{erf}\left(2 * \frac{a}{\mathrm{sqrt}\left(4 * \mathrm{D} * (\mathrm{x} - \mathrm{x}0)\right)} \right) - \frac{\mathrm{sqrt}\left(4 * \mathrm{D} * (\mathrm{x} - \mathrm{x}0)\right)}{\mathrm{sqrt}(4 * 3.1416 * \mathrm{a}^2)} \right.
$$
$$
\left. * \left(1 - \exp\left(-4 * \frac{\mathrm{a}^2}{4 * \mathrm{D} * (\mathrm{x} - \mathrm{x}0)} \right) \right) \right)^2 - A2
$$
$$
* \exp\left(-\mathrm{koff} * (\mathrm{x} - \mathrm{x}0) \right)
$$

(Equation 4)

Here, **A** denotes the depth of the photobleached region, **y0** denotes percentile of unbound molecules, **x0** corresponds to the last time point before the photobleach, **a** corresponds to a size of the phtobleached region, **D** – diffusion coefficient, **k$_{off}$** - disassociation rate (release event per second). The accuracy of the equation was evaluated by Dr. Malte Wachsmuth (Cell Biology and Biophysics, EMBL, Heidelberg). The results presented in the result section combine the measurement from at least 10 cells per condition tested. The measurement spot was chosen randomly, however nucleoli and nuclear periphery were avoided. Only cells with very similar or almost identical levels of GFP signal were chosen for the measurements. During imaging the cells were kept in CO2-independent imaging medium (Gibco) supplemented with 10 % (v/v) FBS (Gibco), 1 mM sodium pyruvate (Sigma) and 2 mM L-glutamine (Sigma), 100 U/ml penicillin and 100 μg/ml streptomycin (Sigma).

The average residence time (**t_{res}**, seconds) in the chromatin bound state was calculated according to the equation 5:

$$t_{res} = 1/k_{off}$$

(Equation 5)

3.16 Fluorescence Loss in Photobleaching (FLIP)

FLIP experiments were performed on a Leica SP2-AOBS confocal microscope with 63×/1.4–numerical objective water-immersion objective. The microscope was equipped with the FLIP wizard. After each photo-bleach, a photo was acquired. Each photobleach was followed by one imgae frame, till the total fluorescence from the cell was depleted. The bleach spot was fixed across all the cells spanning- height (14 μm) and width (1 μm). Images were analysed with ImageJ software. Only cells with very similar or almost identical levels of GFP signal were chosen for the measurements. During imaging the cells were kept in CO_2 - independent imaging medium (Gibco) supplemented with 10 % FBS (Gibco), 1 mM sodium pyruvate (Sigma) and 2 mM L-glutamine (Sigma), 100 U/ml penicillin and 100 μg/ml streptomycin (Sigma).

3.17 Time lapse microscopy

Time lapse imaging of cells expressing human-ERα-GFP and cells transfected with PARP1-mCherry or ALC1-mCherry (upon estrogen treatment) was performed on a Zeiss AxioObserver Z1 confocal spinning-disk microscope equipped with an AxioCam HRm CCD camera (Zeiss) through a Zeiss Plan/Apo 63×/1.4 oil-immersion objective lens. The images were taken every 30 – 60 seconds for 1 or 2 hours. Images were analysed using ImageJ. During all of the fluorescence microscopy experiments cells were kept at 37°C in a CO_2 - independent imaging medium (Gibco) supplemented with 10 % FBS (Gibco), 1 mM sodium pyruvate (Sigma) and 2 mM L-glutamine (Sigma), 100 U/ml penicillin and 100 μg/ml streptomycin (Sigma). Only cells with very similar or almost identical levels of GFP signal were chosen for the measurements.

3.18 Immunofluorescence (IF)

Cells grown on Lab-Teks (3 x 10^4 cells/well) were washed once in PBS (RT) and fixed with a freezing solution (methanol 70 % and acetone 30 %) for 10minutes in -20°C or 4 % formaldehyde for 10 minutes at RT. Formaldehyde fixation was used only in case of PAR staining upon progesterone treatment. Subsequently the cells were rinsed 3 times in PBS (4°C in case of MeOH, or RT in case of formaldehyde) and kept in blocking solution (5 % milk and 0.05 % Tween20 in PBS) for 60 minutes at RT and stained with primary antibodies (1:1000) at 4°C o/n. The next day, the cells were washed three times in PBS (0.05 % Tween20) for 10minutes (each time). Secondary antibody (1:500) was kept for 1 hour at RT and was followed by three washes with PBS (0.05 % Tween20) for 10 minutes (each time) and processed. During the second wash the PBS contained Hoechst 33342 (final concentration: 0.1 μg/ml) in order to stain nuclei. The used antibodies are the following: anti-PAR (H10; Ladurner laboratory stock), Alexa Fluor® 488 anti-mouse (Invitrogen, no. A11001), Alexa Fluor® 488 anti-rabbit goat (Invitrogen, no. A11008), Alexa Fluor® 568 anti-mouse (Invitrogen, no. A11004). The images were acquired with Zeiss AxioObserver Z1 confocal spinning-disk microscope equipped with an AxioCam HRm CCD camera (Zeiss). The results were analysed with freely available Cell Profiler software http://www.cellprofiler.org/.

4 Results and Discussion I

The mechanism of PARP1's binding to DNA *in vivo*

4.1 PARP1 is primarily activated upon binding to DNA

There are two models regarding the mechanism of PARP1 activation. According to the widely accepted model, PARP1 is activated by DNA breaks (see also 2.2.2-2.2.4). The less established model proposes that PARP1 is activated by its posttranslational modifications and by histone variants (see also 2.2.4-2.2.5). The first model is aligned with PARP1 functions in DNA repair, and the second model was proposed to explain PARP1 functions in transcription. A major difference between the models is that PARP1 activation is either coupled to or decoupled from DNA binding. The predominant model relies on the fact that PARP1 binds to DNA via its N-terminal DNA Binding Domain (DBD). Upon DNA binding, PARP1 undergoes an intramolecular conformational rearrangement and subsequently becomes activated. This conformational rearrangement is supported by the X-ray structure of the nearly full-length PARP1 bound to blunt ended DNA (Langelier et al., 2012). The structural evidence for the alternative model is missing. It is not known how exactly the DBD-mediated interactions of PARP1 with chromatin differ between the models in space and time *in vivo*. A proper understanding of PARP1's chromatin interactions and activation would provide valuable insight into PARP1's functions in DNA repair and transcription. Thus it is crucial to fully understand and validate the DNA-coupled and decoupled activation of PARP1.

The predominant model is based on the critical function of the DBD that triggers PARP1 activation upon DNA binding. The DBD is composed of two zinc fingers: zinc finger 1 (ZF1) and zinc finger 2 (ZF2). The exact roles and importance of these two zinc fingers recognizing DNA breaks have been debated for the last 30 years (for details see 2.2.2-2.2.3). Unfortunately, the three recent X-ray structures of zinc fingers bound to DNA are mutually exclusive and thus inconclusive in solving the debate. These structures disagree in ZF2's importance in DNA break recognition and transmission of the bound state to the catalytic domain of PARP1. The X-ray structure of the DBD (two zinc fingers together) bound to broken DNA suggests that ZF2 plays the major role in DNA break recognition. But the X-ray structures of individual zinc fingers and the nearly full-length PARP1 (lacking ZF2 and BRCT domains) indicate that ZF2 is dispensable

for DNA binding (Langelier et al., 2011 and 2012). The structures also show different DNA binding modes. The individual zinc fingers bind DNA via the minor groove (Langelier et al., 2011), whereas the DBD structure binds DNA via the major groove (for details see 2.2.3). In addition, the DBD structure reveals that ZF1 engages in a hydrophobic interface between ZF1 and ZF2. This interface is possible due to dimerization of PARP1 molecules over the DNA break. The X-ray structures of individual zinc fingers and the nearly full-length PARP1 instead favor monomerization of PARP1 (for details see 2.2.3). These contrasting functions of zinc fingers require a comprehensive reevaluation in order to fully understand PARP1's binding to DNA and subsequent activation.

The mechanism of PARP1 activation has mainly been studied *in vitro*. However these biochemical and structural approaches do not account for the effect of cellular architecture on studied biochemical processes. The contribution of macromolecular crowding, confinement and adsorption are difficult to recapitulate in a sample tube (Minton, 2006). Yet PARP1's *in vivo* interactions with chromatin are affected by many soluble macromolecules, which foster or weaken PARP1's specific or non-specific interactions across multiple crowded micro environments. The *in vivo* insights into the mechanism of PARP1 activation and PARP1's association with chromatin in its dormant state are missing.

Therefore, I investigated the properties of PARP1's chromatin interactions using cellular and biophysical approaches. In particular, I aimed to:

o   Measure quantitatively, via diffusion-reaction models, PARP1's diffusion and chromatin associations with high spatiotemporal resolution.

o   Identify the minimal unit of PARP1 required for PARP1's binding to DNA/chromatin.

o   Identify specific roles of each of the two zinc fingers in the DNA Binding Domain with respects to binding initiation and control of a bound state, which is the prerequisite for PARP1 activation.

## 4.2 Towards the *in vivo* dynamics of PARP1 binding to DNA

My work on the molecular mechanism of PARP1 activation was facilitated by a collaboration with Dr. Lawrence Pearl from Sussex University (United Kingdom). The Pearl laboratory solved

the X-ray structure of DBD bound to a DNA duplex molecule with a single base 5´ overhang. The structure revealed which ZF1 and ZF2 residues are important for DNA binding (for more details see 2.2.3). As shown in Figure 4.1, the Arg34 (ZF1) and Arg138 (ZF2) are critical for zinc finger binding of DNA via the phosphate group. I mutated these residues (R34 and R138) from arginine to glutamic acid (R34E, R138E) and evaluated their importance in zinc finger binding of DNA.
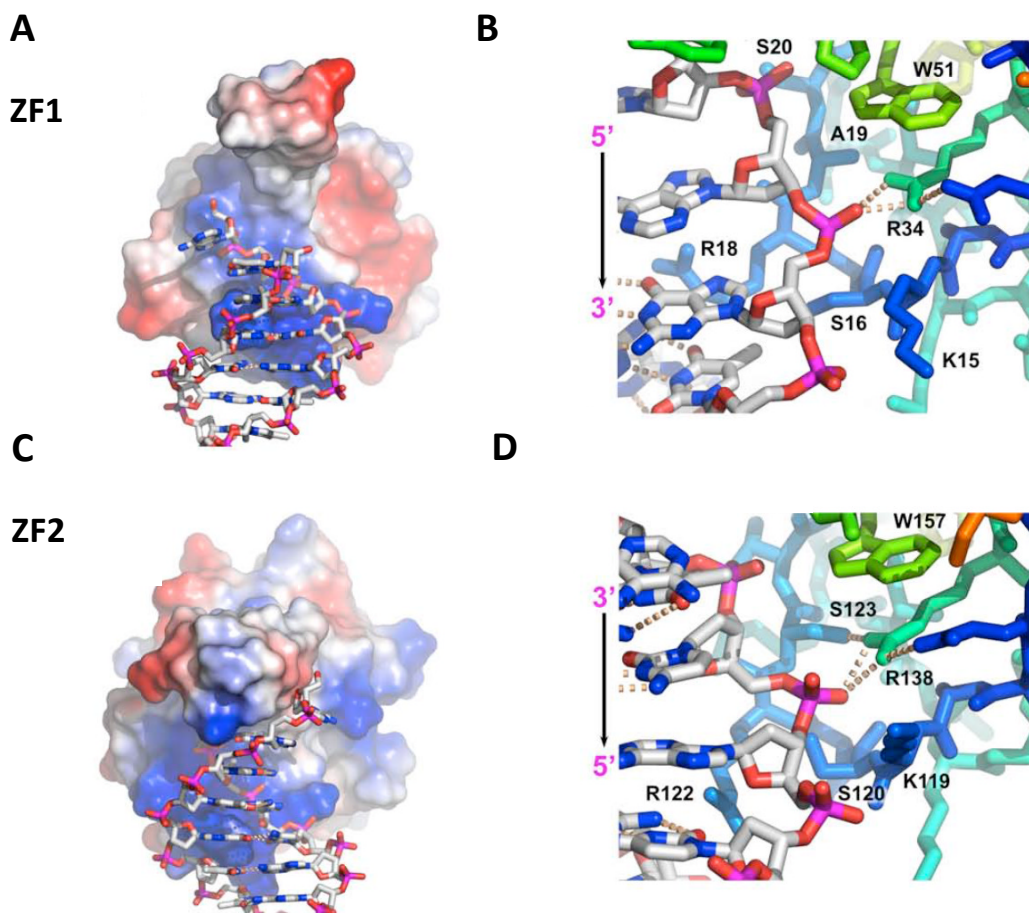

Figure 4.1 Interactions of PARP1 zinc fingers with DNA (modified from Ali et al., 2012). The interactions are based on the X-ray structure of DNA Binding Domain (DBD) bound to DNA with a single base 5´ overhang. **A)** Zinc finger 1 (Z**F1**) DNA-interacting surface (colored by electrostatic potential, with positive in blue and negative in red) interacts with the sugar-phosphate backbone of the overhanging strand and the major groove. **B)** Details of ZF1 and DNA interactions, centered on the polar interaction of Arg34 (R34) and a DNA phosphate group. **C)** Zinc finger 2 (**ZF2**) DNA-interacting surface (colored by electrostatic potential, with positive in blue and negative in red) interacts with the sugar-phosphate backbone of the recessed strand and the minor groove. **D)** Details of ZF2 and DNA interactions, centered on the polar interaction of Arg138 (R138) and a DNA phosphate group.

These single residue changes were introduced via site-directed mutagenesis of both PARP1 full-length (PARP1-FL) and DBD-only (PARP1-DBD) constructs. In addition, I obtained the constructs with individual domains deleted: zinc finger 1, zinc finger 2 or the catalytic domain (CD). All the constructs were tagged consistently on the carboxyl-terminus with enhanced green fluorescent protein (EGFP; Figure 4.2; for details see Materials and Methods). Together, the constructs provided eleven possible combinations for testing the importance of PARP1 domains in binding DNA and PARP1 activation.
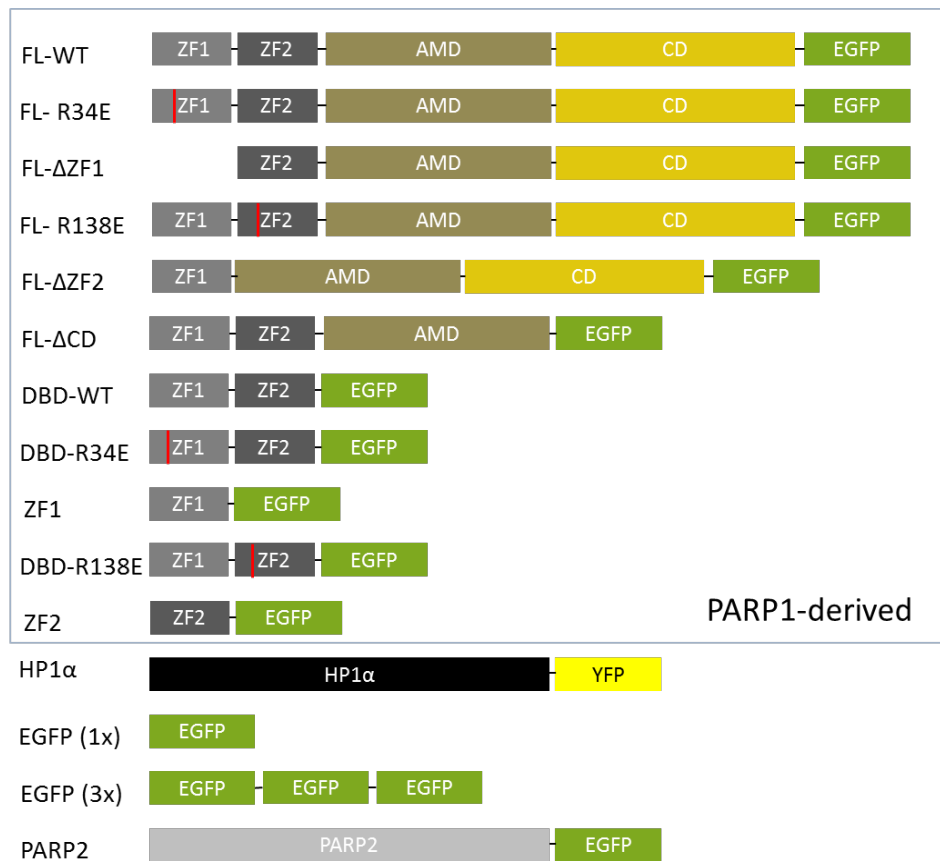

Figure 4.2 Schematic overview of the constructs investigated in this study. All constructs in the box are derived from poly-ADP-ribose polymerase 1 (PARP1). The used abbreviations correspond to: **AMD –** automodification domain, **CD –** catalytic domain, **ΔCD –**deletion of the catalytic domain, **DBD** – DNA Binding Domain, **FL -** full length, **R34E** – arginine to glutamic acid mutation of residue 34, **R138E** – arginine to glutamic acid mutation of residue 138, **WT -** wild type, **ZF1** – zinc finger 1, **ΔZF1-** deletion of the zinc finger 1, **ZF2-** zinc finger 2, **ΔZF2 –** deletion of the zinc finger 2, **HP1α -** heterochromatin protein 1 alpha, **EGFP-** enhanced Green Fluorescent Protein: monomeric (**1x**) and triple (**3x**), **PARP2** – poly-ADP-ribose polymerase 2, **YFP** – Yellow Fluorescent Protein. The domain composition was simplified. PARP1, PARP2 and HP1α were tagged on C-terminus with EGFP (PARP1 and PARP2) or YFP (HP1α). The red bar in zinc fingers indicates the introduced mutation.

The study was conducted in HeLa Kyoto cells with stably depleted endogenous PARP1 via siRNA-mediated knock down (previously created in the Ladurner laboratory). I confirmed the efficiency of the knock-down before and throughout the study (Figure 4.3).
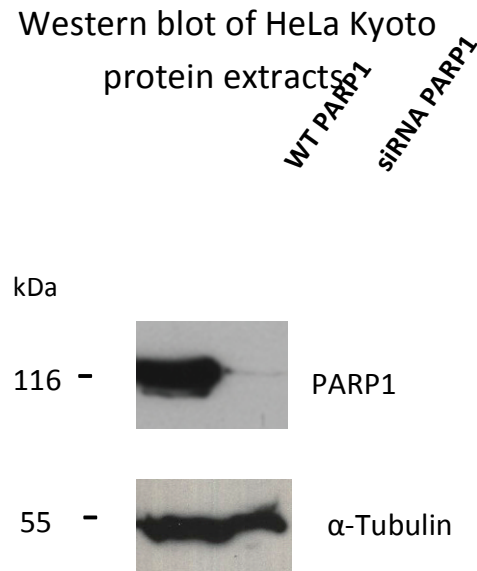
Figure 4.3 PARP1 is efficiently knocked-down in HeLa-Kyoto cell line with stable expression of siRNA anti-PARP1. Whole-cell protein extracts from HeLa-Kyoto *wild-type* (WT) cells (on the left) and Hela-Kyoto with stable expression of siRNA anti-PARP1 (siRNA PARP1) cells (on the right) were analyzed via SDS-PAGE and visualized by western blot with anti-PARP1 and anti-Tubulin (loading control) antibodies. Both antibodies detected proteins of the expected size: 116 kDa for PARP1 and 55 kDa for Tubulin. PARP1 is efficiently depleted in the HeLa Kyoto siRNA PARP1 cell line (upper panel). Loading of protein extract on SDS-PAGE was identical, as indicated by α-Tubulin levels (lower panel). Marker indicating the size of the protein is indicated on the left in kilodaltons (kDa). WT PARP1 corresponds to cells treated with non-target specific siRNA (mock control).

The generated PARP1 constructs were transiently expressed in these cells and only cells with very similar fluorescence intensity were chosen for the analysis. Upon transient expression, the PARP1 variants showed homogenous distribution across cell nuclei with enrichment within nucleoli, as expected from immunofluorescence staining of endogenous PARP1. The DBD constructs did not contain a nuclear localization signal (NLS), so as expected both nucleoplasmic and cytoplasmic localizations were observed (Figure 4.4).
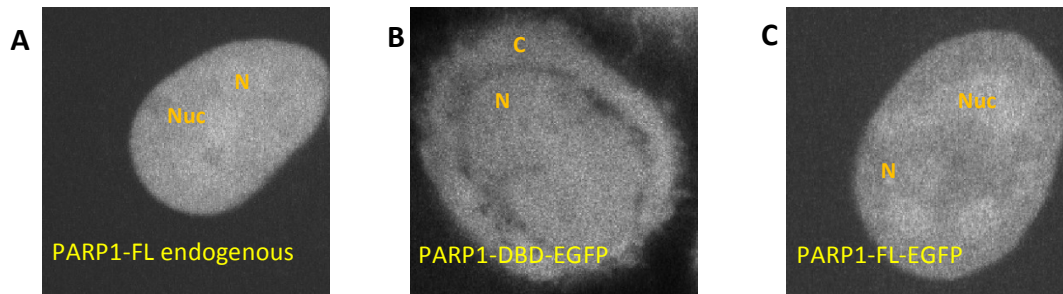
Figure 4.4 Evaluation of expression pattern of PARP1-FL and PARP1-DBD in HeLa cells. **A)** Endogenous poly-ADP-ribose polymerase 1 (**PARP1**) full length (**FL**) is homogenously distributed within nucleus (**N**), with partial enrichment in nucleolus (**Nuc**). PARP1 was detected with anti-PARP1 antibody via immunofluorescence (IF) conducted on fixed HeLa wild type cells. **B)** PARP1- DNA Binding Domain (**DBD**), fused to enhanced Green Fluorescent Protein (**EGFP**), is distributed within nucleus (**N**) and cytoplasm (**C**). **C)** PARP1-FL fused to EGFP shows identical cellular distribution to endogenous PARP1-FL. PARP1-DBD and PARP1-FL (B and C) were transiently expressed in HeLa Kyoto cells depleted of endogenous PARP1. The constructs were visualized via live cell imaging based on EGFP fluorescence. Showed photos are representative of all PARP1-DBD and PARP1-FL constructs used in this study. Fluorescent signal is shown in gray.

The generated PARP1 constructs were used in a comprehensive, spatio-temporal analysis of PARP1's mobility and binding to chromatin *in vivo*. I primarily used two fluorescence microscopy techniques: Fluorescence Correlation Spectroscopy (FCS) and Fluorescence Recovery After Photobleaching (FRAP). These two non-invasive methods are complementary to each other and ideal to probe PARP1's activation mechanism in living cells, as explained below.

4.3 Basis of Fluorescence Correlation Spectroscopy and Quantification

FCS requires that the protein of interest is fluorescently labelled, however it is not an imaging technique. FCS measures fluorescence intensity and its fluctuations in time. Because PARP1 is fluorescently labelled with EGFP, upon laser excitation, PARP1-EGFP becomes a source of fluorescence intensity via emission. This intensity is not stable in time, because proteins are mobile and they leave or enter the position (confocal volume) where the measurement is taken with variable frequency. Thus, mobility of labelled proteins is a source of fluorescence intensity fluctuations. The average length and amplitude of these fluctuations are determined by a temporal autocorrelation analysis. The FCS results are represented as ACF - autocorrelation function curve - $G(\tau)$, which provide information on the number of tested molecules (Y-axis) and the mean diffusion time (τ) in microseconds (μs) that the molecules spend in the observation volume (X-axis; Figure 4.5). In summary, FCS measures the fluctuations, which can be

biophysically modeled to determine the mobility (diffusion) of the fluorescently tagged protein. Mobility of proteins can change for example by binding to chromatin (Wachsmuth et al., 2008).

## A scheme representing the typical steps in FCS analysis
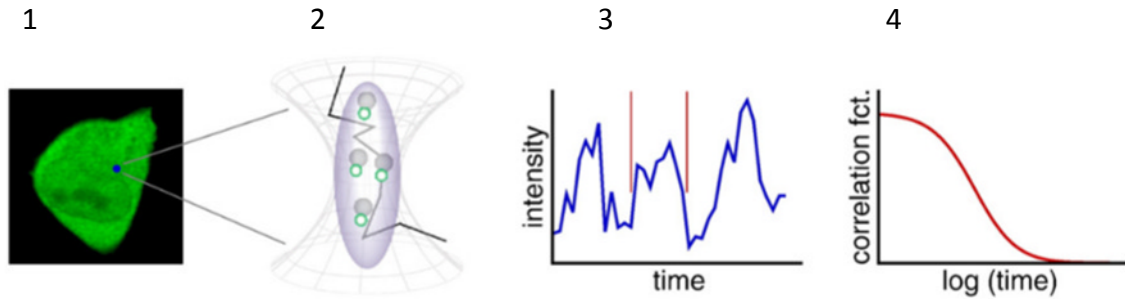
Figure 4.5 Fluorescence Correlation Spectroscopy (FCS) monitors fluctuations in fluorescence intensity in time (modified from Wachsmuth et al., 2008). **1)** A cell contains a fluorescently labelled protein (green). A laser is focused within the cell (blue dot) and a measurement of fluorescence is acquired. **2)** A magnified view of the confocal focus (the place where the laser is placed and the measurement taken), across which fluorescently tagged proteins can enter and leave, as shown by black line trajectories. The protein of interest (gray circle) is tagged with a fluorescent protein e.g. EGFP (green circle). **3)** Movement of fluorescently tagged proteins results as fluctuation of fluorescence intensity in time. **4)** Intensity fluctuations are represented as a graph: the autocorrelation function curve of number of molecules (Y-axis) and time (X-axis).

At first, the FCS results can be analysed qualitatively. A qualitative difference in mobility between two proteins or two tested conditions will be represented by a distinctive separation of the FCS curves when plotted together. As shown in Figure 4.6, the investigated pentameric EGFP diffuses slower in the nucleolus (higher τ) than in the nucleus (lower τ). The difference in diffusion of pentameric EGFP is caused by the higher molecular crowding environment in the nucleolus (Bancaud et al., 2009).

In addition to qualitative analysis, the FCS results could be fitted with biophysical models. The modelling of FCS data allows quantification of the mean time (µs) spent by the investigated protein in the confocal volume, **the diffusion time (τ).** Identification of the mean diffusion time value enables calculation of the **diffusion coefficient (D**, µm^2/sec) for each of the proteins tested. Lower diffusion time will correspond to a higher diffusion coefficient. FCS offers a high temporal resolution in a scale of microseconds (µs) thus even small changes in mobility among tested proteins can be detected (Wachsmuth et al., 2008).

Qualitative diffusion difference measured by FCS
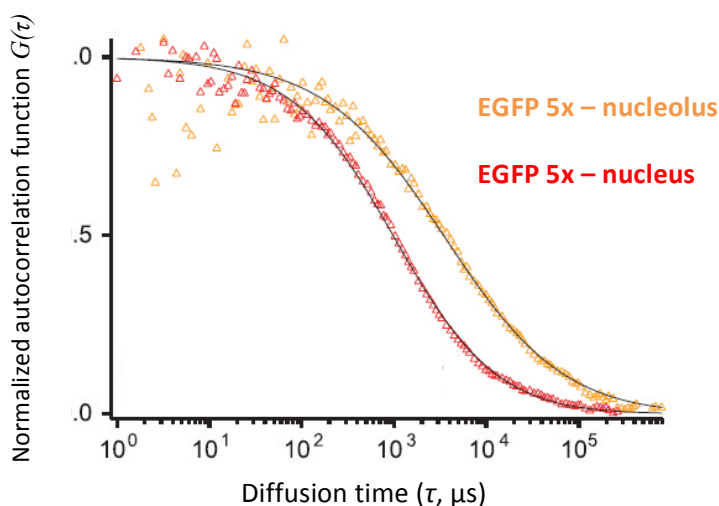
Figure 4.6 Pentameric EGFP (5x) diffuses slower in nucleolus (orange) than it diffuses in nucleus (red) (modified from Bancaud et al., 2009). Autocorrelation function curves (normalized to 1 - representing 100 % of molecules) are distinctive and separated in diffusion time (τ) due to different molecular crowding in nucleus and nucleolus. The mobility of EGFP 5x is reduced and thus FCS curve is shifted to the right, when compared with the FCS curve of EGFP 5x in the nucleus. Measured FCS data (red and orange triangles) are fitted only with a trend line.

The standard models used for FCS fitting are: anomalous diffusion model with one component and anomalous diffusion model with two components. Each component represents a population that can be characterized by the same mean diffusion time. If fitting of the model with measured data results in detection of one component, it means that all measured molecules undergo a homogenous behavior, for instance free diffusion. If two components (two populations) were detected, it means that measured molecules undergo heterogenous behavior, for instance: diffusion (first component) and diffusion coupled with binding (second component). Kinetic modeling of FCS data allows one to determine a percentage of molecules belonging to each component (Michelman-Ribeiro et al., 2009; for details see Materials and Methods). In my FCS experiments, I used two previously characterized controls: enhanced Green Fluorescent Protein (EGFP) and heterochromatin protein 1 alpha (HP1α). EGFP does not bind to chromatin, thus it served as a negative control. HP1α was shown to associate with chromatin, thus it served as a positive control (diffusion plus chromatin binding).

FCS data representative of EGFP and HP1α

A

B
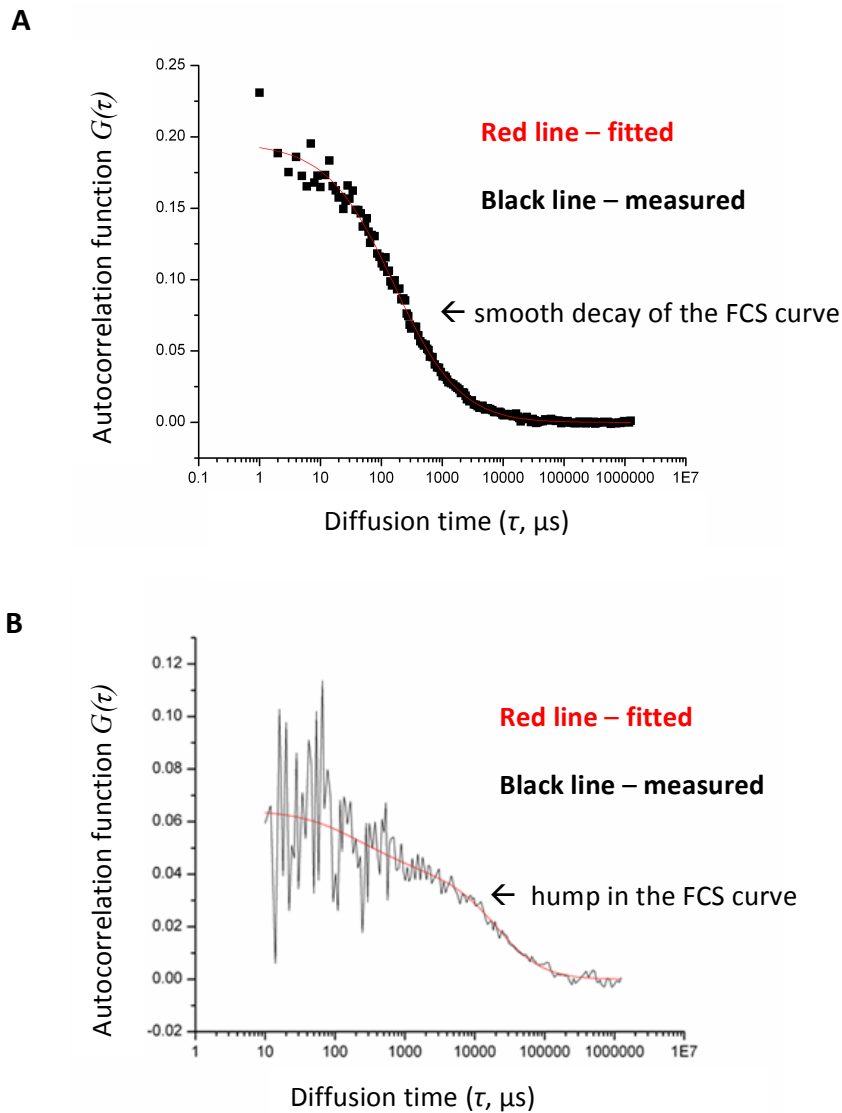
Figure 4.7 Representative fitting of EGFP and HP1α FCS measurements with anomalous diffusion model. A) The FCS curve of EGFP has a typical smooth decay typical for the samples with one component only. **B)** The FCS decay curve for HP1α has a typical hump, suggestive of two components and indeed the best fit of HP1α FCS measurements was achieved with two component anomalous diffusion model. The construct names indicate: **EGFP** – enhanced Green Fluorescent Protein, **HP1α** – heterochromatin protein 1 alpha. FCS measurements were conducted in: (i) HeLa Kyoto (siRNA PARP1) cells transiently transfected with EGFP (24 hours) and (ii) U2OS cells stably expressing HP1α-YFP. FCS measurements were acquired only within nuclei at randomly chosen positions avoiding the nucleoli and nuclear periphery (n > 15 cells per construct).

EGFP and HP1α were fitted with one and two component anomalous diffusion models, respectively (Figure 4.7). The identified mean diffusion time and diffusion coefficients for both controls in my experiments were consistent with previously reported results (Wachsmuth et al., 2000, Müller et al., 2009).
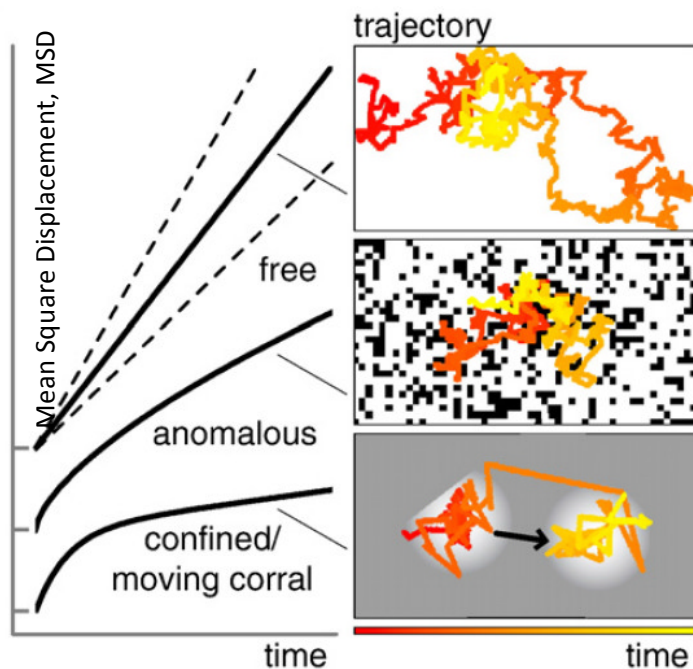
Figure 4.8 Types of diffusion (from Wachsmuth et al., 2008). Time trajectory of a molecule is represented by color transition from red (beginning) to yellow (end). The diffusion types: **Free diffusion** with a linear correlation of distance and time. **Anomalous diffusion** occurs in the presence of (randomly organized) obstacles where the distance deviates from linear correlation with time. The area covered by molecules is smaller. In the case of **confined diffusion**, the motion of a particle is restricted to the highlighted confinement area. The distance does not change significantly in time.

In addition to the quantification of the **diffusion time (τ)**, the fitting of measured FCS data with kinetic models identifies the **anomaly parameter (α).** Each protein diffuses across a certain area of space. This movement in space is measured in square micrometers per second (μm^2/sec), the unit representing the **diffusion coefficient** (**D**). The anomaly parameter refers to diffusion of observed proteins taking consideration of space and time and their mutual correlation. So, for each diffusing protein a correlation between a diffused distance (mean square displacement, MSD) and time needed for it can be calculated. For freely diffusing molecules, the correlation between the distance and time is linear. In such a case, the anomaly parameter is equal to 1.

However when diffusion slows down for example due to chromatin binding, the correlation between distance and time is no longer linear. The anomaly parameter is thus not equal to 1, but it deviates towards 0 or above 1 ($\alpha < 1$, or $\alpha > 1$; Figure 4.8; Wachsmuth et al., 2003 and 2008). In my experiments, the measured anomaly parameter for EGFP was 1 ($\alpha = 1$) and HP1α above 1 ($\alpha > 1$), which agreed with previously reported results (Wachsmuth et al., 2000, Müller et al., 2009).

4.4 PARP1-DBD primarily diffuses within the nucleus, with weak chromatin associations

The PARP1 protein is composed of three functional fragments: a DNA binding domain (DBD), an automodification domain (AMD) and a catalytic domain (CD). An *in vitro* evaluation of the DNA binding affinity of each of these fragments indicated that the DBD has the highest affinity towards DNA. The AMD showed only weak affinity towards DNA and the CD did not bind DNA at all (for details see 2.2.2 and 2.2.4). The role of the DBD and its affinity to chromatin *in vivo* however is not known. Therefore to directly test it, I used FCS to analyze the diffusion and chromatin binding of the DBD in living cells. The FCS analysis of PARP1 DBD constructs was conducted in cells during interphase, under normal cell culture conditions, with no external stimuli. In this condition, nuclear PAR is not detectable by immunofluorescence (IF) with antibodies against PAR (see Figure 5.5 A).

At first, I evaluated via FCS the DBD-WT (wild type), and found the mobility to be as high as that of EGFP (a negative control). A high mobility means that DBD-WT molecules diffuse rapidly within the nucleus. The FCS measurements of DBD-WT and EGFP formed two distinct populations when plotted as the autocorrelation function (ACF; Figure 4.9). However this distinction in slightly different diffusion time (X-axis) is not a true indication of the differences in diffusion, due to the different size of the evaluated molecules. The bigger DBD molecules (44 kDa, including EGFP) are less mobile than smaller EGFP molecules (27 kDa).

Qualitative FCS comparison between DBD and EGFP diffusion

DBD-WT measurements

EGFP measurements
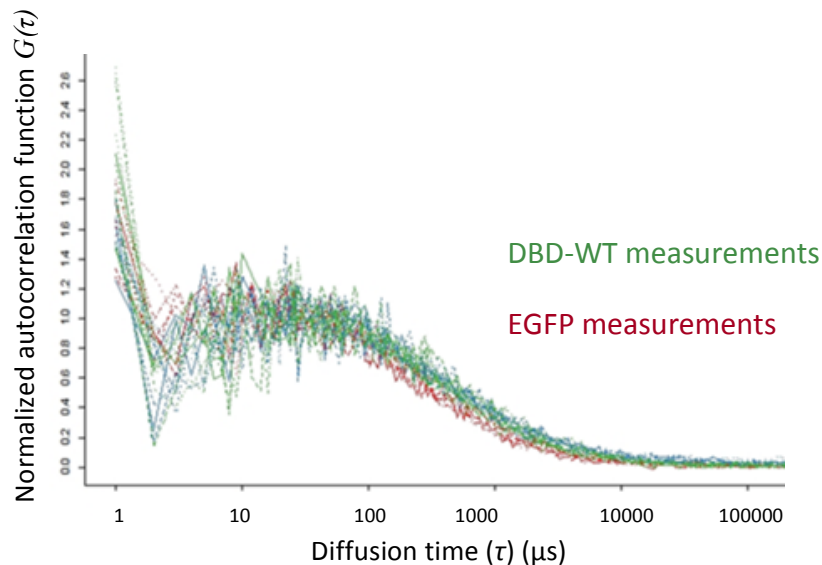
Figure 4.9 Mobility of PARP1-DBD is similar to EGFP molecule within nucleus. HeLa Kyoto siRNA PARP1 cells were transiently expressed (24 hours) with PARP1-DBD-EGFP or EGFP. The mobility of the transfected constructs was evaluated with FCS. The results were plotted as autocorrelation function normalized to 1, representing 100 % of molecules (Y-axis), τ - time spent in a confocal volume (observation volume; X-axis). **DBD-WT** – PARP1 DNA Binding Domain wild-type (**green**); **EGFP** – enhanced Green Fluorescent Protein (**red**). Each ACF curve represents a single FCS measurement in a new cell (n > 20 cells per construct).

The mobility of EGFP in living cells is unobstructed, meaning that EGFP freely diffuses within the nucleus with no binding to chromatin or other proteins (Wachsmuth et al., 2000). Similar FCS results between DBD-WT and EGFP suggested that DBD-WT does not bind extensively to chromatin. In order to evaluate this, FCS was conducted on DBD constructs with mutagenized single residues crucial in DNA binding (R34E and R138E). In addition the FCS measurements were biophysically modelled. The best fit of DBD measurements was with one component anomalous diffusion model. All the DBD constructs (wild-type, R34E and R138E) have similar mean diffusion time (τ) ~ 600 microseconds ± 150 microseconds (Figure 4.10). An introduction of the mutation into either of the two zinc fingers did not change the mobility of the DBD. To rule out a possibility that perhaps one zinc finger mediates short-lived interactions with chromatin, individual zinc fingers were tested as well. The resulting diffusion times for ZF1 and ZF2 are lower than for the DBD, but again the size of the ZFs plays a role (~35 kDa, including EGFP). Thus decrease of diffusion time is caused by the size of ZF vs. DBD (Figure 4.10).
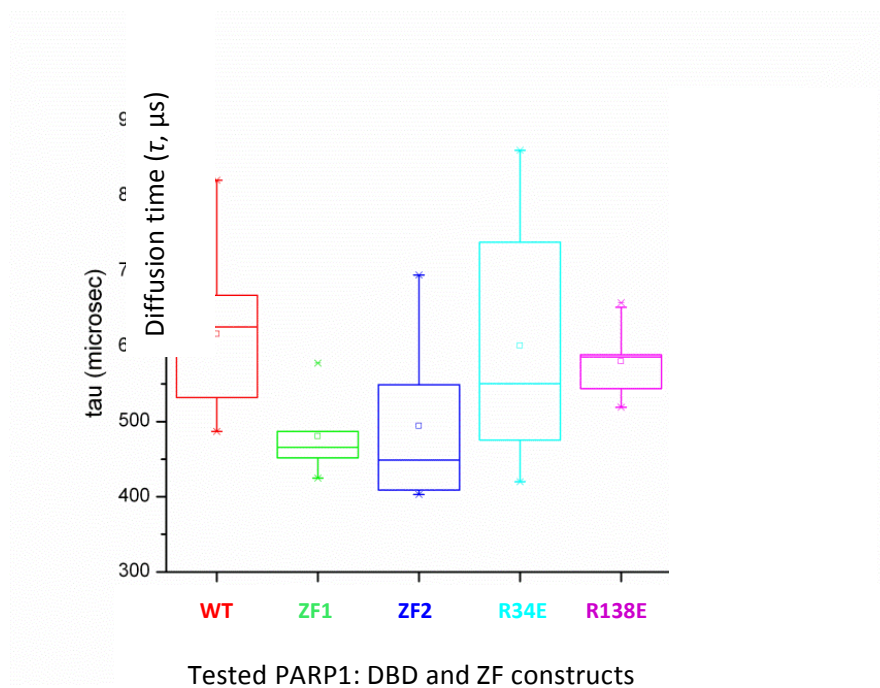
Figure 4.10 PARP1-DBDs require similar diffusion time to diffuse across the measured position (confocal volume). HeLa Kyoto siRNA PARP1 cells were transiently transfected (24 hours) with individual **PARP1-DBD-EGFP** constructs or individual **PARP1-ZF-EGFP** (X-axis): **WT** – wild-type (red), **ZF1** - zinc finger 1 (green), **ZF2** – zinc finger 2 (dark blue), **R34E** – DNA Binding Domain with single residue mutation R34E (light blue), **R138E** – DNA Binding Domain with single residue mutation R138E (pink). The mobility of transfected constructs was evaluated with FCS. The curve fitting yielded mean diffusion time (τ) across the confocal volume. Each box plot is composed of FCS measurements taken in more than 10 cells. In each cell the measurement was taken in 3 randomly chosen sites in the nucleus avoiding nucleoli and nuclear periphery. Only cells with similar fluorescence intensity were selected. The horizontal lines (whiskers) represent the maximum and minimum values, the box signifies the upper (75th) and lower quartiles (25th), the median is represented by a short line within the box and the mean is represented by a square within the box.

A calculation of mean and comparison of diffusion coefficients between the constructs further confirms low binding of the DBD to chromatin. The diffusion coefficients (*D*) of the tested DBDs are not significantly different, taking into account the standard deviation (SD): DBD-WT with *D* = 13.50, ± 3.04 μm^2/sec, DBD-R34E with *D* = 11.57 ± 3.54 μm^2/sec, and DBD-R138E with *D* = 13.72 ± 1.5 μm^2/sec (Table 4.1). In summary, this data suggests that the DBD *in vivo,* unlike *in vitro,* does not bind extensively or retain on chromatin. If DBD engaged with

chromatin, these interactions would have to be infrequent and undetectable in comparison to predominant diffusion.

Table 4.1 Summary of FCS results for PARP1: DNA Binding Domain (DBD) and zinc fingers (ZFs).

| Tested protein	Diffusion coefficient (D) mean ± SD* (μm^2/sec)	Anomaly parameter (α) mean ± SD*
PARP1-DBD-wild type	**13.50** ± 3.04	0.92 ± 0.07
PARP1-DBD-mutated (R34E)	**11.57** ± 3.54	1.00 ± 0.07
PARP1-DBD-mutated (R138E)	**13.72** ± 1.50	0.98 ± 0.05
PARP1-zinc finger 1	**17.23** ± 2.48	0.95 ± 0.05
PARP1-zinc finger 2	**18.00** ± 5.72	0.98 ± 0.07
(1x) EGFP (negative control)	**23.14** ± 3.87	1.00 ± 0.05

*SD-Standard Deviation.

4.5 PARP1-FL primarily diffuses within the nucleus, with weak chromatin associations

An *in vitro* evaluation of the DNA binding affinity of PARP1 full-length and PARP1 DNA Binding Domain indicated that the full-length binds DNA with up to several fold higher affinity than DBD (for details see 2.2.4). Thus, it can be that in a crowded *in vivo* environment the DBD alone is not stable in binding to, or cannot be retained, on chromatin, and therefore the high diffusion coefficient for DBD-WT was observed. It could be that other domains of PARP1 are important for *in vivo* DNA binding by PARP1. I directly tested this using the same approach and same cellular conditions as for FCS tests of DBD constructs. I tested analogous constructs like DBDs however in PARP1 full-length context. The results of FCS were biophysically modelled and the best fit was achieved with one component anomalous diffusion model.

The PARP1 full-length wild-type molecules surprisingly again showed a relatively high mean diffusion time, and the DNA binding mutants were not significantly different. All the full-length constructs, including the proteins with deleted individual zinc fingers had a similar mean diffusion time of ~ 1800 ± 150 microseconds (Figure 4.11). The FCS analysis of heterochromatin protein 1 alpha (HP1α) revealed two fractions of molecules via a fit with two component anomalous diffusion model, in agreement with previously published results (Müller et al., 2009). HP1α is a protein well-known to bind chromatin: the first fraction of HP1α

represents molecules that are predominantly diffusing, and the second fraction with the mean diffusion time above 31 milliseconds represents HP1α bound to chromatin (see Figure 7.2).

FCS analysis of PARP1-FL diffusion times
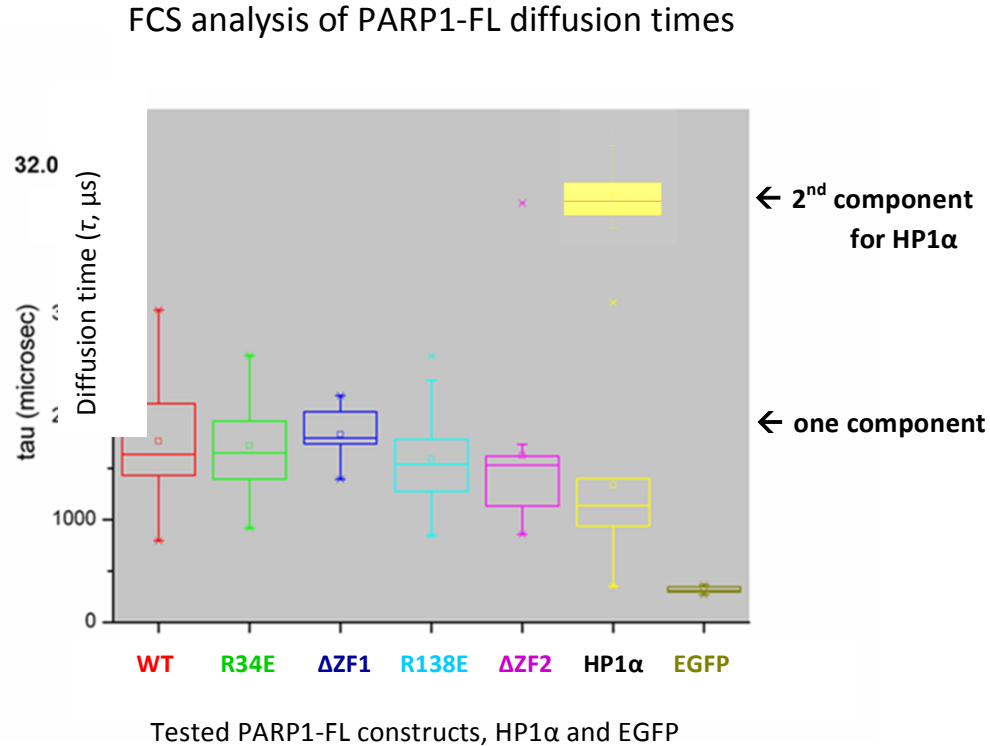
Figure 4.11 PARP1 full-length (FL) constructs require similar diffusion time to diffuse across the confocal volume. HeLa Kyoto siRNA PARP1 cells were transiently transfected (24 hours) with individual PARP1-FL-EGFP constructs: **WT** – wild-type (red), **R34E** – single residue mutation R34E (green), **ΔZF1** – deleted zinc finger 1 (dark blue), R138E –single residue mutation R138E (light blue), ΔZF2 –deleted zinc finger 2 (pink). **HP1α**– heterochromatin protein 1 alpha, and **EGFP** – monomeric enhanced Green Fluorescent Protein were also FCS tested and plotted. Each box plot is composed of FCS measurements taken in at least 15 cells. In each cell the measurement was taken in 3 randomly chosen sites in the nucleus avoiding nucleoli and nuclear periphery. Only cells with similar fluorescence intensity were selected. The horizontal lines (whiskers) represent the maximum and minimum values, the box signifies the upper (75th) and lower quartiles (25th), the median is represented by a short line within the box and the mean is represented by a square within the box. The second component for HP1α was superimposed, for detailed view see Figure 7.2.

The high mobility of the PARP1 full-length molecule is consistent with the observed high mobility of PARP1-DBD. The difference in the mean diffusion time is caused by size differences: PARP1-FL (143 kDa) and PARP1-DBD (44 kDa). These FCS results indicate that PARP1 *in vivo* is a protein that is predominantly not associated with chromatin, in contrast to the *in vitro* results. Quantification of a diffusion coefficient for each of the full-length PARP1

constructs (Table 4.2) further supports a conclusion that PARP1 in unstimulated cells (no excessive DNA damage) does not bind stably to chromatin and freely diffuses within the nucleus with $D = 4.64 \pm 1.04$ μm^2/sec.

Table 4.2 Summary of FCS results for PARP1-FL (full length) constructs.

| Tested protein	Diffusion coefficient (D) mean ± SD* (μm^2/sec)	Anomaly parameter (α) mean ± SD*
PARP1-FL-wild type	**4.64** ± 1.04	0.89 ± 0.05
PARP1-FL-mutated (R34E)	**4.93** ± 1,41	0.94 ± 0.07
PARP1-FL-Δ zinc finger 1	**4.51** ± 0.69	0.90 ± 0.07
PARP1-FL-mutated (R138E)	**5.15** ± 1.16	0.90 ± 0.06
PARP1-FL-Δ zinc finger 2	**5.90** ± 1.20	0.93 ± 0.05
HP1α (1st component; positive control)	**6.74** ± 2.73	0.98 ± 0.06
HP1α (2nd component; positive control)	**0.28** ± 0.08	>1.00
(1x) EGFP (negative control)	**23.14** ± 3.87	1.00 ± 005

*SD-Standard Deviation.

4.6 Free diffusion is characteristic of all nuclear PARP1 molecules

The identification of PARP1 molecules as freely diffusing and not bound to chromatin *in vivo* was surprising. *In vitro* findings suggest that PARP1 is chromatin-associated, thus I considered possible limitations of FCS that could potentially affect the *in vivo* understanding of PARP1 interactions with chromatin. FCS is an approach that can investigate from 1 to 1000 molecules present within the region of interest, at width of ~ 200 nanometers. The highest temporal resolution of FCS is 1 second. I considered a hypothetic scenario, where perhaps some PARP1 molecules are chromatin-associated, even longer than the detectable second component of HP1α protein (Figure 4.11 and 7.2). If this was the case, it would be possible that FCS measurements missed the PARP1 chromatin-associated molecules. Therefore, I investigated diffusion of all PARP1 molecules present in nuclei via Fluorescence Loss in Photobleaching (FLIP).

FLIP is an imaging technique that measures redistribution of fluorescent proteins in time. The fluorescence intensity is continuously decreased via photobleaching (high laser intensity illumination). A repetitive series of photobleaching alternates with a repetitive time series of images that record fluorescence redistribution. Usually, one bleach cycle is followed by one image acquisition cycle until the fluorescence is completely depleted. The loss of fluorescence intensity (Y-axis) is recorded in time (X-axis). The results thanks to the steepness of the curve

allow one to qualitatively distinguish between molecules that diffuse within the nucleus, from those that do not diffuse but for example are bound to chromatin (Figure 4.12; Wachsmuth et al., 2008).

A scheme representing typical steps in FLIP
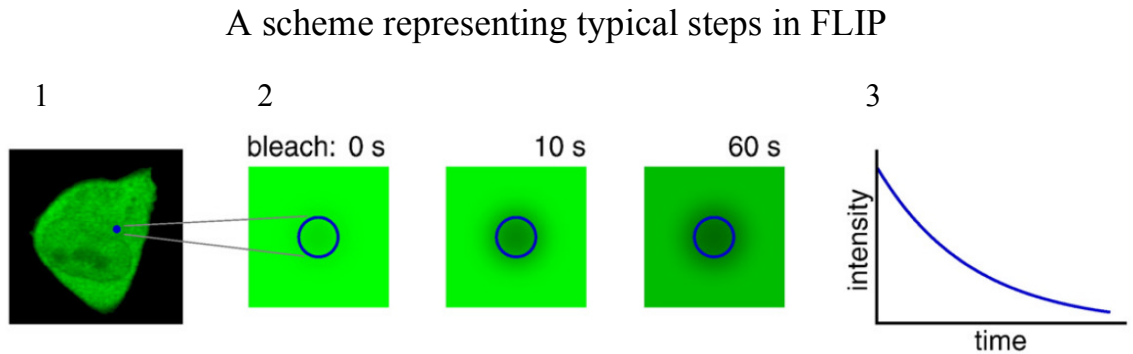
Figure 4.12 Fluorescence Loss in Photobleaching (FLIP) monitors redistribution of fluorescence intensity (modified from Wachsmuth et al., 2008). **1)** A cell contains a fluorescently labelled protein (green). A pre-bleach time series of images is acquired in a state of equilibrium, where fluorescence intensity is evenly distributed within a cell. The initial level of fluorescence intensity is normalized to 1 representing 100 % of the signal. **2)** A magnified view of the confocal focus. In a region of interest (ROI), the fluorescence is reduced via a rapid photobleach (high intensity laser illumination). The bleached ROI is seen as a black circle depleted of fluorescence. Usually one bleach cycle is followed by one image acquisition cycle untill the fluorescence is completely depleted. **3)** The change of fluorescence intensity (Y-axis) in time (X-axis) is plotted as a FLIP curve.

In case of free diffusion of molecules like EGFP, the fluorescence signal is depleted in the order of minutes. When proteins are characterized by diffusion coupled with binding interactions, the fluorescence signal is depleted in a significantly longer time. The FLIP experiments determined that PARP1-EGFP signal is completely lost in 600 seconds (Figure 4.13). Triple EGFP (81 kDa), with no interaction partners, was photobleached only slightly faster (500 seconds). PARP2 (90 kDa, including EGFP) of a similar size to EGFP, is photobleached in a similar time as EGFP. This result confirms that there are no tightly chromatin-bound subpopulations of PARP1 that could have been missed with FCS. PARP2 contains DNA-binding motifs, however PARP2 molecules showed a similar behavior to PARP1. This suggests that lack of chromatin association by nuclear PARPs could be shared within the PARP family.

FLIP analysis of PARP1, PARP2 and EGFP (3x) mobility
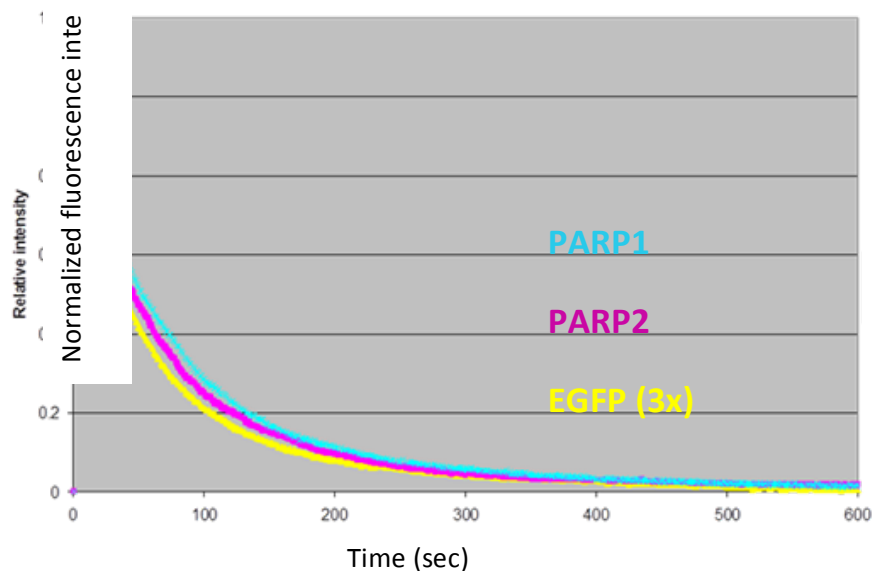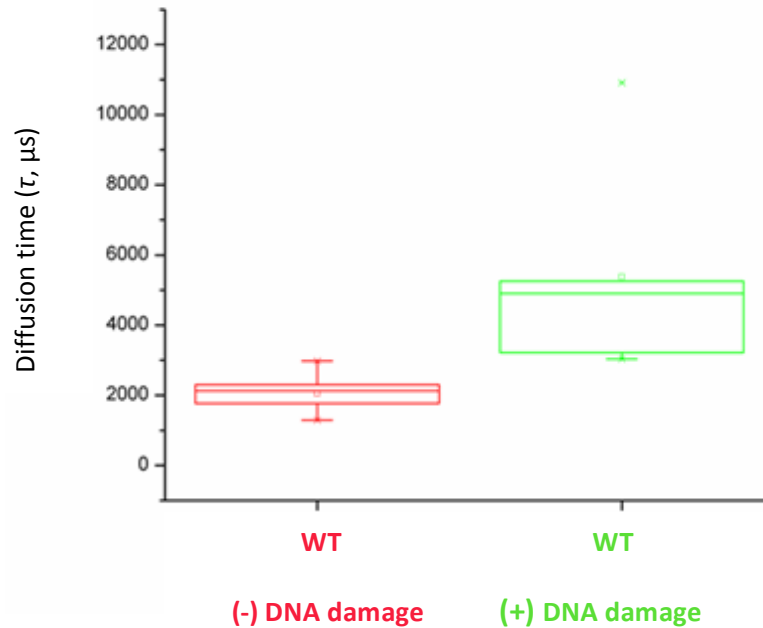

PARP1

PARP2

EGFP (3x)

Figure 4.13 FLIP confirms that PARP1 is freely diffusing protein. Mobility of PARP1-FL-EGFP, PARP2-EGFP and EGFP (3x) were analyzed via fluorescence loss in photobleaching (FLIP). Experiments were conducted in HeLa Kyoto (siRNA PARP1) cells transiently transfected with **PARP1** (light blue) **PARP2** (pink) and **EGFP (3x)** (yellow) constructs. The fluorescence (normalized to 1, Y-axis) of all constructs was depleted within 600 seconds or less, as was the case for EGFP (X-axis) suggesting that none of the proteins is tightly bound to chromatin. Each curve is an average of at least 10 measurements for each condition.

4.7 PARP1 binds to DNA upon induction of DNA damage

According to the established model, PARP1 is activated upon binding to a DNA break. Under the standard cell culture conditions deprived of stressful stimuli like heat shock or DNA damage, PAR levels are not detectable. Upon induction of DNA damage, for example via laser irradiation, PARP1 binds to DNA breaks and PAR cellular levels are rapidly elevated (see Figure 2.11). From the kinetic modelling, I knew that my FCS measurements are conducted on a number of molecules from 50 to 200 within a ~ 200 nanometer-wide confocal volume (for details see Materials and Methods). Thus, I considered the possibility that there are not enough DNA target sites (DNA breaks) across the genome for PARP1 to bind under standard cell culture conditions. I tested this hypothesis via FCS measurements on cells that underwent DNA damage. Single and double-stranded DNA breaks were induced within the whole nucleus with a 405 nanometer laser (for details see Materials and Methods). The FCS measurements were acquired,

immediately following DNA damage induction. Strikingly, the fitting of FCS results with one component anomalous diffusion yielded 2.6-fold increased values of diffusion time for PARP1-WT molecules (Figure 4.14).

FCS analysis of PARP1-FL diffusion times upon DNA damage

Figure 4.14 PARP1-full length-wild type molecules undergo diffusion coupled with binding upon DNA damage induction. HeLa Kyoto siRNA PARP1 cells were transiently transfected (24 hours) with PARP1-FL-WT construct. FCS measurements were taken in two conditions: **no DNA damage (red)** and **DNA damage (green)**. The DNA damage was induced with a 405 nm laser on cells pretreated with Hoechst 33342 (final concentration: 0.1 μg/ml) for at least 10 minutes. Each box plot is composed of FCS measurements taken in at least 10 cells. In each cell the measurement was taken in 3 randomly chosen sites in the nucleus avoiding nucleoli and nucleus periphery. Only cells with similar fluorescence intensity were selected. The horizontal lines (whiskers) represent the maximum and minimum values, the box signifies the upper (75th) and lower quartiles (25th), the median is represented by a short line within the box and the mean is represented by a square within the box.

The increase of diffusion time suggests that under DNA damage PARP1 undergoes a transition from freely diffusing protein (no DNA damage) to a protein with limited diffusion. This means that PARP1 could bind chromatin frequently. Under DNA damage, it was possible to fit PARP1 FCS data with two component anomalous diffusion similarly to HP1α. The outcomes were the

following: the first freely diffusive fraction was present in the majority (at least 64 % of molecules) and the second fraction which underwent diffusion coupled with binding started to be detectable (up to 36 % of molecules). The diffusion time of the second fraction was in the range of 20 – 200 milliseconds (data not shown). These FCS experiments of PARP1 diffusion post-DNA damage induction were however difficult to conduct, due to high photobleaching of PARP1-EGFP molecules while FCS measurements were acquired. Thus, many measurements had to be discarded during the analysis. FCS therefore was no longer an adequate technology to reliably investigate mobility of the remaining PARP1-FL constructs. FCS measurements are suitable to investigate interactions of molecules which are short lived, below 1 second in time (Michelman-Ribeiro et al., 2009). Upon increase of DNA binding sites due to DNA damage, PARP1 presumably becomes immobilized on chromatin and apparently the mean diffusion time in a confocal volume exceeds the upper limit of FCS. Therefore a different complementary approach had to be deployed. I continued the analysis with use of FRAP, which has a time resolution over 1 second (from a few seconds to a few minutes).

4.8 Two functional ZFs are essential and sufficient for PARP1 to bind DNA

A free diffusion of PARP1-DBD and PARP1-FL constructs was explicitly evaluated via FCS in no DNA damage conditions. I employed FRAP to test PARP1-DBD and PARP1-FL construct (wild type and DNA binding mutants) diffusion and chromatin binding under laser-induced DNA damage condition.

FRAP is an imaging technique that measures redistribution of fluorescent proteins in time. The first images (pre-bleach) are taken when a cell is in the state of equilibrium. This series of images serves for normalization purpose where 100 % of fluorescence intensity is represented as 1. At equilibrium, the fluorescently tagged proteins are evenly distributed within a cell, according to the endogenous protein localization. This equilibrium is perturbed via a photobleach (high laser intensity illumination) of fluorescence in the selected region of the cell (region of interest, ROI). The bleach results in spatial reduction of fluorescence intensity in ROI. Post-bleach, a series of images is taken in order to record the redistribution of fluorescence intensity from the non-bleached region to the bleached region. Observation is continued until the fluorescence equilibrium is reached again. This redistribution of fluorescence intensity (Y-axis) is recorded in time (X-axis) and plotted as a FRAP recovery curve (Figure 4.15; Wachsmuth et al., 2008). The

redistribution of fluorescence intensity can change by diffusion and binding of the investigated protein. Thus FRAP is ideal to study PARP1 *in vivo* interactions with chromatin. The FRAP data can be biophysically modelled.

A scheme representing the typical steps in FRAP
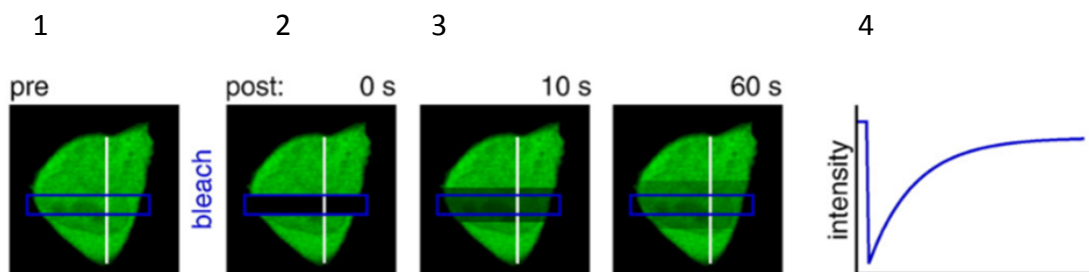
Figure 4.15 Fluorescence Recovery After Photobleaching (FRAP) monitors redistribution of fluorescence intensity (modified from Wachsmuth et al., 2008). **1)** A cell contains a fluorescently labelled protein (green). A pre-bleach time series of images is acquired in a state of equilibrium, where fluorescence intensity is evenly distributed within a cell. **2)** In a region of interest (ROI), the fluorescence is reduced via a rapid bleach (high intensity laser illumination). The bleached ROI is seen as a black stripe across the cell. **3)** The post-bleach time series of images is acquired until the equilibrium is reached again. The grey stripe represents diffusion of fluorescent molecules from non-bleached region to the bleached region. **4)** The change of mean fluorescence intensity (Y-axis) in time (X-axis) is plotted as a FRAP curve.

At first, I tested the diffusion and binding of PARP1-DBD molecules: wild-type and DNA binding mutants (R34E and R138E). Prior to the FRAP measurements, the cells underwent DNA damage induction via a laser treatment exclusively within the nucleus (for details see Materials and Methods). Upon induction of DNA breaks, the DBD-WT molecules showed full fluorescence recovery in about 15 seconds. Under the same DNA damage conditions, the DBD DNA binding mutants (R34E or R138E) showed full fluorescence recovery in only 6 seconds. The diffusion of DNA binding mutants was identical to diffusion of DBD-WT mutants but in no DNA damage conditions (Figure 4.16). Thus, only the DBD-WT with two functional zinc fingers showed reduced diffusion upon DNA damage conditions. A mutation of any of the residues important for the DNA binding by DBD, results in no change in diffusion. Thus these results suggest that DBD-WT undergoes slower diffusion because of temporal immobilization due to

DNA break recognition and binding. This result suggested that both functional zinc fingers are essential for DNA binding by DBD (Figure 4.16).

FRAP analysis of PARP1-DBD under DNA damage conditions
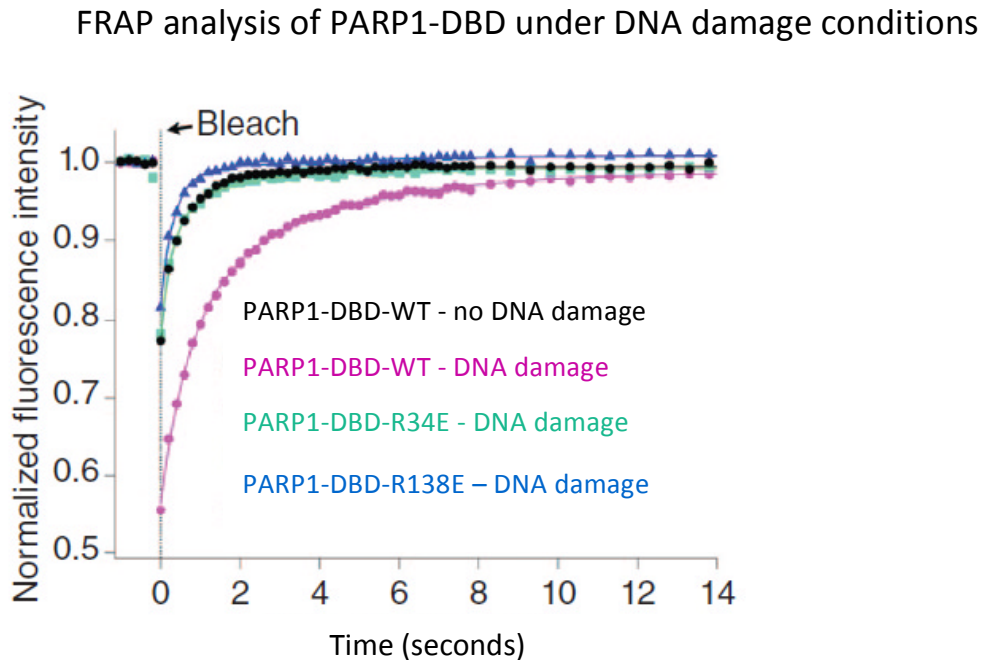
Figure 4.16 Only PARP1-DBD-WT binds DNA upon induction of DNA damage. FRAP experiment were conducted in HeLa Kyoto cells (siRNA PARP1) which transiently expressed individual DNA Binding Domain (DBD) poly-ADP-ribose polymerase 1 (PARP1) constructs: WT – wild-type (black and purple), R34E – single residue mutation R34E (turquoise), R138E – single residue mutation R138E (dark blue). The mutated single residues interfere with DNA binding. Prior to DNA damage induction with a 405nm laser, cells were pretreated with Hoechst 33342 (final concentration of 0.1 μg/ml). Plotted FRAP curves are the mean measurements from at least 15 cells for each construct. FRAP recovery curves were superimposed with trend lines.

According to the *in vitro* evaluation of DNA binding affinity of PARP1 full-length and PARP1 DNA Binding Domain, the full-length molecule has at least a several fold higher affinity to DNA than DBD alone (for details see 2.2.4). Thus, I tested the importance of domains outside of the DBD for PARP1 binding to the DNA breaks *in vivo*. The identical DNA damage and FRAP conditions to the PARP1-DBD FRAP analysis were used for measurements of PARP1-full length diffusion and binding to chromatin. I tested analogous constructs to DBDs however in a PARP1 full-length context. The FRAP analysis indeed showed that PARP1-FL-WT molecules become significantly immobilized on chromatin stronger than PARP1-DBD. Strikingly, despite laser-induced DNA damage neither of the PARP1-FL-R34E nor the PARP1-FL-R138E had

reduced mobility and immobilization. Both of the PARP1 full-length mutants deficient in DNA binding recovered in the same time as PARP1-FL in no DNA damage conditions (Figure 4.17). Thus, only the PARP1-WT with two functional zinc fingers showed reduced diffusion in DNA damage conditions. These results suggest that domains outside of DBD are important for immobilization of PARP1 molecule on the break, however after PARP1 is already bound to DNA thanks to DBD. In summary, both zinc fingers composing the DBD function in a cooperative unit in DNA binding by PARP1. The DBD is sufficient for DNA break recognition and actual break binding.

FRAP analysis of PARP1-FL under DNA damage
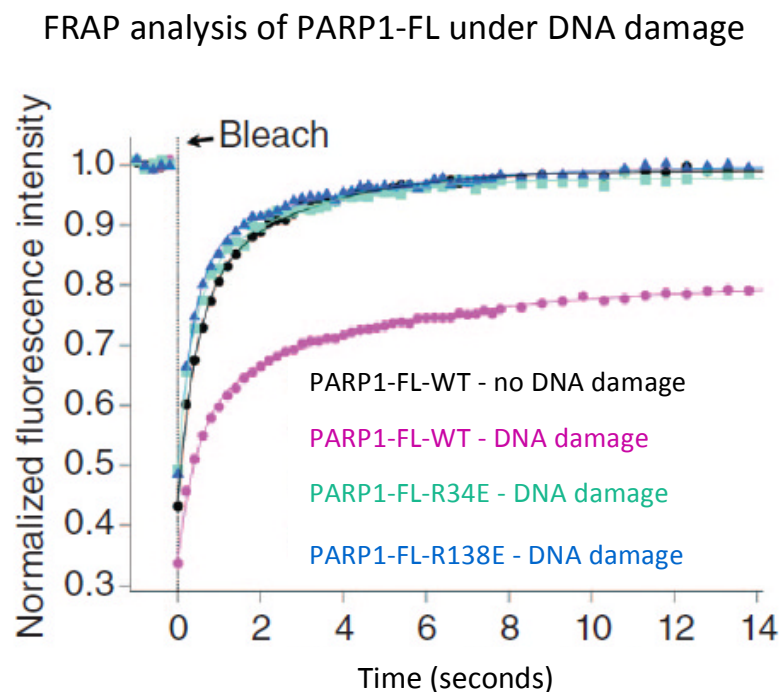
Figure 4.17 Only PARP1-FL-WT binds DNA upon induction of DNA damage. FRAP experiment were conducted in HeLa Kyoto cells (siRNA PARP1) which transiently expressed individual full-length poly-ADP-ribose polymerase 1 (PARP1) constructs: WT – wild-type (black and purple), R34E – single residue mutation R34E (turquoise), R138E – single residue mutation R138E (dark blue). The single reside mutations interfere with DNA binding. Prior to DNA damage induction with 405nm laser, cells were pretreated with Hoechst 33342 (final concentration of 0.1 µg/ml). Plotted FRAP curves for each construct are the averaged measurements from at least 15 cells.

In order to precisely quantify how long PARP1 is bound to DNA breaks - **residency time (t_{res})**, the FRAP curves representing PARP1-FL molecules (wild-type, R34E and R138E) were fitted with a two-dimensional model accounting for diffusion and binding (for details see Materials and Methods). The modeling allows one to quantify a **diffusion coefficient (D)**, and **dissociation**

rate (k_{off}) meaning how often PARP1 dissociates from a DNA break in a given time (here, one second). Under no DNA damage conditions, thus low number of DNA breaks, PARP1 was calculated to be represented by $D = 2.92 \pm 0.51$ μm²/sec. In the presence of DNA breaks, the diffusion coefficient was on average ~ 20-fold reduced to $D = 0.15 \pm 0.16$ μm²/sec. A reduction of diffusion coefficient due to induction of DNA damage was only detectable for PARP1 wild-type molecules and none of the DNA binding PARP1 mutants. Thus, the reduced diffusion was caused by PARP1's association to chromatin. The immobilization of PARP1 on chromatin lasts on average ~ 18.2 seconds. The results of fitting are summarized in Table 4.3. Due to the predominant diffusion of PARP1-FL DNA-binding mutants (R34E and R138E) it was not possible to determine residency time or dissociation rate for these constructs.

Table 4.3 Summary of FRAP results for PARP1 full-length constructs.

Tested protein	Diffusion coefficient (D) mean ± SD* (μm²/sec)		k_{off} (sec^{-1}) mean ± SD	t_{res} (seconds) mean ± SD
	No DNA damage	**Under DNA damage**		
PARP1-FL-wild type	2.92 ± 0.51	0.15 ± 0.16	0.055 ± 0.055	18.18 ± 18.18
PARP1-FL-mutated (R34E)	2.92 ± 0.51	2.92 ± 0.51	n.d	n.d
PARP1-FL-mutated (R138E)	2.92 ± 0.51	2.92 ± 0.51	n.d	n.d

*SD – Standard Deviation, n.d – not possible to determine, K_{off} - disassociation rate (release event per second), t_{res} – residence time on chromatin (seconds).

The results depicted on Figure 4.16 and Figure 4.17 have been published as:

Ali AA, Timinszky G, Arribas-Bosacoma R, **Kozlowski M**, Hassa PO, Hassler M, Ladurner AG, Pearl LH, Oliver AW. . The zinc-finger domains of PARP1 cooperate to recognize DNA strand breaks. *Nat Struct Mol Biol*. 2012 Jun 10;19(7):685-92

4.9 Dissociation of PARP1 from DNA is coupled to PARP1 activity

According to the FRAP findings, the functional DBD is sufficient for PARP1 to bind DNA. However with PARP1-FL is at least 4 times longer immobilized on chromatin in comparison to PARP1-DBD. Full fluorescence recovery of PARP1-FL molecules takes about 70 seconds (Figure 4.18 A) whereas PARP1-DBD recovers in just 15 seconds. Thus once PARP1 is bound

to chromatin, other domains seem to regulate PARP1 chromatin association. According to the predominant model, PARP1 is activated due to DNA binding. I tested how activation sequentially regulates the chromatin-bound state of PARP1. The PARP1-FL-ΔCD (catalytic domain) was assayed via FRAP under typically used DNA damage conditions. Strikingly, PARP1 with a deleted catalytic domain is immobilized on chromatin even longer than PARP1-FL molecules. The fluorescence recovery of PARP1-FL-ΔCD molecules is minimal, which means that diffusion of PARP1 molecules is no longer predominant, but PARP1 is stably bound to DNA breaks (Figure 4.18 A and B).

FRAP analysis of importance of domains outside of DBD for chromatin immobilization :rol
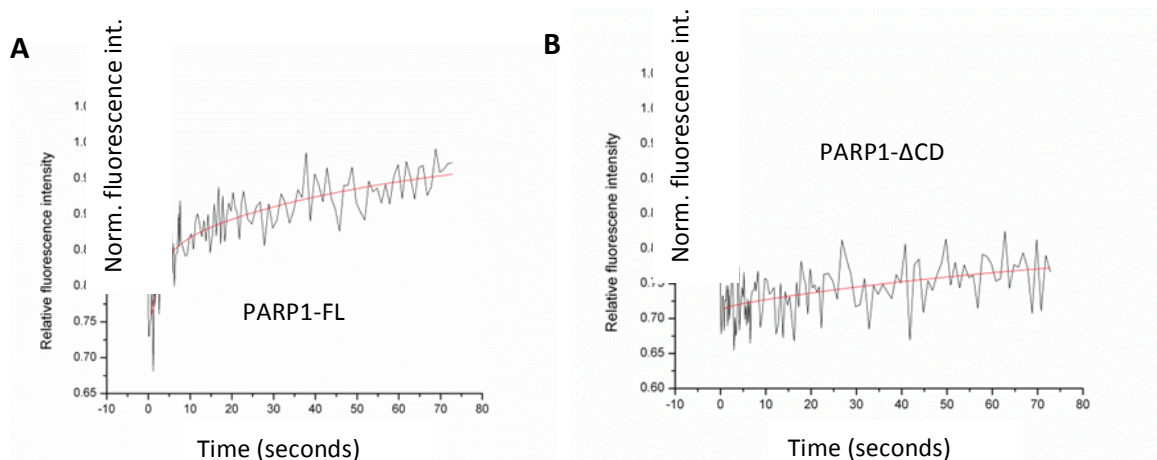
Figure 4.18 PARP1's release from chromatin is coupled to PARP1's catalytic activation. FRAP experiments were conducted in HeLa Kyoto cells (siRNA PARP1) which transiently expressed individual full-length poly-ADP-ribose polymerase 1 (PARP1) constructs: **A)** WT – wild-type and **B)** ΔCD – deleted catalytic domain. Prior to DNA damage induction with a 405nm laser, cells were pretreated with Hoechst 33342 (final concentration of 0.1 μg/ml). Plotted FRAP curves for each construct are the mean measurements from at least 15 cells. FRAP recovery curves were superimposed with trend lines.

4.10 Discussion

The outcome of my work provides for the first time a comprehensive and quantitative *in vivo* analysis of: (i) PARP1's nuclear diffusion coupled to DNA target site selection, together with (ii) specifics of DBD's each zinc finger role in binding to DNA, a prerequisite to PARP1's activation.

(i) PARP1 diffuses freely within the nucleus

Presented findings of PARP1 as freely scanning the nuclear milieu with diffusion coefficient above 4.64 ± 1.04 μm^2/sec (in no DNA damage conditions; FCS tested) challenge the predominant view of PARP1 as a constantly chromatin-associated protein. This past notion came in majority from *in vitro* studies, where indeed PARP1 showed high affinity towards DNA and nucleosomes promoting chromatin condensation and replacement of histone 1 (H1) from linker DNA (Kim et al., 2004; see also 2.2.4). My *in vivo* findings suggest the opposite – that PARP1 only weakly associates with chromatin, under no excessive DNA damage. And only upon the induction of DNA breaks, does PARP1 bind these breaks and become temporally immobilized on chromatin (Figure 4.17). The free diffusion of PARP1 agrees with findings that most of the molecules probed in the nucleus show rapid exchange between various chromatin sites (Lippincott-Schwartz et al, 2001; Patterson and Lippincott-Schwartz, 2002, Hager et al, 2002; Phair et al, 2004; Beaudouin et al, 2006).

The first insights into the nature of PARP's association with chromatin *in vivo* came from PARP1 mobility studies in *Drosophila melanogaster* (Pinnola et al., 2007; see also 2.2.4). The fly genome encodes only one PARP (corresponding to PARP1; Tulin et al, 2002), whereas the human genome encodes 17 PARPs (Vyas et al., 2013). FRAP analysis in the salivary glands of flies revealed that *Drosophila melanogaster* PARP (dPARP) exchanges between chromatin domains faster than a canonical histone H2A. The exchange rate of dPARP varied between euchromatin and heterochromatin regions. On average the FRAP half-time recovery (representing 50 % recovery of the bleached spot) was around 100 seconds. The half time FRAP recovery for human PARP1 was significantly shorter, less than 5 seconds. This high difference between FRAP results for fly and human PARP1 may be attributed to the fact that flies contain only one PARP protein in comparison to 8 nuclear PARPs in humans with perhaps redundant functions and thus weaker chromatin association. Of course, the difference in size of the genome

or differences in chromatin organization (additional histone variants and chromatin factors in higher eukaryotes) may play a difference as well.

In addition, I did not observe significant differences in PARP1 nuclear mobility that would suggest different diffusion within euchromatin or heterochromatin regions in mammalian cells, unlike dPARP. Particular enrichment of PARP1 (endogenous or transiently expressed) within nuclei, if PARP1 was trapped in heterochromatin region, neither was observed in cells evaluated via fluorescence microscopy (HeLa Kyoto, U2OS, MCF-7 and MDA-66). However I did not test PARP1 mobility in environment with labelled euchromatin or heterochromatin allowing me to distinguish between two chromatin states.

(ii) All of the PARP1 molecules show analogous cellular behavior

In addition to the FRAP study of dPARP, another study that evaluated human PARP1 via FRAP was conducted. This PARP1 mobility study in HeLa cells found PARP1 to be gradually enriched over laser-induced DNA damage as fast as 1 second (Haince et al., 2007). This past *in vivo* study provided insights into PARP1's chromatin associations in living cells and suggested that PARP1 may not be constantly chromatin-associated. However the used classical and only qualitative FRAP approach was limited in its spatial and temporal resolutions. The bleached areas in the experiment encompassed a big part of the nucleus (Haince et al., 2007). Thus the final information on PARP1 mobility was only an average of hundreds of thousands of PARP1 molecules, which could have undergone completely different mobility, when considered individually. Moreover, no analysis of the actual mechanism and domain importance for target DNA selection and binding by PARP1 was conducted. I investigated the PARP1 diffusion and interaction behavior in living cells with FRAP and two additional, complementary methods: Fluorescence Correlation Spectroscopy (FCS; 1-1000 molecule resolution) and Fluorescence Loss in Photobleaching (FLIP; 100 % of tagged molecules in a cell). The outcomes of my work suggest that PARP1 recognizes its target sites via free diffusion, which is representative of all molecules.

A free diffusion of PARP1 allows the protein to weakly and frequently interact with multiple genome sites. This type of PARP1 interaction with chromatin allows PARP1 to monitor DNA target sites constantly and rapidly engage with chromatin when required, for example upon

detection of a DNA break. According to the predominant model of PARP1 activation, the protein becomes activated upon DNA binding. The fast diffusion of PARP1 molecules and lack of continuous binding to chromatin, unless there are DNA breaks, may thus explain very low levels of PAR within a cell (see Figure 5.5 A). Simply, no binindg corresponds to lack of PAR within the nucleus.

The PARP1 DBD binds to DNA 4 times shorter than the PARP1 full-length molecules (Figure 4.16 and 4.17). PARP1 with deleted the catalytic domain becomes strongly immobilized on chromatin (Figure 4.18). A variation in chromatin-immobilization time of PARP1, depending on domain composition suggests that there is most likely an intramolecular interaction between PARP1 domains leading to catalytic activation based on the signal originating from DNA-bound zinc fingers. Such an intradomain communication was suggested by the X-ray crystal structure of nearly full-length PARP1 molecule bound to DNA (see also 2.2.3), however the X-ray structure misses the ZF2 and BRCT domains, thus it is not clear what the final interaction between the domains is. Prolonged immobilization of PARP1 missing the catalytic domain could be caused by three mechanisms, which could be addressed experimentally. First, PARP1 does not automodify itself with PAR, thus its association with chromatin has no negative feedback promoting disaasociation. Second, PAR modification is required to recruit proteins (kinases or ubiquitinases) that will negatively regulate association of PARP1 with chromatin (for details see 2.2.5 and 2.3.3). Third, perhaps the catalytic domain, upon NAD^+ binding, releases zinc fingers from a DNA break.

(iii) PARP1's mobility is hindered

Interestingly, my observations suggest that PARP1 could interact with chromatin or other proteins, when not bound to chromatin. This conclusion is based on the fact that the predicted diffusion coefficient (*D*) for PARP1 based on the proteins size is ca. 6 μm^2/sec. Quantification of FCS data for PARP1 full-length found the molecules to diffuse with diffusion coefficient of 4.64 ± 1.04 μm^2/sec. There are two possible explanations for the difference between predicted and measured *D*. The first could be that PARP1 forms a homo/hetero complex with other molecules and thus diffuses slower. The second would be that PARP1 diffuses slower due to PAR modification or other posttranslational modifications (see also 2.2.5). A combination of these two models is possible as well. For example, if PARylated PARP1 diffused across the nucleus it

could be recognized and temporally immobilized by a macroH2A1.1 histone variant that specifically recognizes and binds PAR. This hypothesis needs an evaluation. For example, PARP1 mobility could be evaluated by FCS in the presence of PARP1 activity-specific inhibitors or mutated known PTM sites. In addition, a possibility of homo- or hetero-dimer formation of PARP1 can be tested with Fluorescence Cross-Correlation Spectroscopy (FCCS). This experiment would evaluate a mobility of two populations of PARP1 or additional candidate molecules (e.g. ALC1) labeled with two different fluorescent proteins (e.g. EGFP and mCherry). If the two populations diffused together, the cross-correlation of FCCS experiment would be positive, thus two tested populations would show identical diffusion times in space and time.

(iv) PARP1's binding to chromatin is zinc finger-dependent

An evaluation of dPARP association at the heat-shock loci revealed that dPARP resides at the TSS and in the gene body of *hsp70* in a PAR modification-independent and -dependent manner, respectively (for details see 2.2.4). No importance of zinc fingers for TSS association was however tested in these previous studies. My data suggests that zinc fingers are critical in PARP1 chromatin-association. Lack of functional zinc fingers results in lack of PARP1 binding, even in the presence of high amount of DNA breaks (Figure 4.17). It is thus not clear how PARP1 would associate with chromatin due to posttranslational modification of histones. Such a mechanism was suggested by dPARP association with heat shock loci due to presence of H2A.V histone variant and its phosphorylation (for details see 2.2.4; Kotova et al., 2011, Thomas et al., 2014). The study of dPARP chromatin association was conducted at *hsp70* loci during transcription initiation. My study was conducted in the context of PARP1 binding to DNA lesions. Although it is not clear that dPARP actually does not become activated at *hsp70 promoter* due to DNA damage (see Outlook, chapter 6) it is possible that PARP1 associates differently at DNA lesion sites vs. transcriptional sites. A comprehensive study of PARP1's domain importance for mobility and chromatin association in defined transcriptional context would be appreciated.

(v) Both zinc fingers are essential for PARP1's binding to DNA

The investigation of the importance of each zinc finger revealed that ZF1 and ZF2 form a functional unit, which is essential and sufficient for PARP1's association with chromatin (in DBD and full-length contexts). None of the zinc fingers alone was sufficient to even transiently

immobilize the PARP1 molecule over the target site. In such a case where both zinc fingers are important, the model which disregards zinc finger 2 and importance of the linker contact between the zinc fingers may be simply incorrect (see more 2.2.3). Instead, the X-ray structure of the full-length PARP1 molecule bound to various DNA structures would be highly appreciated. Zinc finger 2 *in vitro* was shown to have 100-fold higher affinity to DNA than zinc finger 1 (for details see 2.2.3). The *in vitro* differences observed in DNA affinity between ZF1 and ZF2 are not visible *in vivo*. Both zinc fingers *in vivo* are equally important and most likely bind DNA breaks simultaneously.

5 Results and Discussion II
Functions of PARP1 and ALC1 in transcription

5.1 ALC1 is recruited to DNA damage sites and activated via PAR

The amplified in liver cancer 1 (*ALC1*) gene was originally identified as an amplified region of chromosome 1 in more than 50 % of hepatocellular carcinomas (HCC). The oncogenic role of ALC1 was next confirmed via its ectopic expression in transgenic mice, which developed tumors in consequence. In HCC patients, the elevated expression level of ALC1 was correlated with shorter disease-free survival time (for details see 2.4). ALC1 is a member of the SNF2 ATPase superfamily, some members of which function as chromatin remodelers. ALC1 was found to remodel a mono-nucleosome position *in vitro* (Gottschalk et al., 2009). Thus ALC1's oncogenic functions are most likely mediated via its roles in regulation of chromatin structure. However the details of this process *in vivo* are not known. Dynamics of chromatin structure reorganization will affect DNA accessibility and all DNA-based processes (Clapier and Cairns, 2009). There are two possible models that could explain ALC1 oncogenic functions. The first model describes that ALC1's activity regulates DNA repair mechanisms. The second model involves ALC1 roles in transcriptional deregulation of other oncogenes.

ALC1 is recruited to the sites of DNA damage in an exclusively PARP1-dependent manner. The recruitment is possible due to ALC1's macrodomain, a globular domain that specifically recognizes and binds PAR, which is product of PARP1 enzyme (Karras, et al., 2005, Gottschalk et al., 2009). In the transcriptional context, one study has to date reported ALC1 binding to a few genome sites that included exons, introns and intergenic regions. A possible DNA sequence motif recognized by ALC1 was proposed (Chen et al., 2010). However the validity of these findings was not confirmed. Moreover the importance of PAR in ALC1 recruitment to transcriptional sites was not tested. A clear understanding of ALC1 recruitment mechanism to the genome sites in a transcriptional context matters in order to understand the mechanism of ALC1 activation and resulting cellular functions.

Our current understanding of ALC1 significance in transcription regulation is not clear. To date, there are two reports of two individual genes, *ARHGEF9* and *SPOCK1*, whose expression is regulated by ALC1. The evidence is based on the fact that changes of ALC1 cellular level,

results in changed ARHGEF9 and SPOCK1 expression levels. These findings were followed up and ALC1 was found, via ChIP, in the vicinity of transcriptional start sites (TSS) for these genes. However, the ChIP results were only qualitative and the authors showed a specific localization only for *SPOCK1* (for details see 2.4). The authors did not provide a true enrichment (detected percentage of input DNA) of ALC1 over the investigated loci. Neither the molecular basis of ALC1 recruitment to these sites was investigated and reported. This is important, because ALC1 as a chromatin remodeler may affect chromatin organization across the genome, which may result in deregulation of expression for certain genes. Although these genes not necessarily need to be direct targets of ALC1 and the effect does not necessarily need to originate from ALC1's transcriptional role, but may instead be a consequence of ALC1 roles in DNA repair. It is widely accepted that genome of cancerous cells is unstable. Changes in DNA repair will contribute to transcriptional changes and thus deregulation of gene expression, common in carcinogenesis (Burgess et al., 2012).

Therefore, I investigated the properties of ALC1 dependence on PARylation and ALC1 roles in transcription. In particular, I aimed to:

o   Identify, if indeed and how ALC1 regulates transcription.

o   Identify the molecular mechanism of ALC1 recruitment and regulation of chromatin structure in the context of transcription.

## 5.2 PARP1 and ALC1 appear not to function in ER-regulated transcription

ALC1 via its macrodomain binds *in vitro* exclusively to chains of PAR, which play a crucial role in activation of ALC1's ATPase-dependent remodeling functions (for details see 2.4). Similar to the *in vitro*, thanks to the macrodomain, ALC1 is recruited to the sites of extensive PARylation *in vivo* (laser induced DNA lesions). A functional macrodomain is essential in ALC1 recruitment to PARP1 activity sites (Gottschalk et al., 2009). Thus, it appears that ALC1 is highly dependent on its macrodomain interactions with PAR for both, the genomic localization and the chromatin remodeling function. A dependence of ALC1 on macrodomain and PAR was never tested in the context of transcription. Knowing recruitment mechanism of ALC1 to the transcriptional sites would facilitate understanding of ALC1's functions as an oncogene.

Cellular PAR originates in majority from the activity of PARP1 enzyme (see also 2.3). To date, a few transcriptional mechanisms that depend on PARP1 activity and PAR presence were reported. For example, PARP1 was found to co-activate transcription together with various nuclear receptors (estrogen and progesterone receptors) upon the presence of a respective ligand (estrogen or progesterone; Ju et al., 2006, Wright et al., 2012, Zhang et al., 2013a). Therefore I used one of the breast cancer cell lines (MDA-MB231-human ERα, see Materials and Methods) responsive to estrogen. In this cell line, upon the ligand addition, ERα target genes are transcriptionally up-regulated or down-regulated within minutes and hours (depending on the gene) following estrogen addition (Ju et al., 2006, Reid et al., 2003, Hah et al., 2012). I hypothesized that ALC1 could play a role in estrogen-dependent transcription regulation, if ALC1's macrodomain recognizes PAR originating from activated PARP1 in this process. Thus, I evaluated up-regulation of mRNA levels (via RT-PCR) for known ERα-regulated genes (*GREB1*, *TFF1* and *CASP7*) in the presence of the ligand across eight different conditions. The conditions were the following (for details see Materials and Methods):

(i)   no estrogen treatment (negative control)

(ii)   estrogen treatment (positive control)

(iii)   chemical inhibition of PARP1 activity with 5 µM olaparib and estrogen treatment

(iv)   PARP1 siRNA-mediated knock down (48 hours) and estrogen treatment

(v)   ALC1 siRNA-mediated knock down (48 hours) and estrogen treatment

(vi)   chemical inhibition of PARP1 activity with 15 µM AG14361 and estrogen treatment

(vii)   chemical inhibition of PARP1 activity with 5 µM AG14361 and estrogen treatment

(viii)   chemical inhibition of PARP1 activity with 2.5 µM AG14361 and estrogen treatment

The results of RT-PCR analysis are shown in Figure 5.1. As expected, a chemical inhibition of PARP1 activity with the highest concentrations of AG14361 resulted in decreased up-regulation of estrogen receptor target genes. Surprisingly, a chemical inhibition of PARP1 activity with olaparib or PARP1 down-regulation via siRNA (48 hours) did not interfere with up-regulation of the same genes upon estrogen treatment. In addition, siRNA-mediated down-regulation of ALC1 did also not prevent up-regulation of estrogen receptor target genes.
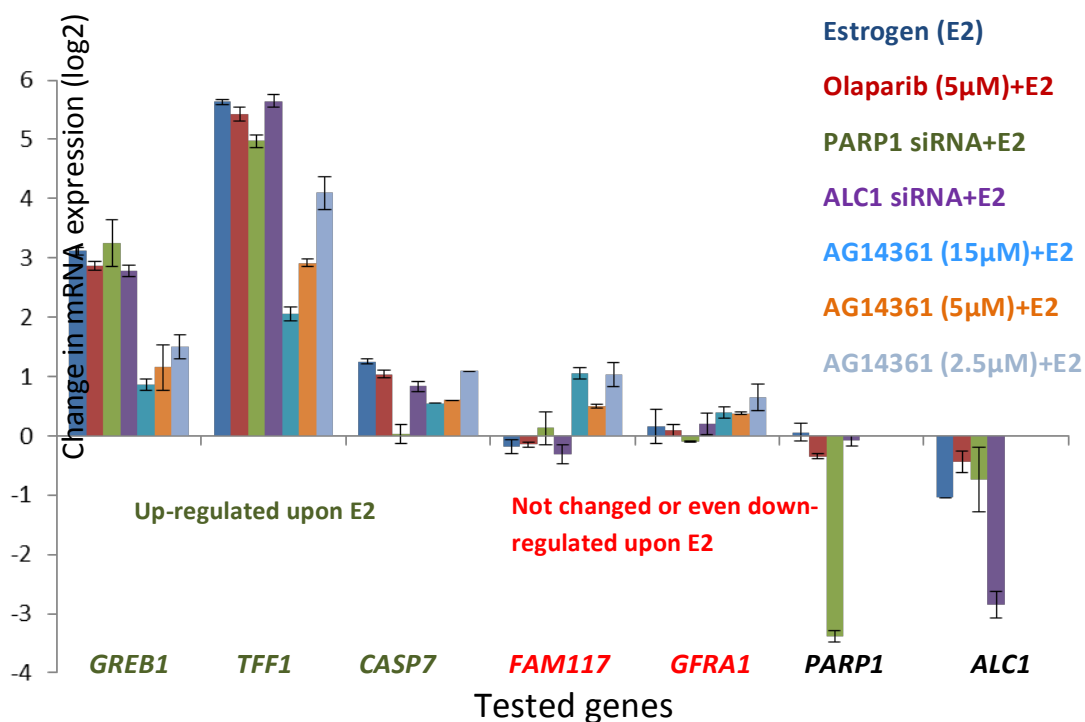
Figure 5.1 Chemical inhibition of PARP1 and siRNA of PARP1 or ALC1 does not interfere with up-regulation of estrogen receptor-dependent genes. Breast cancer cells (MDA-MB231-human ERα) were treated with chemical inhibitors of PARP1 (**olaparib** or **AG14361**) with the indicated concentrations (15, 5 or 2.5 μM) for 40 minutes prior to estrogen (**E2**) treatment, or the MDA-MB231-human ERα cells were treated with siRNA (48 hours) to knock-down PARP1or ALC1 and then treated with estrogen (E2). Estrogen treatment (100 nM) lasted 3 hours, after which total RNA was extracted. Shown on the graph are mRNA levels of the respective genes (post estrogen treatment) normalized to the levels prior estrogen addition (indicated as 0 on the logarithmic scale, on the **Y-axis**). PARP1 and ALC1 mRNA levels post-siRNA were normalized to mRNA levels of cells treated with non-specific siRNAs (mock control). PARP1 and ALC1 mRNA levels were not evaluated in cells treated with AG14361 compound. Tested genes were: **GREB1 -** growth regulation by estrogen in breast cancer 1, **TFF1** – trefoil factor 1, **CASP7** – caspase 7 apoptosis-related cysteine peptidase, **FAM117** – family with sequence similarity 117, **GFRA1** – GDNF family receptor alpha 1, **PARP1**- poly-ADP-ribose polymerase 1, **ALC1** – amplified in liver cancer 1. Error bars represent Standard Error of Mean from at least 3 experiments.

The importance of ALC1 in estrogen receptor-regulated transcription is not known and the main goal of this experiment was to test it. However, the outcome of the experiment was surprising. I expected to see a functional role of PARP1 in deregulation of transcription of estrogen receptor responsive genes upon PARP1 chemical inhibition or siRNA knock-down. PARP1's role in this process was not observed, unless high concentration of AG14361 (15 μM) were used, suggesting

that PARP1 is not important for estrogen receptor transcription control. Thus, my data contradicts the previously published results from Ju and co-workers (2006) and Zhang and co-workers (2013a), where PARP1 and its activity were shown to play a co-activation role in up-regulation of estrogen receptor dependent genes upon estrogen treatment (see also 2.1.2).

However, technical differences between my study and the published studies exist. A major difference is the choice of PARP1 chemical inhibitors. The Ju and Zhang study deployed the early generations of PARP1 chemical inhibitors: 3-aminobenzamide (3AB; Purnell and Whish, 1980) and PJ-34 (phenanthridinone derivative; Soriano et al., 2001). 3AB is a very weak PARP1 inhibitor with inhibitory constant (Ki) of 500 nM (Gallmeier et al., 2005), thus the authors used high 10 mM concentration of 3AB in the study. The PJ-34 in Zhang study was used at 10 μM concentration. Unfortunately, at concentration of 5 μM and higher, PJ-34 was shown to have off target proteins, including the PIM family of serine/threonine kinases (Antolin et al., 2012). Recently, 3AB was additionally judged to be a very poor PARP1 inhibitor thanks to mass spectrometry (MS) results (Zhang et al., 2013b). In this study, five different chemical inhibitors of PARP1 were compared with respects to their efficiency in inhibition of protein PARylation in cells with or without oxidative DNA damage (induced via hydrogen peroxide, H_2O_2). Use of 3AB at high concentrations (50 μM) did not prevent PARylation of proteins upon DNA damage, and the PAR modified protein profiles between two conditions (no inhibitor or plus inhibitor) in cells with or without DNA damage, poorly matched. In contrast, the chemical inhibitors, olaparib and AG14361 used at low concentrations (1-3 μM) were found to specifically inhibit PARylation of target proteins in relevant conditions. PJ-34 inhibitor was unfortunately not tested in the study (Zhang et al., 2013b). Therefore I used recent generation of PARP1 inhibitors: olaparib and AG14361 to evaluate PARP1's role in estrogen receptor dependent transcription.

The use of AG14361 resulted in decreased transcriptional response of ERα target genes, however this response was especially present in higher 15 μM and 5 μM AG14361 concentrations. Therefore, I conducted siRNA-mediated knock down of PARP1 to re-confirm chemical inhibition study. The knock-down efficiency (48 hours) of RNA levels was high, with only 10 % PARP1 mRNA remaining. At the protein levels PARP1 was detectable in higher levels than 10 % of the siRNA mock-treated control (Figure 5.2 A; for details see Materials and Methods). The

siRNA-mediated knock down of PARP1 further favored no role of PARP1 in ERα-regulated transcription.

Western blot of MDA cell protein extracts
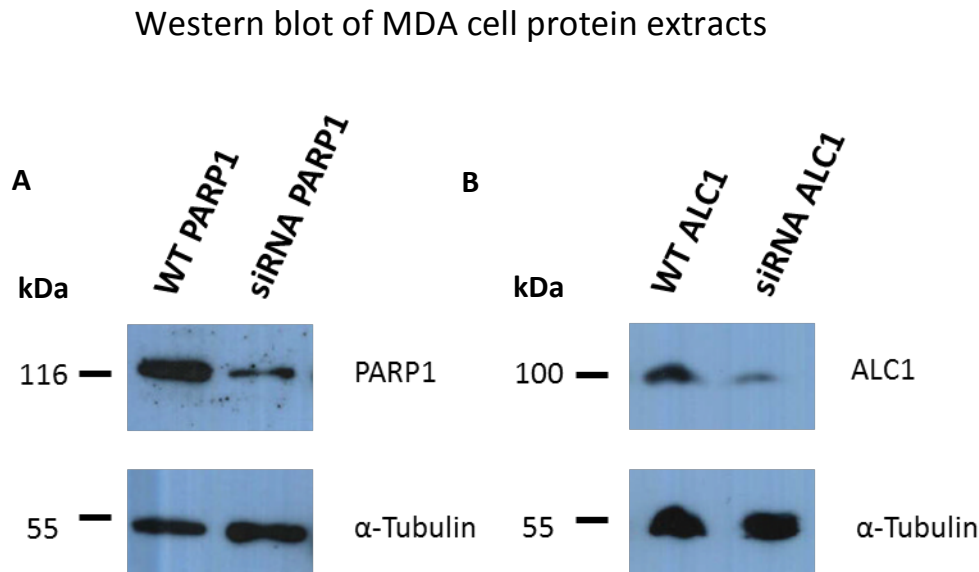
Figure 5.2 PARP1 and ALC1 are efficiently knocked down in MDA cell lines. Whole-protein extracts from MDA-MB231-human ERα cell lines upon transient expression of siRNA specific to **A)** PARP1 or **B)** ALC1, were analyzed via SDS-PAGE and visualized by western blot with anti-PARP1, anti-ALC1 and anti-Tubulin (loading control) antibodies. All antibodies detected proteins of the expected size: 116 kDa for PARP1, 100 kDa for ALC1 and 55 kDa for Tubulin. **A)** PARP1 – poly-ADP-ribose polymerase 1 and **B)** ALC1 – amplified in liver cancer 1, are significantly depleted in the MDA-MB231-human ERα cell lines (upper panels, respectively). Loading of protein extract on SDS-PAGE was similar, as indicated by α-Tubulin levels (lower panels, respectively). Marker indicating the size of the protein is indicated on the left in kilodaltons (kDa). WT PARP1 and WT ALC1 correspond to cells treated with non-specific siRNA (mock control).

The Ju and Zhang studies deployed siRNA targeting PARP1 to confirm the involvement of PARP1 in estrogen receptor-dependent transcription as well. The siRNA used by Ju and co-workers is no longer in stock (Qiagen). BLAST analysis of this siRNA accuracy showed that this siRNA targets other coding regions in addition to *PARP1*. BLAST analysis of the siRNA used by Zhang and co-workers did not yield non-specific coding sequences in addition to PARP1, however 3 non-coding regions (each 12 base pair long) were identified. The importance of these non-coding sequences is not known.

Importantly, despite confusing results concerning PARP1 co-activation role, the main goal was to evaluate ALC1 importance in estrogen receptor alpha regulated transcription. Upon ALC1

knock down tested genes responded as genes in wild type cells (control) and no change in mRNA levels of ERα regulated genes was observed (Figure 5.1) This result likely diminishes ALC1's importance in the studied process. ALC1 was efficiently down-regulated at RNA and protein levels (Figure 5.1 and 5.2 B).

5.3 ERα foci formation is unaffected by interference with PARP1 activity

According to my data PARP1's activity in not essential for ERα-dependent transcription. This result was surprising and opposite to the one expected based on the previously published reports. Therefore, I further tested PARP1's importance in estrogen-stimulated transcription from another perspective - formation of estrogen receptor alpha (ERα) foci across the genome upon ligand addition. Such foci are formed by ERα presumably being bound to estrogen responsive element (ERE; Reid et al., 2003, Sharp et al., 2006, Kwon et al., 2007). A rationale for PARP1's possible function in the foci formation was based on the fact that PARP1 was shown to PARylate ERα *in vitro*. Also, both PARP1 and ERα were found to co-immunoprecipitate each other (Zhang et al., 2013a).

If PARP1 indeed regulated ERα-dependent transcription, I expected changes to ERα foci formation upon interference with PARP1 activity. I tested this using live cell imaging of ERα labelled with EGFP constructs stably expressed in two estrogen-responsive cell lines: MCF-7-human-ERα-EGFP and MDA-MB231-human-ERα-EGFP. In addition to estrogen treatment (condition i, control), the cells were pretreated with PARP1 chemical inhibitor - olaparib or AG14361 (condition ii and iii) or had transiently expressed (24 hours) PARP1 or ALC1 (condition iv and v, respectively). As expected, the cells expressing ERα-EGFP formed significantly distinct foci within 2 minutes of estrogen addition (Figure 5.3 A). Pre-treatment of cells with any of the PARP1 inhibitors, olaparib or AG14361, did not prevent foci formation (Figure 5.3 B and C). Olaparib was tested at 1 μM and 5 μM and AG14361 at 15 μM concentrations. Foci formation was followed for 2 hours since ligand addition. During this time, the control (i) and PARP1 chemical inhibition (ii and iii) conditions were indistinguishable in terms of foci formation.

Live cell imaging of foci formation by ERα, PARP1 and ALC1 in cells upon E2 treatment
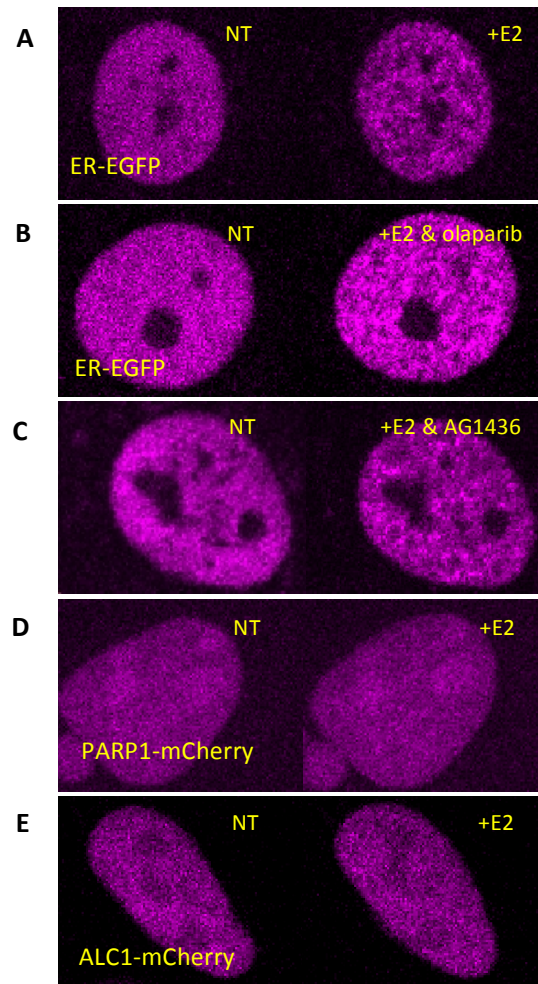
Figure 5.3 ERα foci form despite chemical inhibition of PARP1 and ERα does not co-localize with PARP1 or ALC1. MDA-MB231-human ERα-EGFP cells depleted of endogenous estrogen receptor (**ERα**) were stably transfected with human ERα tagged with enhanced Green Fluorescent Protein (**EGFP**) shown as magenta. **NT** – no E2 treatment (left column) photos prior to the ligand addition, the same cells were next treated with 100 nM estrogen (**E2**; right column) and imaged continuously for 2 hours (image frame every 30 seconds). Photos on the right represent foci formation or not, upon 15 minutes of the ligand addition. **A**) ERα forms distinctive foci upon E2 treatment (right column). **B**) ERα foci formation is not affected by presence of PARP1 chemical inhibitor - 1 or 5 μM olaparib (right column). **C)** ERα foci formation is not affected by presence of PARP1 chemical inhibitor - 15 μM AG14361 (right column). **D**) Poly-ADP-ribose polymerase 1 (PARP1) tagged with mCherry (shown as magenta) does not form foci upon E2 treatment (right column). **E**) Amplified in liver cancer 1 (ALC1) tagged with mCherry does not form foci upon E2 treatment (right column). Shown images are representative of results acquired from evaluation of at least n = 10 cells for each condition. Foci are visible as circules of magenta.

In addition, if PARP1 and ERα co-immunoprecipitate (Zhang et al, 2013a), I expected both to co-localize in the cells treated with estrogen. However no co-localization between PARP1-mCherry and ERα-EGFP was observed, neither did PARP1-mCheery form foci at all (Figure 5.3 D). Similarly to PARP1, ALC1-mCherry did not co-localize or form foci in cells treated with estrogen (Figure 5.4 E). In summary, these results suggest that PARP1 or ALC1 are not important for ERα association to genome sites and foci formation.
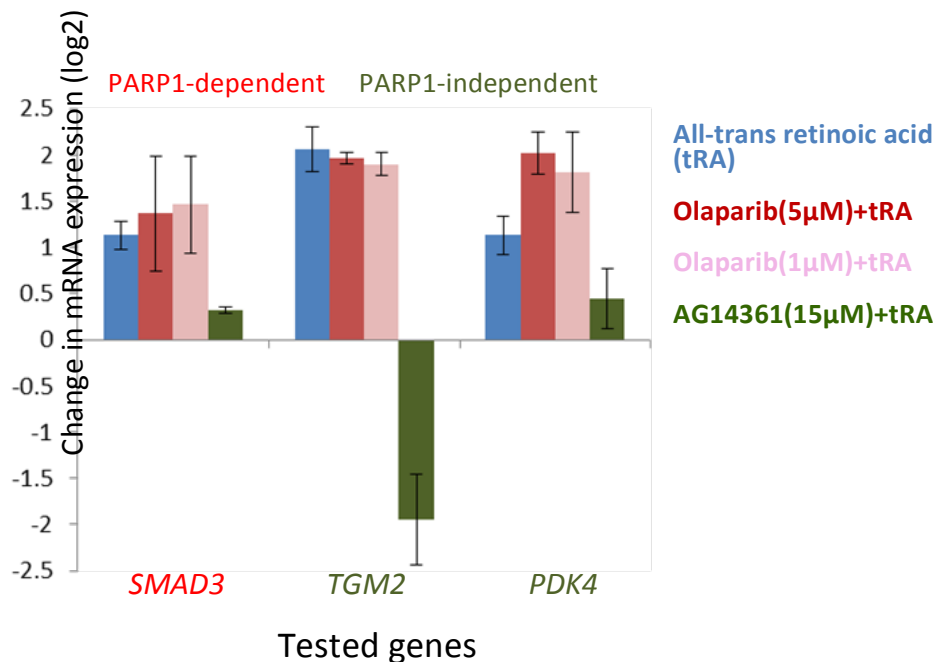
5.4 Olaparib and AG14361 lead to different transcriptional outcomes

Chemical inhibition of PARP1 activity with olaparib or AG14361 did not affect ERα foci formation in the presence of estrogen. However, mRNA levels of estrogen responsive genes were reduced in presence of AG14361 inhibitor, but not when the olaparib was used. I wanted to know why two recent, specific PARP1 inhibitors lead to two different transcription outcomes. Therefore, I tested both the PARP1 inhibitors in another transcription-based assay. I used cells in which transcription is regulated by another nuclear receptor called retinoic acid receptor (RAR). In these cells, transcription activation via a RAR ligand, all-trans retinoic acid (tRA), was shown to be negatively regulated by PAR (Le May et al., 2012).

I evaluated up-regulation of mRNA levels for known tRA regulated genes (*TGM2* and *PDK4)* in the presence of the ligand and chemical PARP1 inhibitor, either olaparib or AG14361. Pretreatment of HeLa cells, prior the ligand addition, with olaparib (1 or 5 μM) did not lead to change of the PAR-independent gene *SMAD3* mRNA levels, however did affect as expected one of the PAR-dependent genes (*PDK4*). In contrast, AG14361 at 15 μM concentration inhibited transcription of all the tested genes, PAR-dependent and -independent (Figure 5.4). This result suggests that the effect observed at estrogen regulated genes due to high concentration of AG14361 may be not specific to PARP1 functions, but simply result from AG14361 off-target effects.

RT-PCR analysis of mRNA levels for retinoic acid receptor-dependent genes

Figure 5.4 Chemical inhibition of PARP1 with olaparib or AG14361 leads to different transcription response. HeLa cells were treated with chemical inhibitors of PARP1 (olaparib or AG14361) with the indicated concentrations (5 μM, 1 μM or 15 μM) for 40 minutes prior to all-trans retinoic acid (**tRA**) treatment. tRA treatment (10 μM) lasted for 3 hours, after which total RNA was extracted. Shown on the graph are mRNA levels of the respective genes (post-tRA treatment) normalized to the levels prior to tRA addition (indicated as 0 on the logarithmic scale, on the **Y-axis**). Tested genes were: ***SMAD3*** – SMAD family member 3, ***TGM2*** – transglutaminase 2, ***PDK4*** - pyruvate dehydrogenase kinase isoform 4. Error bars represent Standard Error of Mean from 4 experiments.

5.5 Olaparib and AG14361 inhibit PARP1 activity *in vivo*

My results suggest that PARP1 activity is not essential for ERα-dependent transcription. In a major experimental part that led to me to this conclusion I used chemical inhibitors of PARP1 whose inhibitory function had to be confirmed. Thus, I used a cellular system in which upon induction of oxidative DNA damage with hydrogen peroxide (H_2O_2), PARP1 undergoes rapid activation. Activity of PARP1 can be visualized by direct immunofluorescent staining of the PARP1 product, poly-ADP-ribose (PAR). In a positive control, in cells treated with hydrogen peroxide, PAR is readily detectable within 10 minutes of the DNA damage induction (Figure 5.5 B). Presence of any of the PARP1 inhibitors used throughout my work (olaparib or AG14361)

abolished PAR, confirming that chemical inhibitors of PARP1 activity are working properly (Figure 5.5 C and D).

Evaluation of PAR levels via Immunofluorescence
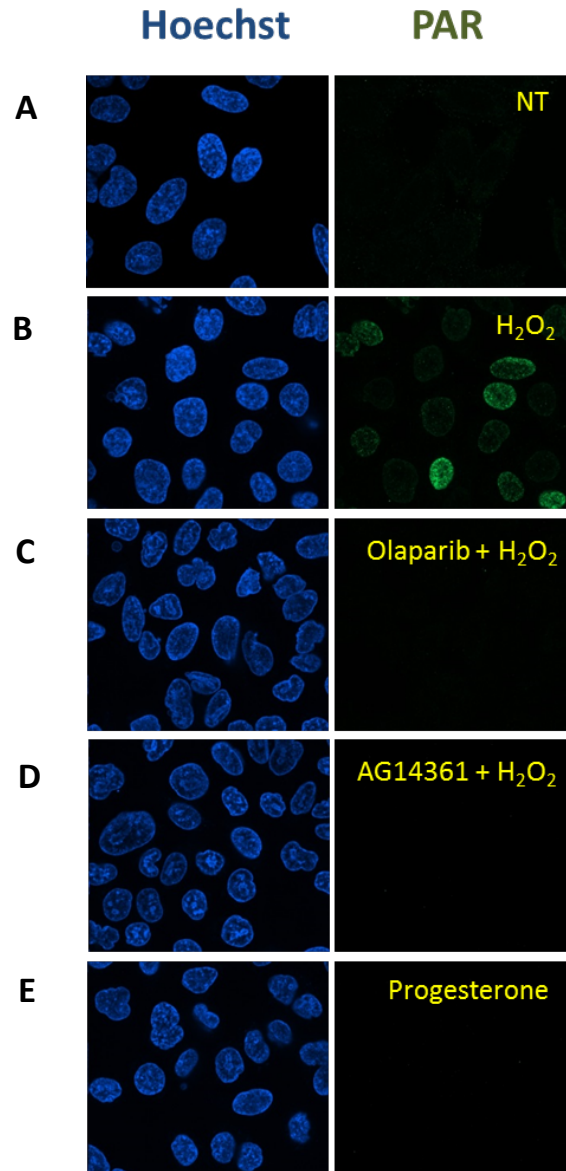
Figure 5.5 Olaparib and AG14361 inhibit PARP1 activity. Progesterone does not lead to increased PAR levels. T47D cells were stained for poly-ADP-ribose (PAR) with anti-PAR antibody post-treatment: **A)** no treatment (negative control). **B)** hydrogen peroxide (H_2O_2; 1μM) treatment for 10 minutes. **C)** olaparib (5μM or 1μM) treatment for 40 minutes, followed by H_2O_2 (as in B). **D)** AG14361 (15μM/5μM/1μM) treatment for 40 minutes, followed by H_2O_2 (as in B). **E)** progesterone (R5020) treatment for 20 minutes (10 nM) and 30 minutes (10 nM and 100 nM). Nuclei were visualized with Hoechst 33342 (final concentration of 0.1 μg/ml; column on the left).

The predominant model of PARP1 activation assumes that PARP1 binds DNA breaks and the enzyme becomes subsequently activated. According to the less-established model, PARP1 is activated by its post-translational modifications and histone variants. The first model is aligned with PARP1 roles in DNA damage. The second model is aligned with PARP1 functions in transcription. I wanted to rule out a possibility that perhaps the inhibitors used in transcriptional assays do not inactivate PARP1 due to a different mode of enzyme activation. This possibility was unlikely when one takes into account that olaparib and AG14361 are NAD^+ analogs, however I aimed to test PARP1 inhibition in transcription-based assay. Wright and co-workers (2012) showed that PAR levels are increased upon progesterone treatment in ductal carcinoma (T47D) cells. Progesterone is a ligand of progesterone receptor (nuclear receptor) that leads to transcriptional activation of various genes, similarly to ERα. I treated the T47D cells with progesterone, however did not observe PAR elevation, thus could not test PARP1 inhibitors (Figure 5.5 E). This result was different from the reported one (Wright et al., 2012; see Figure 2.3). Importantly, I confirmed that the used cells respond to progesterone treatment based on up-regulation of PR dependent genes: DUSP1 and EGFR (Figure 5.6).
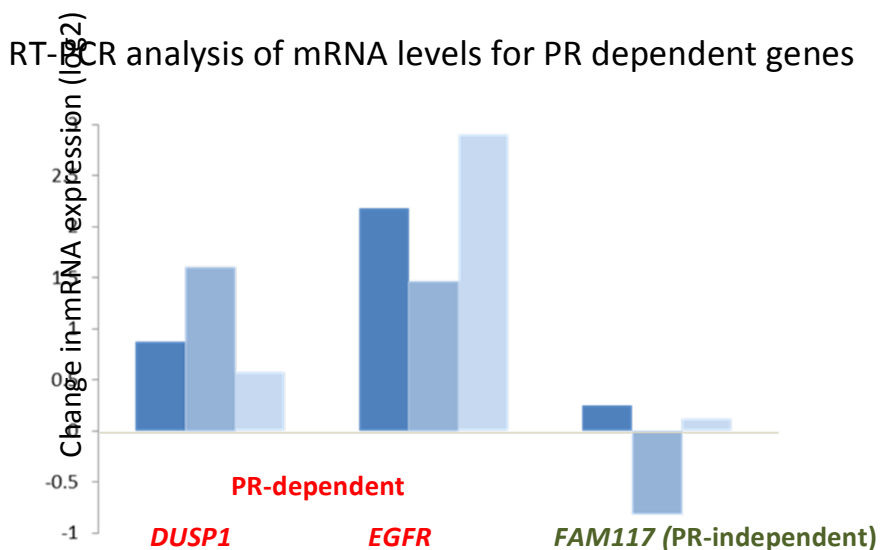
Figure 5.6 Cells respond to progesterone treatment. T47D cells were treated with 100 nM progesterone (R5020) for 3 hours and after the treatment total RNA was extracted. Each column represents a single biological sample (total 3) for each gene. mRNA levels of PR dependent genes (*DUSP1* and *EGFR*) and PR independent genes (*FAM117*) were tested. Shown on the graph are mRNA levels of tested genes post-PR treatment normalized to to the mRNA levels prior to PR treatment (indicated as 0 on the logarithmic scale, **X-axis**). ***DUSP1*** - dual specificity phosphatase 1, ***EGFR*** - epidermal growth factor receptor, ***FAM117*** - family with sequence similarity 117.

5.6 ALC1 regulates transcription similarly to PARP1

My initial plan to study ALC1 functions in transcription, via a robust PARP1-dependent transcription activation system, had to be discontinued. I could not recapitulate dependence of nuclear receptor regulated gene expression on PARP1 activity, as previously reported (Ju et al., 2006, Wright et al., 2012, Zhang et al., 2013). Lack of robust reproducibility of previously published results undermined the validity of use hormone responsive cells as adequate to study ALC1 functions. In addition, a direct evaluation of ALC1 importance for ERα-regulated transcription and ERα association with chromatin (both upon ligand addition) suggested that ALC1 does not play a role in these processes.

Therefore, I employed a new cellular system to study ALC1 functions in transcription. Again, I assumed that PAR is critical in regulating macrodomain-containing ALC1 activity. PARP1 and PAR were reported to regulate gene expression at the transcription level in no hormone stimulated cells. PARP1 candidate genes were identified via a microarray study of mRNA levels in cells with stably knocked-down PARP1. The study identified 115 and 89 genes, which were up- or down- regulated in absence of PARP1, when compared to wild-type cells that expressed PARP1 (Frizzell et al., 2009). PARP1 was found to reside at the TSS of the candidate genes and promote an open chromatin structure via PARylation and subsequent removal of demethylase 5B (KDM5B demethylase; Krishnakumar and Kraus, 2008 and 2010, for details see 2.1.2).

I selected a few extensively studied PARP1 dependent genes (see Figure 2.4) and tested possible ALC1 functions in transcription regulation of these genes as well. The candidate genes were the following: *GDF15* and *ITPR1*, including a negative control *ABDH*. I transiently knocked-down (48 hours) PARP1 or ALC1 individually and checked the expression level of the candidate target genes. As shown on Figure 5.7, knock-down of ALC1 results in similar deregulation of mRNA levels of evaluated genes as PARP1 knock-down. ALC1 depletion leads to transcription up-regulation or down-regulation of the tested genes, whereas mRNA levels of the negative control *ABDH* remained unchanged. Both PARP1 and ALC1 were significatntly down-regulated at the RNA and protein levels (Figure 5.7 and 5.8).

RT-PCR analysis of mRNA levels for ALC1 regulated candidate genes
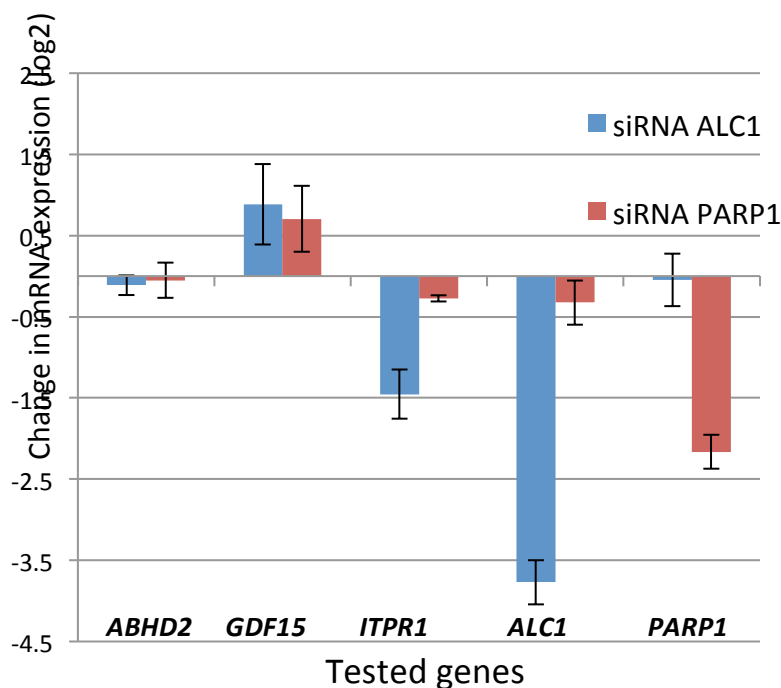
Figure 5.7 ALC1 knock-down recapitulates an effect of PARP1 knock-down on PARP1 target genes. Breast cancer cells (MCF-7) were treated with siRNA to knock-down individually PARP1 or ALC1. Post-siRNA treatment (48 hours) the cells were collected and total RNA was extracted. Shown on the graph are mRNA levels of the respective genes (post-siRNA treatment: PARP1 or ALC1) normalized to the mRNA levels of the respective genes from cells treated with non-specific siRNA (mock control) (indicated as 0 in the logarithmic scale, on the **Y-axis**). Tested genes were: ***ABHD2 -*** abhydrolase domain-containing 2, ***GDF15*** – growth differentiation factor 15, ***ITPR1*** – inositol 1,4,5-trisphosphate receptor 1, ***ALC1*** – amplified in liver cancer 1, ***PARP1-*** poly-ADP-ribose polymerase 1. Error bars represent Standard Error of Mean from 4 experiments.

The evaluation of mRNA levels for the candidate genes was conducted at 48 hours post-siRNA knock-down, of PARP1 or ALC1. At this time point, ALC1 was significantly down-regulated at the RNA level, however the protein down-regulation was not as strong as expected based on RNA leftover around 10 % (see Figure 5.8). Thus, I tested the efficiency of ALC1 knock-down after 72 hours of specific ALC1 siRNA addition (for details see Materials and Methods). As shown on Figure 5.9, at the 72 hour time point after siRNA treatment, ALC1 is further down-regulated at the protein level. I have not tested the mRNA levels of PARP1 target genes upon 72 hours of ALC1 siRNA.

Western blot of MCF-7 cell protein extracts
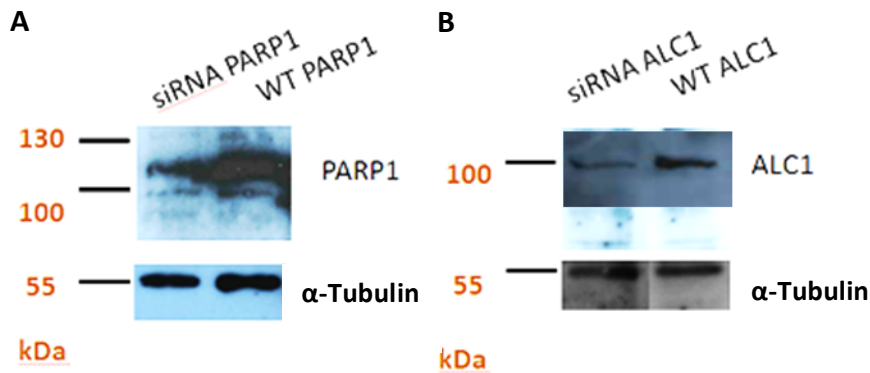
Figure 5.8 PARP1 and ALC1 are efficiently knocked down. Whole-protein extracts from MCF-7 cell lines upon transient expression of siRNA specific to PARP1 (**A**) or ALC1 (**B**) were analyzed via SDS-PAGE and visualized by western blot with anti-PARP1, anti-ALC1 and anti-Tubulin (loading control) antibodies. All antibodies detected proteins of the expected size: 116 kDa for PARP1, 100 kDa for ALC1 and 55 kDa for Tubulin. PARP1 (**A**) and ALC1 (**B**) are significantly depleted in the MCF-7 cell lines (upper panels, respectively). Loading of protein extract on SDS-PAGE was similar, as indicated by α-Tubulin levels (lower panels, respectively). Markers indicating the size of the protein are indicated on the left in kilodaltons (kDa). WT PARP1 and WT ALC1 correspond to cells treated with non-specific siRNA (mock control).

Western blot of MCF-7 cell protein extracts
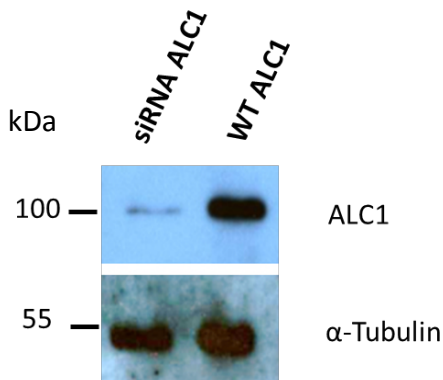
Figure 5.9 ALC1 is efficiently knocked down at 72 hours after siRNA treatment. Whole-protein extracts from MCF-7 cell lines upon transient expression of siRNA specific to ALC1were analyzed via SDS-PAGE and visualized by western blot with anti-ALC1 and anti-Tubulin (loading control) antibodies. All antibodies detected proteins of the expected size: 100 kDa for ALC1 and 55 kDa for Tubulin. ALC1 is significantly depleted in the MCF-7 cell lines (upper panels). Loading of protein extract on SDS-PAGE was similar, as indicated by α-Tubulin levels (lower panels). Marker indicating the size of the protein is indicated on the left in kilodaltons (kDa). WT ALC1 corresponds to cells treated with non-target specific siRNA (mock control).

5.7 Generated antibodies anti-ALC1 specifically recognize the target protein

In order to facilitate studies of the molecular mechanism of ALC1's role in transcription regulation, I generated ALC1-specific polyclonal antibodies. Each of the individual ALC1 domains (macrodomain and ATPase domain) was used as an antigen in rabbit immunization (for details see Materials and Methods). The resulting serum from immunized animals was then analyzed on the whole-protein extracts from cells: (i) expressing endogenous levels of ALC1, (ii) overexpressing ALC1 labelled with YFP, and (iii) cells with siRNA knocked-down ALC1 (72 hours). As shown on Figure 5.10 both newly generated polyclonal antibodies specifically recognize endogenous ALC1 or overexpressed ALC1-YFP and as expected no signal was detected in cells depleted of ALC1.
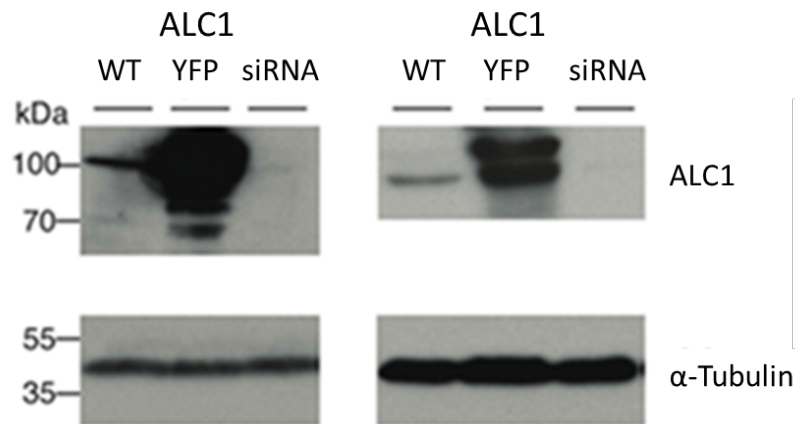
Figure 5.10 Generated polyclonal antibodies specifically recognize ALC1. Whole-protein extracts from U2OS cell lines: with endogenous ALC1 levels (wild type, **WT**), overexpressed ALC1 tagged with Yellow Fluorescent Protein (**YFP**), and cells with depleted ALC1 via siRNA specific to ALC1 (**siRNA**; 72 hours) were analyzed via SDS-PAGE and visualized by western blot with anti-ALC1 and anti-Tubulin (loading control) antibodies. Used ALC1 antibodies were: unpurified serum recognizing ALC1 macrodomain (left) and unpurified serum recognizing ALC1 ATPase domain (right). All antibodies detected proteins of the expected size: 100 kDa for ALC1 and 55 kDa for Tubulin. Loading of protein extract on SDS-PAGE was similar, as indicated by α-Tubulin levels (lower panels). Markers indicating the size of the protein are indicated on the left in kilodaltons (kDa). No ALC1-specific signal was detected lanes with knocked down ALC1.

5.8 The generated polyclonal antibody immunoprecipitates ALC1

I planned to use the newly generated antibodies against ALC1 to test ALC1 chromatin association, especially at the sites of identified candidate genes (see Figure 5.7). The pattern of ALC1 association with these genes, would shed light on the mechanism behind de-regulation of *GDF15* and *ITPR1* expression upon ALC1 knock-down.

At first, I tested the suitability of ALC1 antibodies to specifically immuno-precipitate (IP) ALC1 in various conditions, including the typical conditions for chromatin immuno-precipitation (ChIP, for details see Materials and Methods). Predominantly I used osteosarcoma cells (U2OS) that express ALC1 tagged with YFP. The level of ALC1 in this cell line is a few times higher than the endogenous level of ALC1 (see Figure 5.10). A use of cell line that overexpressed ALC1 facilitated optimization of IP and ChIP conditions. I optimized the IP conditions in:

    (i)   cells that were not treated with formaldehyde

    (ii)   cells in which proteins were crosslinked to chromatin via 1 % formaldehyde treatment.

    (iii)   Cells which underwent formaldehyde treatment as in (ii), plus the cells after formaldehyde treatment were sonicated with Covaris in order to shear DNA to desirable size (200 bp and 500 bp).

In order to pull down ALC1, I used antibodies against YFP and directly against ALC1. An antibody against YFP was generated with GFP as an antigen (Ladurner laboratory own stock). Between YFP and GFP is only one amino acid difference, and the anti-GFP antibody recognizes YFP very well.

In tested conditions, an antibody against GFP readily precipitated ALC1-YFP from cells not treated with formaldehyde and the cells treated with formaldehyde (indicated as crosslinked, Figure 5.11 A). Once I established good IP conditions with the anti-GFP antibody, I tested the suitability of generated ALC1 antibodies on the same cellular material. As shown on Figure 5.11 B, the generated ALC1 antibody immunoprecipitates ALC1 from cells that underwent formaldehyde treatment (crosslinked). Whereas precipitation of ALC1 was straightforward in no formaldehyde or with formaldehyde treated cells, the addition of sonication to the crosslinked material caused difficulties in ALC1 precipitation.
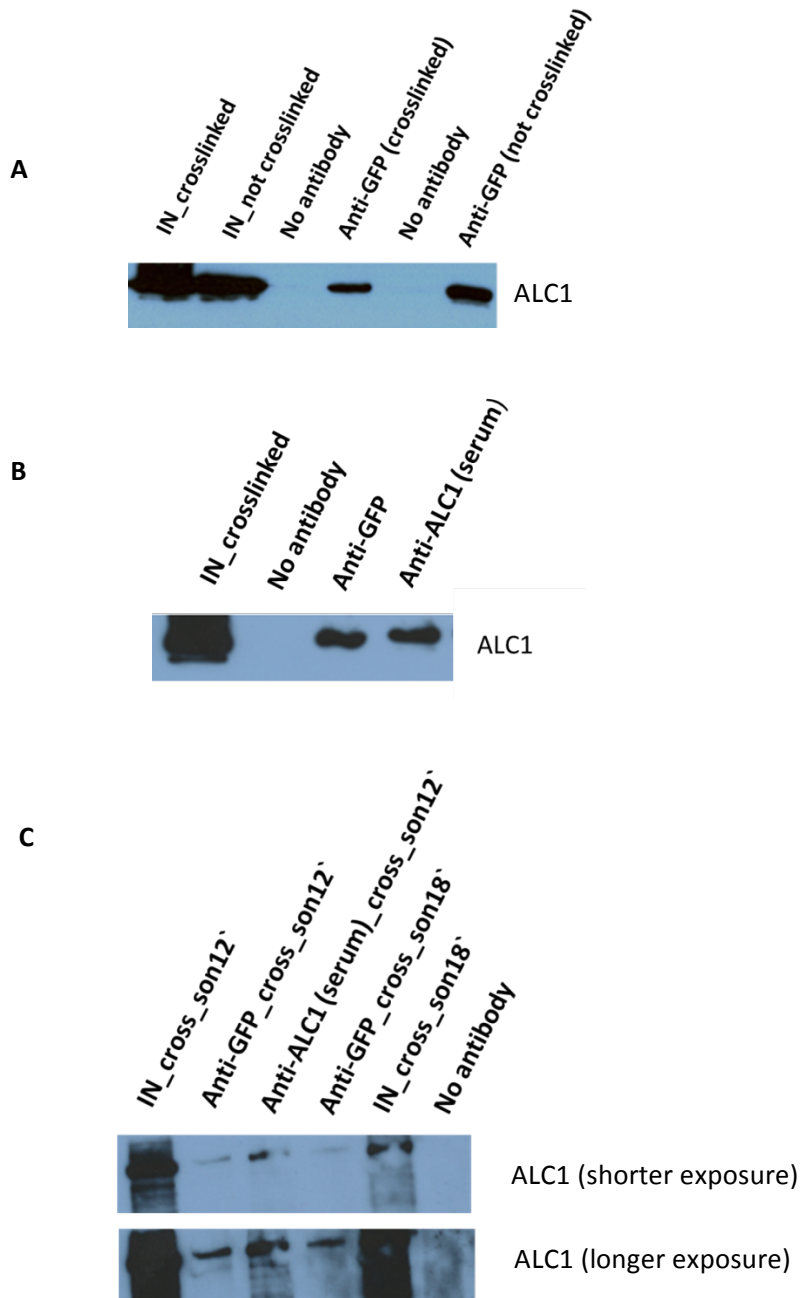
Figure 5.11 Generated ALC1 polyclonal antibody specifically immunoprecipitates ALC1. U2OS ALC1 was immunoprecipitated from cells that express ALC1 labelled with yellow fluorescent protein (**YFP**). The following antibodies were used: anti - green fluorescent protein (**GFP**) and anti – amplified in liver cancer 1 (**ALC1**) generated with ALC1 macrodomain as antigen. The cells were: **A)** not treated (not crosslinked) or treated with 1% formaldehyde for 10 minutes at RT (crosslinked). IN – input, 30 %. **B)** cells were treated with 1% formaldehyde for 10 minutes at RT (crosslinked). 30 % input. **C)** cells were treated with 1% formaldehyde for 10 minutes at RT (**crosslinked/cross**) and Covaris sonicated (**son**) for indicated time - **12** or **18** minutes. 7 % input.

Eventually, an increase of input material and modification of sonication conditions (time and sonication temperature) allowed for ALC1 precipitation (Figure 5.11 C). Afterwards, the same conditions were used to pull down DNA fragments that are presumably crosslinked to ALC1. qPCR was performed on the pull-down DNA with the primers spanning TSS and up- and down-stream regions from the TSS of ALC1 candidate genes. However, the results of ALC1 residence at these sites were inconsistent and not robustly reproducible (data not shown).

5.9 Discussion

(i) ALC1's transcriptional functions depend on PARP1 activity

My data suggests that ALC1 plays a role in transcription regulation. The functions of ALC1 seem to be restricted to certain transcriptional programs, importantly downstream of PARP1 (Figure 5.7). The previously published reports, which linked ALC1 to transcription, lacked the underlying mechanism for ALC1 association with chromatin. As shown in Figure 5.12 ALC1 is highly mobile within nucleus (similar to PARP1, FRAP evaluated), thus ALC1 associations with chromatin are most likely transient and only prolonged upon specific stimuli.
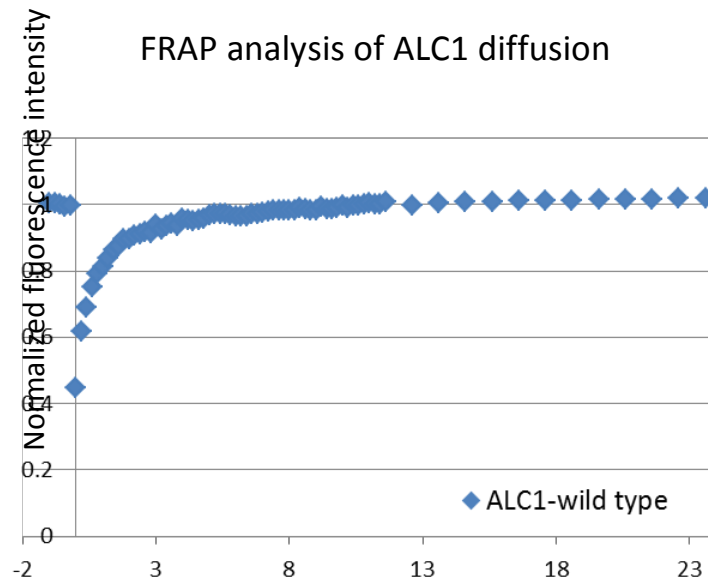
Figure 5.12 ALC1 is a freely diffusive molecule within the nucleus. Amplified in liver cancer 1 (**ALC1**) was transiently expressed (24 hours) in breast cancer cells (MCF-7) and FRAP measured. Only cells with low fluorescence intensity were chosen for the analysis. Showed FRAP curves for each construct are the averaged measurements from at least 10 cells.

Knock down of ALC1 results in a similar outcome on the target genes as the knock-down of PARP1. This result suggests that prolonged chromatin association of ALC1 will depend on PAR signal in the transcriptional context, similarly to DNA damage. However no macrodomain mutants of ALC1 (unable to bind PAR) were evaluated in transcription assays.

(ii) ALC1 acts as co-activator and co-repressor of transcription

Based on deregulation of target genes (*GDF15* and *ITPR1*) upon ALC1 knock-down, it appears that ALC1 can act as a transcription activator or repressor, similarly to PARP1. It will be interesting to find out how exactly ALC1, as a chromatin remodeler, achieves its bi-functionality at the chromatin structure level. Deciphering a role for ALC1 in nucleosome position, or nucleosome composition is of great importance. Mass spectrometry study of ALC1 interactors identified H2A and H2B histones as immunoprecipitated with ALC1 (Gottschalk et al., 2009). For example, enrichment or depletion of these histones or histone variants could be tested at ALC1 target genes upon ALC1 wild type knock-down or overexpression. As well, an evaluation of chromatin structure organization, upon presence of non-functional macro and ATPase mutants of ALC1, could shed light on the chromatin remodeler functions. It would however be critical in these steps first to know the occupancy profiles of ALC1 genome-wide (TSS, gene body, enhancers, etc.). A difficulty in this respect may be overcome by further optimizing ChIP conditions with alternative fragmentation of DNA e.g. enzymatic or modification of crosslinking conditions. Presumably PARP1 is not activated at the target genes as robustly as it is at sites of DNA damage. Thus it may be that the number of ALC1 molecules recruited to the sites of PARP1 activity at genes is low or even that the function of ALC1 is short lived. This may explain difficulties in consistency of ALC1 ChIP at the target genes.

(iii) Functions of PARP1 and ALC1 in ER-dependent transcription need a re-evaluation

PAR levels in unstressed cells (no DNA damage, no heat shock) are very low. The use of estrogen-inducible transcription system to study PARP1-dependent genes (as reported previously) seemed to be desirable to decipher ALC1 functions in transcription. The hormone and nuclear receptor-regulated transcription was supposed to rely on high PAR levels, which were assumed to promote robust chromatin association of PAR readers, including ALC1.

Strikingly, my data questions the previously reported essential role of PARP1 in transcriptional activation of estrogen receptor-dependent genes (Figure 5.1, 5.3 and 5.5).

Both chemical inhibitors of PARP1 used in this study effectively prevent activation of PARP1 (PAR levels are not detectable *in vivo*). Only AG1436 deregulated expression of ERα-responsive genes, however mainly at high concentrations (5 μM and 15μM). This effect is most likely caused by secondary off-target effects of the AG14361 molecules (see Figure 5.4). The possible secondary targets of AG14361 are not known. The analysis of commonly used PARP1 inhibitors in the field, suggests that most of them are not exclusively PARP1-specific. Often at high concentrations, in addition to PARP1, other PARPs or non-PARP family members can be targeted (Wahlberg et al., 2012). The off-target effects stem from a fact that used PARP1 inhibitors are actually NAD^+ analogs, thus not specific to PARP1 only. In this study, the most recent PARP1 inhibitors were used (olaparib and AG14361) with higher specificity than 3-AB or PJ-34 used by authors of previous reports of PARP1 importance in nuclear receptor gene expression regulation (see also 5.1).

Another explanation may be that PARP1 plays an important role in activation of these genes however the PARP1's role is highly resolved in time. It would be important to look at mRNA levels of ERα-responsive genes post-estrogen stimulation in time (30 minutes, 45 minutes, 60 minutes and 90 minutes). However, no changes in ERα chromatin association in early time points, upon transcription stimulation with estrogen were, observed suggesting, the changes in that mRNA level may not be noticeable either.

Importantly, the evidence so far rules out the importance of ALC1 in ERα-dependent transcription, when ALC1 was evaluated directly (Figure 5.1 and 5.3).

6 Outlook

The significance of PAR metabolism in regulating human health is widely recognized. It even seems that it is only a matter of time before we see chemical compounds prescribed by doctors as medicines in order to modify cellular PAR signaling in a benefit to the patient. Recent progress regarding the mechanisms driving occurrence and degradation of PAR metabolism further increases the chances of more adequate diagnosis and treatment in cases of human pathophysiology, involving PAR. The recent progress regarding the molecular mechanism of PARP1 activation is promising, however some questions are still not answered.

How does PARP1 associate with transcriptional sites?

The conclusions of my work suggest that binding of PARP1 to DNA breaks is zinc finger-mediated. However the dependence of zinc fingers for PARP1 binding to transcriptional sites is not clear and not extensively evaluated *in vivo.* Thanks to recent work, it is for example known that PARP1 needs to be already activated (presumably elsewhere) and PAR modified, in order to associate with androgen receptor (AR)-dependent genes (Schiewer et al., 2012) or *c-FOS* promoter (O'Donell et al., 2013). In the presence of chemical inhibitors of PARP1, the association of PARP1 is no longer detectable at these genes (Schiewer et al., 2012, O'Donell et al., 2013). In contrast, at DNA damage sites, bound PARP1 is stably trapped in the presence of chemical inhibitors (Timinszky et al., 2009). An investigation of PARP1 domain importance for chromatin association in well defined transcriptional context is necessary.

How does PARP1 become activated at transcriptional sites?

It is not clear how PARP1 becomes activated at transcription sites. In recent studies where PARP1 is claimed to regulate the co-activation of transcription, PARP1 activation was linked to its phosphorylation (Wright et al., 2012, O'Donell et al., 2013). Genome-wide profiling of PARP1 and CDK2 kinase reveled only 31 % overlap between the two. CDK2 was suggested to play a critical role in PARP1's activation upon progesterone stimuli (Wright et al., 2012). However, the knock-down of CDK2 reduced PAR levels in a cell, but did not abolish then completely (Wright et al., 2012). These results suggest that indeed phosphorylation of PARP1 enhances its activity but is not essential for PARP1 activation. In addition, the nearly full-length

X-ray structure of PARP1 bound to blunt ended DNA stress the importance of intramolecular interactions between the ZF1, ZF3 and WGR for PARP1 catalytic domain activation (Langelier et al., 2012). The intramolecular interactions are triggered by PARP1 binding to DNA. Thus PARP1 activation exclusively due to posttranslational modification needs further evidence.

Drosophila melanogaster PARP activation was proposed to depend on phosphorylation of the H2A.V histone variant (Kotova et al., 2011, Thomas et al., 2014). Presence of H2A.V histone variant exposes H4, which supposedly stimulates dPARP *in vitro* (Pinnola et al., 2007, Thomas et al., 2014). This stimulatory effect of H4 on PARP1 activity was however not seen by others (Kim et al., 2004, Clark et al., 2012). Depletion of H2A.V in flies leads to increased association of dPARP at *hsp70* loci (Kotova et al., 2011). Thus, if activated dPARP was released from chromatin due to H2A.V stimulation, indeed it would not be surprising to see increased levels of dPARP in the absence of H2A.V. However, upon H2A.V depletion, dPARP would have to remain inactive and PAR levels not detectable at *hsp70 loci*. These assumptions need to be tested.

Does PARP1 regulate transcription due to functions in DNA repair?

It is not clear that PARP1 does not associate and become activated at some of the transcription sites due to the presence of DNA breaks. The comprehensive analysis of *hsp70* loci prior to heat shock revealed that PARP1 association with *hsp70* TSS is PAR activity-independent and PARP1 is inactive. The importance of zinc fingers for PARP1 association was unfortunately not tested (Petesch and Lis, 2012). Upon heat shock, Topoisomerase I (Top I) is recruited to the *hsp70* loci within seconds post-RNA polymerase II recruitment (Zobeck et al., 2010). It is highly probable that Top I is recruited to the heat shock regulated loci in order to release the DNA topological stress introduced by transcription. Top I could introduce the DNA break, which has not been tested. Thus, it is possible that PARP1 could be activated due to the presence of DNA breaks at the highly transcribed *hsp70* loci. For example, in differentiating adipocytes, PAR and transcript levels of PARP1-dependent genes are reduced upon chemical inhibition of Topoisomerase II (Top II) activity (Erener at al., 2012). Unfortunately, an association of PARP1 with PARP1 target genes upon chemical inhibition of Top II was not tested. In addition, the phosphorylation of H2A.V is considered a DNA damage marker in flies, analogous to H2A.X phosphorylation in higher eukaryotes (Baldi and Becker, 2013).

Heat shock and hormonal treatment are sources of stress for a cell. It is known that excessive proliferation upon e.g. estrogen, progesterone or androgen treatment contributes to genome instability due to stalled DNA replication forks and their incorrect repair (Halazonetis et al., 2008, Williamson et al., 2011). The ERα signaling down-regulates the DNA damage response, further increasing DNA instability (Caldon, 2014). Importantly, the DNA breaks were detected at ERα-regulated *pS2* promoter upon estrogen treatment (Ju et al., 2006). The peculiar finding only PAR modified PARP1's presence at *c-FOS* gene and androgen responsive genes suggests that DNA lesions could be in the vicinity to these promoters. If so, PARP1 could be activated at DNA breaks and spread into the evaluated promoters in a PAR-dependent fashion.

In summary, it is of high interest to resolve the DNA break presence at and near the transcription sites upon rapid transcription induction, in order to re-solve PARP1's binding to transcription sites and subsequent activation mechanisms. It is probable that PARP1 initiates DNA repair at highly transcribed genome regions. Thus some of the roles of PARP1 in transcription could still be PARP1's classic functions in DNA repair.

PARP1's association with DNA matters

Understanding PARP1's association with chromatin at DNA damage and transcription sites matters. If the mechanisms behind the chromatin association were similar, it would allow for universal modification of PARP1 activity via chemical compounds in various physiological conditions. If the mechanisms of PARP1 and chromatin interactions are different, then the chemical inhibition of PARP1 activity has to be carefully tailored depending on the actual molecular mechanism underlying the PAR metabolism malformation. Not tailored interference with PARP1 activity may be not beneficial and moreover lead to the off-target side effects. For example, where it is known that PARP1 associates with chromatin due to zinc fingers, the use of PARP1 inhibitors (NAD^+ analogs) results in trapped PARP1 at the DNA breaks, increasing toxicity and cancer cell death (Murai et al., 2012 and 2014).

Specific PARP1 inhibitors are needed

PARP1 inhibitors (NAD^+ analogs), which are used commonly in basic research laboratories, are often not specific to a single target (Wahlberg et al., 2012, Antolin et al., 2012, Zhang et al., 2013b). Olaparib, the compound proposed to Food and Drug Administration (FDA) as a treatment for a subset of ovarian cancers, was found to target PARP1, PARP2, PARP3, PARP4, PARP12, PARP15 and PARP16 (Wahlberg et al., 2012). Whereas in disease treatment non-specificity of the compound can be beneficial, like it is with kinase inhibitors (Goreschi et al., 2009), in basic research laboratories the non-specificity of the compound is a major limitation. The observed biological phenomena that are attributed exclusively to one of the PARPs may in reality be a summary of various unknown off-target effects. The commonly used 3-AB inhibitor of PARP1 actually shows low potency and specificity in inhibiting PAR modification of the acceptor proteins (Zhang et al., 2013b). Another commonly used PARP1 inhibitor, PJ-34, targets other PARPs and PIM kinases (Antolin et al., 2012).

Luckily a need for specific chemical compounds exclusively modulating PARP1 activity has been recognized. A new approach takes advantage of intramolecular domain interactions that are specific to PARP1 based on the X-ray structure (Langelier et al., 2012). The authors developed the high throughput assay to screen for the compounds that interfere with intramolecular interactions of PARP1 domains and thus exclusively inhibit PARP1 (Steffen et al., 2014).

PARP1 and ALC1 co-regulate each other

ALC1's chromatin remodeling functions depend on PAR. This dependence is manifested in ATPase domain activation, upon macrodomain-mediated PAR binding and possibly ALC1 protein PAR modification (Gottschalk et al., 2009). Thus, ALC1 functions in transcription and DNA repair are coupled to PARP1 roles in transcription and DNA repair. A clarification of PARP1 association with, and activation at, chromatin sites will facilitate studies of ALC1 chromatin remodeling roles *in vivo*.

Interestingly, a more detailed investigation of ALC1's dependence on active PARP1 revealed that both ALC1 and PARP1 co-operatively bind to DNA or nucleosomes *in vitro*. This results in formation of a stable PARP1-ALC1-DNA/nucleosome complex and prevents release of PARP1 from the complex (Gottschalk et al., 2012). I tested if ALC1 can modulate PARP1 association
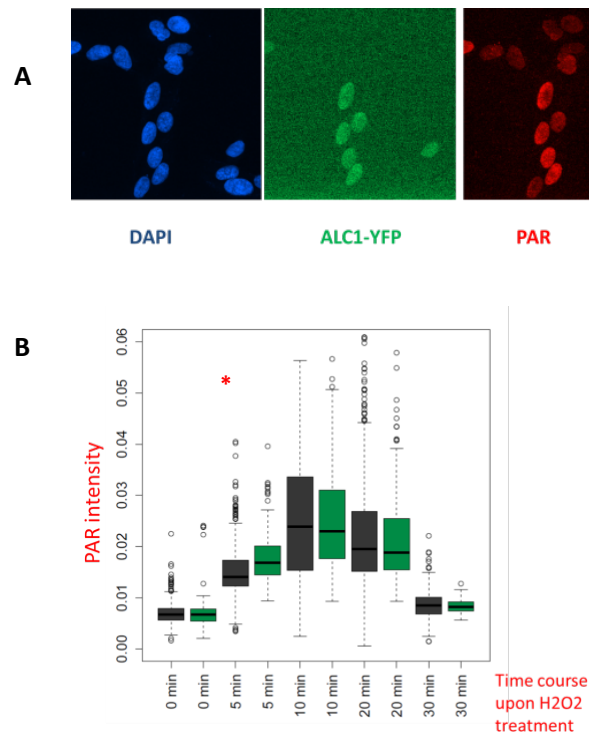
Figure 6.1 ALC1 overexpression leads to elevated PAR levels in 5 minutes after DNA damage induction. A) Cells expressing endogenous ALC1 levels (no yellow fluorescent protein signal – no **YFP**) were mixed with cells overexpressing ALC1 (YFP signal) and stained for poly-ADP-ribose (**PAR**) levels upon DNA damage induction with hydrogen peroxide treatment (1 μM; 5-30 minutes). Shown on the left are all the cells, which nuclei was stained with Hoechst 33285 (blue), in the middle are cells that overexpress ALC1 (green), and on the right are cells that underwent PARylation upon hydrogen peroxide treatment (red; shown is a 5 minute time point during treatment). **B)** Quantification of PAR levels (0 – 30 minutes) upon DNA damage induction. PAR levels were elevated at 5 minute time point in cells that overexpressed ALC1 (* - statistically significant; each condition and each cell line n > 100 cells). PAR levels were quantified with Cell Profiler software.

and activity at chromatin sites *in vivo*. Two cell lines were mixed and cultured together. One that expressed endogenous levels of ALC1 and another that had ALC1 levels a few times elevated when compared to endogenous ALC1 levels (ALC1-YFP). The cells were distinguishable due to YFP tag on ALC1. The cells were treated with hydrogen peroxide to induce oxidative DNA damage, which is known to stimulate PARP1 activity. Next, PARP'1s activity was evaluated via PAR staining. The time course of hydrogen peroxide treatment suggested that PAR is elevated between 5 and 20 minutes. Interestingly, higher levels of ALC1 lead to increased levels of PAR

at 5 minutes after DNA damage induction (Figure 6.1). This result is reproducible and suggests that ALC1 can modulate PARP1 activity *in vivo*. Taking into account that PARP1's activity is coupled to DNA break binding, it appears that PARP1 association with chromatin will be regulated by ALC1 (data not shown). It remains to be determined if the chromatin remodeling function of ALC1 is a main reason behind ALC1 roles in regulation of PARP1 activity.

7 Appendix: Additional Figures

Western blot of HeLa Kyoto
protein extracts
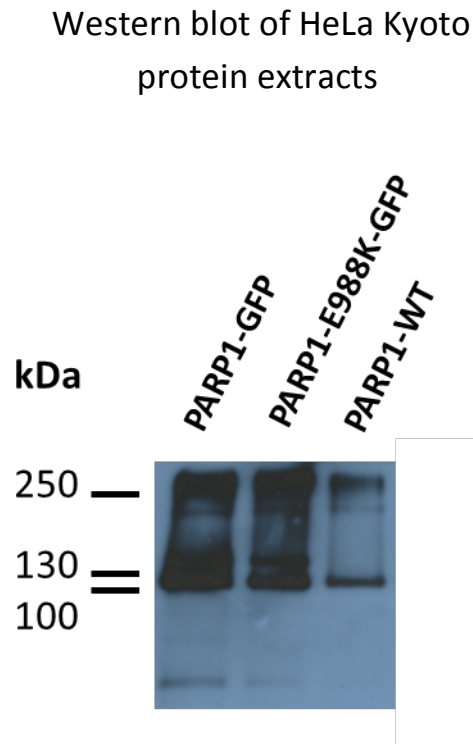
Figure 7.1 Generated polyclonal antibodies specifically recognize PARP1. Whole-cell protein extracts from HeLa-Kyoto *wild type* (WT) cells transiently transfected with PARP1-GFP (first on the left), WT cells transiently transfected with PARP1-E998K-GFP (the mutant capable of mono-ADP-ribosylation, in the middle) and WT (first on the right) were analyzed via SDS-PAGE and visualized by Western blot with anti-PARP1 and anti-Tubulin (loading control) antibodies. Used antibody against PARP1 was an unpurified serum (fourth bleed) from a rabbit injected with zinc finger 1 and zinc finger 2 as antigen. Both antibodies detected proteins of the expected size: Above 130 kDa for PARP1-GFP, above 100 kDa for PARP1. Marker indicating the size of the protein is indicated on the left in kilodaltons (kDa).

FCS analysis of HP1α diffusion and chromatin binding times

HP1α (second component)
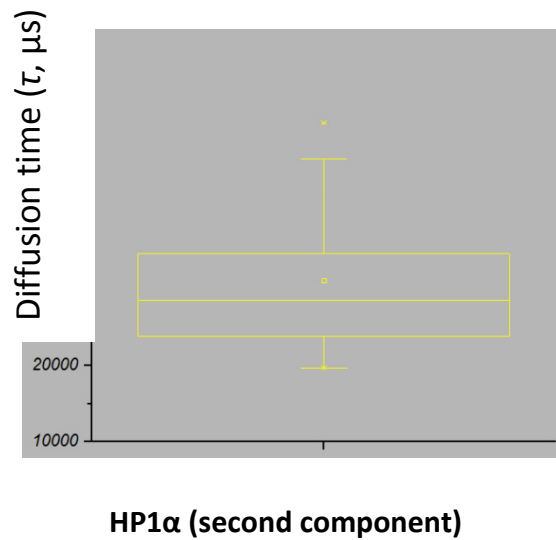
Figure 7.2 Diffusion time of the second component of HP1α-full length is reduced due to chromatin binding. Mobility of **HP1α**– heterochromatin protein 1 alpha stably expressed in U2OS cells was FCS tested. The box plot is composed of FCS measurements taken in more than 10 cells. In each cell the measurement was taken in 3 randomly chosen sites in the nucleus avoiding nucleoli and nuclear periphery. Only cells with identical fluorescence intensity were selected. The horizontal lines (whiskers) represent the maximum and minimum values, the box signifies the upper (75th) and lower quartiles (25th), the median is represented by a short line within the box and the mean is represented by a square within the box.

8 Bibliography

Ahel D, Horejsí Z, Wiechens N, Polo SE, Garcia-Wilson E, Ahel I, Flynn H, Skehel M, West SC, Jackson SP, Owen-Hughes T, Boulton SJ. Poly(ADP-ribose)-dependent regulation of DNA repair by the chromatin remodeling enzyme ALC1. *Science*. 2009 Sep 4; 325(5945):1240-3.

Ali AA, Timinszky G, Arribas-Bosacoma R, Kozlowski M, Hassa PO, Hassler M, Ladurner AG, Pearl LH, Oliver AW. . The zinc-finger domains of PARP1 cooperate to recognize DNA strand breaks. *Nat Struct Mol Biol*. 2012 Jun 10; 19(7):685-92.

Alkhatib, H. M., D. F. Chen, B. Cherney, K. Bhatia, V. Notario, C. Giri, G. Stein, E. Slattery, R. G. Roeder, and M. E. Smulson. Cloning and expression of cDNA for human poly(ADP-ribose) polymerase. *Proc. Natl. Acad. Sci. USA*. 1987, 84:1224–1228.

Althaus FR, Richter C. ADP-ribosylation of proteins. Enzymology and biological significance. *Mol Biol Biochem Biophys*. 1987, 37, I-126.

Althaus FR, Kleczkowska HE, Malanga M, Müntener CR, Pleschke JM, Ebner M, Auer B. Poly ADP-ribosylation: a DNA break signal mechanism. *Mol Cell Biochem*. 1999 Mar; 193(1-2):5-11.

Altmeyer M, Messner S, Hassa PO, Fey M, Hottiger MO. Molecular mechanism of poly(ADP-ribosyl)ation by PARP1 and identification of lysine residues as ADP-ribose acceptor sites. *Nucleic Acids Res*. 2009 Jun; 37(11):3723-38.

Alvarez-Gonzalez, R., Jacobson, M.K. Characterization of polymers of adenosine diphosphate ribose generated *in vitro* and *in vivo*. *Biochemistry*. 1987, 26, 3218–3224.

Alvarez-Gonzalez R, Althaus FR. Poly(ADP-ribose) catabolism in mammalian cells exposed to DNA-damaging agents. *Mutat Res*. 1989, 218(2):67–74.

Anantharaman, V., Koonin, E. V. & Aravind, L. Comparative genomics and evolution of proteins involved in RNA metabolism. *Nucleic Acids Res*. 2002, 30, 1427–1464.

Antolín AA, Jalencas X, Yélamos J, Mestres J. Identification of pim kinases as novel targets for PJ34 with confounding effects in PARP biology. *ACS Chem Biol*. 2012 Dec 21; 7(12):1962-7.

Aubin RJ, Dam VT, Miclette J, Brousseau Y, Huletsky. A., Poirier G.G. Hyper(ADP-ribosyl)ation of histoneH1. *Can. J. Biochem*. 1982, 60, 1085–1094.

Bancaud A, Huet S, Daigle N, Mozziconacci J, Beaudouin J, Ellenberg J. Molecular crowding affects diffusion and binding of nuclear proteins in heterochromatin and reveals the fractal organization of chromatin. *EMBO J*. 2009 Dec 16; 28(24):3785-98.

Bakulski KM, Fallin MD. Epigenetic epidemiology: promises for public health research. *Environ Mol Mutagen*. 2014 Apr; 55(3):171-83.

Baldi S, Becker PB. The variant histone H2A.V of Drosophila--three roles, two guises. *Chromosoma*. 2013 Aug; 122(4):245-58.

Barber LJ, Sandhu S, Chen L, et al. Secondary mutations in *BRCA2* associated with clinical resistance to a PARP inhibitor. *J Pathol* 2013, 229: 422-9.

Barkauskaite E, Jankevicius G, Ladurner AG, Ahel I, Timinszky G. The recognition and removal of cellular poly(ADP-ribose) signals. *FEBS J.* 2013 Aug; 280(15):3491-507.

Barkauskaite E, Brassington A, Tan ES, Warwicker J, Dunstan MS, Banos B, Lafite P, Ahel M, Mitchison TJ, Ahel I, Leys D. Visualization of poly(ADP-ribose) bound to PARG reveals inherent balance between exo- and endo-glycohydrolase activities. *Nat Commun.* 2013, 4:2164

Bauer P. I., Farkas G., Buday L., Mikala G., Meszaros G., Kun, E., Farago A. Inhibition of DNA binding by the phosphorylation of poly ADP-ribose polymerase protein catalysed by protein kinase C. *Biochem. Biophys. Res. Commun.* 1992, 187 (2), 730–6.

Beaudouin J, Mora-Bermúdez F, Klee T, Daigle N, Ellenberg J. Dissecting the contribution of diffusion and interactions to the mobility of nuclear proteins. *Biophys J.* 2006 Mar 15;90(6):1878-94. Epub 2005 Dec 30.

Blomster HA, Hietakangas V, Wu J, Kouvonen P, Hautaniemi S, and Sistonen L. Novel proteomics strategy brings insight into the prevalence of SUMO-2 target sites. *Mol. Cell. Proteomics.* 2009, 8 1382–1390.

Buki KG, Bauer PI, Hakam A, Kun E. Identification of domains of poly(ADP-ribose) polymerase for protein binding and self-association. *J Biol Chem.* 1995 Feb 17; 270(7):3370-7.

Bryant HE, Schultz N, Thomas HD. Specific killing of BRCA2-deficient tumors with inhibitors of poly(ADP-ribose) polymerase. *Nature* 2005, 434: 913-7.

Burgess RC, Misteli T, Oberdoerffer P. DNA damage, chromatin, and transcription: the trinity of aging. *Curr Opin Cell Biol.* 2012 Dec; 24(6):724-30.

Caldon CE. Estrogen signaling and the DNA damage response in hormone dependent breast cancers. *Front Oncol.* 2014 May 14; 4:106.

Chambon P, Weill JD, Mandel P. Nicotinamide mononucleotide activation of new DNA-dependent polyadenylic acid synthesizing nuclear enzyme. *Biochem Biophys Res Commun.* 1963 Apr 2; 11:39-43.

Chen L, Yuan YF, Li Y, Chan TH, Zheng BJ, Huang J, Guan XY. Clinical significance of CHD1L in hepatocellular carcinoma and therapeutic potentials of virus-mediated CHD1L depletion. *Gut.* 2011 Apr; 60(4):534-43.

Chen L, Chan TH, Guan XY. Chromosome 1q21 amplification and oncogenes in hepatocellular carcinoma. *Acta Pharmacol Sin.* 2010 Sep;31(9):1165-71.

Chen L, Chan TH, Yuan YF, Hu L, Huang J, Ma S, Wang J, Dong SS, Tang KH, Xie D, Li Y, Guan XY. CHD1L promotes hepatocellular carcinoma progression and metastasis in mice and is associated with these processes in human patients. *J Clin Invest.* 2010 Apr; 120(4):1178-91.

Cheng W, Su Y, Xu F: CHD1L: a novel oncogene. *Mol Cancer.* 2013. Dec 21;12(1):170.

Clapier CR, Cairns BR. The biology of chromatin remodeling complexes. *Annu Rev Biochem.* 2009; 78:273-304.

Clark NJ, Kramer M, Muthurajan UM, Luger K. Alternative modes of binding of poly(ADP-ribose) polymerase 1 to free DNA and nucleosomes. *J Biol Chem.* 2012. 287(39):32430–32439

Cléry A, Blatter M, Allain FH. RNA recognition motifs: boring? Not quite. *Curr Opin Struct Biol.* 2008. Jun;18(3):290-8.

Curtin NJ. DNA repair dysregulation from cancer driver to therapeutic target. *Nat Rev Cancer.* 2012. 12(12):801–17.

D'Amours D, Desnoyers S, D' Silva I, Poirier GG. Poly(ADP-ribosyl)ation reactions in the regulation of nuclear functions. *Biochem J.* 1999. Sep 1; 342 (Pt 2):249-68.

Davalos AR, Coppe JP, Campisi J, Desprez PY. Senescent cells as a source of inflammatory factors for tumor progression. *Cancer Metastasis Rev.* 2010. Jun; 29(2):273-83

De Lorenzo SB, Patel AG, Hurley RM, Kaufmann SH. The Elephant and the Blind Men: Making Sense of PARP Inhibitors in Homologous Recombination Deficient Tumor Cells. *Front Oncol.* 2013. Sep 11; 3:228.

Doly J., Mandel P. Demonstration of the biosynthesis in vivo of a compound polymer, polyadenosine diphosphoribose in the nucleus of the liver of chickens. C. R. *Acad. Sci. D.* 1967, 264:2687–2690.

Dunstan M, Barkauskaite E, Lafite P, Knezevic C, Brassington A, Ahel M, Hergenrother P, Leys D, Ahel I. Structure and mechanism of a canonical poly(ADP-ribose) glycohydrolase. *Nat Commun* 2012, 3, 878

Durkacz BW, Omidiji O, Gray DA, Shall S. (ADP-ribose)n participates in DNA excision repair. *Nature.* 1980 Feb 7; 283(5747):593-6.

Edwards SL, Brough R, Lord CJ. Resistance to therapy caused by intragenic deletion in *BRCA2*. *Nature* 2008; 451:1111- 5.

Erener S, Hesse M, Kostadinova R, Hottiger MO. Poly(ADP-ribose)polymerase-1 (PARP1) controls adipogenic gene expression and adipocyte function. *Mol Endocrinol.* 2012 Jan;26(1):79-86.

Eustermann S, Brockmann C, Mehrotra PV, Yang JC, Loakes D, West S.C, Ahel I, Neuhaus D Solutionstructures of the two PBZ domains from human APLF and their interaction with poly(ADP-ribose). *Nat. Struct. Mol.Biol.* 2010, 17, 241–243.

Farmer H, McCabe N, Lord CJ, et al. Targeting the DNA repair defect in BRCA mutant cells as a therapeutic strategy. *Nature* 2005; 434: 917-21.

Ferro, AM, Minaga T, Piper WN, Kun W. Analysis of larger than tetrameric poly(adenosine diphosphoribose) by a radioimmunoassay in nuclei separated in organic solvents. *Biochim. Biophys. Acta* 1978, 519:291– 305.

Frizzell KM, Gamble MJ, Berrocal JG, Zhang T, Krishnakumar R, Cen Y, Sauve AA, Kraus WL. Global analysis of transcriptional regulation by poly(ADP-ribose) polymerase-1 and poly(ADP-ribose) glycohydrolase in MCF-7 human breast cancer cells. *J Biol Chem*. 2009 Dec 4;284(49):33926-38.

Gagné JP, Hendzel MJ, Droit A, Poirier GG. The expanding role of poly(ADP-ribose) metabolism: current challenges and new perspectives. *Curr Opin Cell Biol*. 2006 Apr;18(2):145-51. Epub 2006 Mar 3.

Gagné JP, Hunter JM, Labrecque B, Chabot B, Poirier GG. A proteomic approach to the identification of heterogeneous nuclear ribonucleoproteins as a new family of poly(ADP-ribose)-binding proteins. *Biochem J*. 2003 Apr 15;371(Pt 2):331-40.

Gagné JP, Isabelle M, Lo KS, Bourassa S, Hendzel MJ, Dawson VL, Dawson TM, Poirier GG. Proteome-wide identification of poly(ADP-ribose) binding proteins and poly(ADP-ribose)-associated protein complexes. *Nucleic Acids Res*. 2008 Dec;36(22):6959-76.

Gagné JP, Moreel X, Gagné P, Labelle Y, Droit A, Chevalier-Paré M, Bourassa S, McDonald D, Hendzel MJ, Prigent C, Poirier GG. Proteomic investigation of phosphorylation sites in poly(ADP-ribose) polymerase-1 and poly(ADP-ribose) glycohydrolase. *J Proteome Res*. 2009 Feb;8(2):1014-29.

Gallmeier E, Kern SE. Absence of Specific Cell Killing of the BRCA2-Deficient Human Cancer Cell Line CAPAN1 by Poly(ADP-ribose) Polymerase Inhibition. *Cancer Biol Ther*. 2005; 4:703–6.

Ghoreschi K, Laurence A, O'Shea JJ. Selectivity and therapeutic inhibition of kinases: to be or not to be? *Nat Immunol*. 2009 Apr;10(4):356-60.

Gottschalk AJ, Trivedi RD, Conaway JW, Conaway RC: Activation of the SNF2 family ATPase ALC1 by poly(ADP-ribose) in a stable ALC1•PARP1•nucleosome intermediate *J Biol Chem*. 2012 Dec 21;287(52):43527-32.

Gottschalk AJ, Timinszky G, Kong SE, Jin J, Cai Y, Swanson SK, Washburn MP, Florens L, Ladurner AG, Conaway JW, Conaway RC: Poly(ADP-ribosyl)ation directs recruitment and activation of an ATP-dependent chromatin remodeler. *Proc Natl Acad Sci U S A*. 2009 Aug 18;106(33):13770-4.

Gradwohl, G., Menissier de Murcia, J. M., Molinete, M., Simonin, F., Koken, M., Hoeijmakers, J. H., and de Murcia, G. The second zinc-finger domain of poly(ADP-ribose) polymerase determines specificity for single-stranded breaks in DNA. *Proc. Natl. Acad. Sci. U.S.A*. 1990, 87, 2990–2994.

Gradwohl G, Ménissier de Murcia JM, Molinete M, Simonin F, Koken M, Hoeijmakers JH, de Murcia G. The second zinc-finger domain of poly(ADP-ribose) polymerase determines specificity for single-stranded breaks in DNA. *Proc Natl Acad Sci U S A*. 1990 Apr; 87(8):2990-4.

Guan XY, Fang Y, Sham JS, Kwong DL, Zhang Y, Liang Q, et al. Recurrent chromosome alterations in hepatocellular carcinoma detected by comparative genomic hybridization. *Genes Chromosomes Cancer* 2000, 29: 110-116.

Hager GL, Elbi C, Becker M. Protein dynamics in the nuclear compartment. *Curr Opin Genet Dev*. 2002 Apr;12(2):137-41.

Hah N, Danko CG, Core L, Waterfall JJ, Siepel A, Lis JT, Kraus WL. A rapid, extensive, and transient transcriptional response to estrogen signaling in breast cancer cells. *Cell.* 2011 May 13; 145(4):622-34.

Haince JF, McDonald D, Rodriguez A, Dery U, Masson JY, Hendzel MJ. PARP1-dependent kinetics of recruitment of MRE11 and NBS1 proteins to multiple DNA damage sites. *J BiolChem* (2008) 283(2):1197–208.

Haince JF, Kozlov S, Dawson VL, Dawson TM, Hendzel MJ, Lavin MF, Poirier GG. Ataxia telangiectasia mutated (ATM) signaling network is modulated by a novel poly(ADP-ribose)-dependent pathway in the early response to DNA-damaging agents. *J Biol Chem*. 2007 Jun 1;282(22):16441-53. Epub 2007 Apr 11.

Halazonetis TD, Gorgoulis VG, Bartek J. An oncogene-induced DNA damage model for cancer development. *Science*. 2008 Mar 7;319(5868):1352-5.

Han, S.P., Tang, Y.H., Smith, R., 2010. Functional diversity of the hnRNPs: past, present and perspectives. Biochem. J. 430, 379–392.

Hao, B., Wang, H., Zhou, K., Li, Y., Chen, X., Zhou, G., Zhu, Y., Miao, X., Tan, W., Wei, Q., Lin, D., He, F., Identification of genetic variants in base excision repair pathway and their associations with risk of esophageal squamous cell carcinoma. *Cancer Res*. 2004, 64 (12), 4378–4384

Hassa PO, Buerki C, Lombardi C, Imhof R, Hottiger MO. Transcriptional coactivation of nuclear factor-kappaB-dependent gene expression by p300 is regulated by poly(ADP)-ribose polymerase-1. *J Biol Chem*. 2003 Nov 14; 278(46):45145-53. Epub 2003 Sep 5.

Hassa PO, Haenni SS, Elser M, Hottiger MO. Nuclear ADP-ribosylation reactions in mammalian cells: where are we today and where are we going? *Microbiol Mol Biol Rev*. 2006 Sep;70(3):789-829.

Hassa PO, Haenni SS, Buerki C, Meier NI, Lane WS, Owen H, Gersbach M, Imhof R, Hottiger MO. Acetylation of poly(ADP-ribose) polymerase-1 by p300/CREB-binding protein regulates coactivation of NF-kappaB-dependent transcription. *J Biol Chem.* 2005 Dec 9; 280(49):40450-64. Epub 2005 Oct 4.

Hassa PO, Haenni SS, Buerki C, Meier NI, Lane WS, Owen H, Gersbach M, Imhof R, Hottiger MO. Acetylation of poly(ADP-ribose) polymerase-1 by p300/CREB-binding protein regulates coactivation of NF-kappaB-dependent transcription. *J Biol Chem*. 2005 Dec 9; 280(49):40450-64. Epub 2005 Oct 4.

Hassa PO, Hottiger MO. A role of poly (ADP-ribose) polymerase in NF-kappaB transcriptional activation. *J Biol Chem*. 1999 Jul-Aug; 380(7-8):953-9.

Hassler M, Ladurner AG. Towards a structural understanding of PARP1 activation and related signalling ADP-ribosyl-transferases. *Curr Opin Struct Biol*. 2012 Dec; 22(6):721-9

Han, W., Li, X., Fu, X. The macro domain protein family: structure, functions, and their potential therapeutic implications. *Mutat. Res*. 2011, 727, 86–103.

Hanahan D, Weinberg RA. Hallmarks of cancer: the next generation. *Cell* 2011, Mar 4;144(5):646-74.

Hayashi K., Tanaka M., Shimada T., Miwa M., Sugimura T. Size and shape of poly(ADP-ribose): examination by gel filtration, gel electrophoresis and electron microscopy. *Biochem. Biophys. Res. Commun*. 1983, 112 102–107.

He WP, Zhou J, Cai MY, Xiao XS, Liao YJ, Kung HF, Guan XY, Xie D, Yang GF: CHD1L protein is overexpressed in human ovarian carcinomas and is a novel predictive biomarker for patients survival. *BMC Cancer* 2012, 12:437.

Heldin CH. Autocrine PDGF stimulation in malignancies. Ups J Med Sci. 2012 May; 117(2):83-91.

Honegger CG, Krenger W, Langemann H. Changes in amino acid contents in the spinal cord and brainstem of rats with experimental autoimmune encephalomyelitis. *J Neurochem*. 1989 Aug; 53(2):423-7.

Hottiger MO, Hassa PO, Lüscher B, Schüler H, Koch-Nolte F. Toward a unified nomenclature for mammalian ADP-ribosyltransferases. *Trends Biochem Sci*. 2010 Apr; 35(4):208-19.

Horton JK, Watson M, Stefanick DF, Shaughnessy DT,Taylor JA, Wilson SH. XRCC1and DNA polymerase beta in cellular protection against cytotoxic DNA single-strand breaks. *Cell Res* 2008, 18(1):48–63.

Hyeon J, Ahn S, Park CK: CHD1L Is a marker for poor prognosis of hepatocellular carcinoma after surgical resection. *Korean J Pathol* 2013, 47:9–15

Hilz, H., K. Wielckens, P. Adamietz, R. Bredehorst, and A. Kreymeier. Functional aspects of mono- and poly(ADP-ribosyl)ation: subcellular distribution and ADP-ribosyl turnover under conditions of repair and 'starvation. *Princess Takamatsu Symp*. 1983. 13:155–163.

Ikejima M, Marsischky G, Gill DM. Direction of elongation of poly(ADP-ribose) chains. Addition of residues at the polymerase-proximal terminus. *J Biol Chem*. 1987 Dec 25;262(36):17641-50.

Ikejima M, S Noguchi, R Yamashita, T Ogura, T Sugimura, D M Gill and M Miwa. The zinc fingers of human poly(ADP-ribose) polymerase are differentially required for the recognition of DNA breaks and nicks and the consequent enzyme activation. Other structures recognize intact DNA. *J. Biol. Chem.* 1990, 265:21907-21913.

Izumi T, Wiederhold L R, Roy G, RoyR, Jaiswal A,Bhakat KK. Mammalian DNA base excision repair proteins: their interactions and role in repair of oxidative DNA damage. *Toxicology.* 2003, 193(1-2):43–65.

Jankevicius G, Hassler M, Golia B, Rybin V, Zacharias M, Timinszky G & Ladurner AG. A family of macrodomain proteins reverses cellular mono-ADP-ribosylation. *Nat Struct Mol Biol.* 2013, 20, 508–514.

Ji X, Li J, Zhu L, Cai J, Zhang J, Qu Y, Zhang H, Liu B, Zhao R, Zhu Z. CHD1L promotes tumor progression and predicts survival in colorectal carcinoma. *J Surg Res.* 2013 Nov; 185(1):84-91.

Ju BG, Lunyak VV, Perissi V, Garcia-Bassets I, Rose DW, Glass CK, Rosenfeld MG. A topoisomerase IIbeta-mediated dsDNA break required for regulated transcription. *Science.* 2006 Jun 23; 312(5781):1798-802.

Kauppinen TM, Chan WY, Suh SW, Wiggins AK, Huang EJ, Swanson RA. Direct phosphorylation and regulation of poly(ADP-ribose) polymerase-1 by extracellular signal-regulated kinases 1/2. *Proc Natl Acad Sci U S A*. 2006 May 2; 103(18):7136-41

Kameshita I., Matsuda Z, Tanigushi T, Shizuta Y. Poly(ADP-ribose)synthetase. Separation and identilication of three proteolytic firagments as the substrate-binding domain, the DNA binding domain, and the automodilication domain. *J Biol Chem.* 1984, 259, 4770—4776.

Karras, G. I. et al. The macro domain is an ADP-ribose binding module. *EMBO J.* 24, 1911–1920 (2005).

Kato M, Kumasaka MY, Takeda K, Hossain K, Iida M, Yajima I, Goto Y, Ohgami N. L-cysteine as a regulator for arsenic-mediated cancer-promoting and anti-cancer effects. *Toxicol In Vitro.* 2011 Apr; 25(3):623-9.

Kim MY, Mauro S, Gevry N, Lis JT, Kraus WL. NAD-dependent modulation of chromatin structure and transcription by nucleosome binding properties of PARP-1. *Cell.* 2004, 119:803–814.

Kleine, H. et al. Substrate-assisted catalysis by PARP10 limits its activity to mono-ADP-ribosylation. *Mol. Cell* 2008, 32, 57–69.

Kleine H, Herrmann A, Lamark T, Forst AH, Verheugd P, Lüscher-Firzlaff J, Lippok B, Feijs KL, Herzog N, Kremmer E, Johansen T, Müller-Newen G, Lüscher B Dynamic subcellular localization of the mono-ADP-ribosyltransferase ARTD10 and interaction with the ubiquitin receptor p62. *Cell Commun Signal.* 2012 Sep 20;10(1):28.

Kotova E, Lodhi N, Jarnik M, Pinnola AD, Ji Y, Tulin AV. Drosophila histone H2A variant (H2Av) controls poly(ADP-ribose) polymerase 1 (PARP1) activation in chromatin. *Proc Natl Acad Sci U S A*. 2011 Apr 12;108(15):6205-10

Kothe GO, Kitamura M, Masutani M, Selker E, Inoue H. PARPis involved in replicative aging in Neurospora crassa. Fungal *Genet. Biol.* 2010, 47, 297–309.

Kraus WL, Hottiger MO. PARP-1 and gene regulation: progress and puzzles. *Mol Aspects Med*. 2013 Dec;34(6):1109-23.

Kreimeyer, A., K. Wielckens, P. Adamietz, H. Hilz. DNA repair associated ADP-ribosylation in vivo. Modification of histone H1 differs from that of the principal acceptor proteins. *J. Biol. Chem*. 1984, 259:890–896.

Krishnakumar R., Matthew J. Gamble, Kristine M. Frizzell, Jhoanna G. Berrocal, Miltiadis Kininis, W. Lee Kraus. Reciprocal Binding of PARP-1 and Histone H1 at promoters specifies transcriptional outcomes. *Science,* 319, 819 (2008).

Krishnakumar R1, Kraus WL. PARP-1 regulates chromatin structure and transcription through a KDM5B-dependent pathway. *Mol Cell*. 2010 Sep 10;39(5):736-49.

Kurosaki, T., H. Ushiro, Y. Mitsuuchi, S. Suzuki, M. Matsuda, Y. Matsuda, N. Katunuma, K. Kangawa, H. Matsuo, T. Hirose, et al. 1987. Primary structure of human poly(ADP-ribose) synthetase as deduced from cDNA sequence. *J. Biol. Chem.* 262:15990–15997.

Kwon YS, Garcia-Bassets I, Hutt KR, Cheng CS, Jin M, Liu D, Benner C, Wang D, Ye Z, Bibikova M, Fan JB, Duan L, Glass CK, Rosenfeld MG, Fu XD. Sensitive ChIP-DSL technology reveals an extensive estrogen receptor alpha-binding program on human gene promoters. *Proc Natl Acad Sci U S A*. 2007 Mar 20; 104(12):4852-7.

Kim I-K, Kiefer J, Ho C, Stegeman R, Classen S, Tainer J & Ellenberger T Structure of mammalian poly(ADP-ribose) glycohydrolase reveals a flexible tyrosine clasp as a substrate-binding element. *Nat Struct Mol Biol*. 2012, 19, 653–656.

Krietsch J, Rouleau M, Pic É, Ethier C, Dawson TM, Dawson VL, Masson JY, Poirier GG, Gagné JP. Reprogramming cellular events by poly(ADP-ribose)-binding proteins. *Mol Aspects Med*. 2013 Dec; 34 (6):1066-87.

Kusano N, Shiraishi K, Kubo K, Oga A, Okita K, Sasaki K. Genetic aberrations detected by comparative genomic hybridization in hepatocellular carcinomas: their relationship to clinicopathological features. *Hepatology.* 1999, 29:1858-1862.

Lacal PM, Tentori L, Muzi A, Ruffini F, Dorio AS, Xu W, Arcelli D, Zhang J, Graziani G. Pharmacological inhibition of poly(ADP-ribose) polymerase activity down-regulates the expression of syndecan-4 and Id-1 in endothelial cells. *Int J Oncol*. 2009 Mar; 34(3):861-72.

Lakadong RO, Kataki AC, Sharan RN. ADP-ribose polymer--a novel and general biomarker of human cancers of head & neck, breast, and cervix. *Mol Cancer.* 2010 Oct 30;9:286.

Langelier MF1, Planck JL, Roy S, Pascal JM. Structural basis for DNA damage-dependent poly(ADP-ribosyl)ation by human PARP-1. *Science.* 2012 May 11;336(6082):728-32.

Langelier MF1, Planck JL, Roy S, Pascal JM. Crystal structures of poly(ADP-ribose) polymerase-1 (PARP-1) zinc fingers bound to DNA: structural and functional insights into DNA-dependent PARP-1 activity. *J Biol Chem.* 2011 Mar 25;286(12):10690-701.

Langelier MF, Servent KM, Rogers EE, Pascal JM. A third zinc-binding domain of human poly(ADP-ribose) polymerase-1 coordinates DNA-dependent enzyme activation. *J Biol Chem.* 2008 Feb 15;283(7):4105-14. Epub 2007 Nov 30.

Lamarre D, Talbot B, de Murcia G, Laplante C, Leduc Y, Mazen A, Poirier GG. Structural and functional analysis of poly(ADP ribose) polymerase: an immunological study. *Biochim Biophys Acta*. 1988 Jul 13;950(2):147-60.

Lippincott-Schwartz J1, Snapp E, Kenworthy A. Studying protein dynamics in living cells. *Nat Rev Mol Cell Biol*. 2001 Jun;2(6):444-56.

Long JC1, Caceres JF. The SR protein family of splicing factors: master regulators of gene expression. *Biochem J*. 2009 Jan 1;417(1):15-27.

Loseva O, Jemth AS, Bryant HE, Schüler H, Lehtiö L, Karlberg T, Helleday T. PARP-3 is a mono-ADP-ribosylase that activates PARP-1 in the absence of DNA. *J Biol Chem*. 2010 Mar 12;285(11):8054-60.

Lautier D, Lagueu× J, Thibodeau J, M~nard L, Poirier G (1993) Molecular and biochemical features of poly(ADP-ribose) metabolism. *Mol Cell Biothem* 122, 171-193.

Le May N, Iltis I, Amé JC, Zhovmer A, Biard D, Egly JM, Schreiber V, Coin F. .Poly (ADP-ribose) glycohydrolase regulates retinoic acid receptor-mediated gene expression. *Mol Cell*. 2012 Dec 14;48(5):785-98.

Liu Y, Scheurer, M, El-Zein R, Cao Y, Do KA, Gilbert M, Aldape KD, Wei Q, Etzel C, Bondy M.L. Association and interactions between DNA repair gene polymorphisms and adult glioma. *Cancer epidemiology, biomarkers & prevention* : a publication of the American Association for Cancer Research, cosponsored by *the American Society of Preventive Oncology* 2009, 18 (1), 204–214.

Liu C, Wu J, Paudyal SC, You Z, Yu X.. CHFR is important for the first wave of ubiquitination at DNA damage sites. *Nucleic Acids Res*. 2013 Feb 1;41(3):1698-710.

Lockett KL, Hall C, Xu J, Zheng SL, Berwick, M, Chuang, SC, Clark, PE, Cramer SD, Lohman, K, Hu, JJ, The ADPRT V762A genetic variant contributes to prostate cancer susceptibility and deficient enzyme function. *Cancer Res*. 2004, 64 (17), 6344–6348.

Lonskaya I. , Vladimir N. Potaman, Luda S. Shlyakhtenko, Elena A. Oussatcheva, Yuri L. Lyubchenko and Viatcheslav A. Soldatenkov. Regulation of Poly(ADP-ribose) Polymerase-1 by DNA Structure-specific Binding J. *Biol. Chem*. 2005, 280:17076-17083.

Ludwig A, Behnke B, Holtlund J, Hilz H. Immunoquantitation and size determination of intrinsic poly(ADP-ribose) polymerase from acid precipitates. An analysis of the *in vivo* status in mammalian species and in lower eukaryotes. *J Biol Chem* 1988, 263(15):6993–6999.

Ma NF, Hu L, Fung JM, Xie D, Zheng BJ, Chen L, Tang DJ, Fu L, Wu Z, Chen M, Fang Y, Guan XY. Isolation and characterization of a novel oncogene, amplified in liver cancer 1, within a commonly amplified region at 1q21 in hepatocellular carcinoma. *Hepatology*. 2008 Feb; 47(2):503-10.

Mackay J, Szecsei CM. Genetic counselling for hereditary predisposition to ovarian and breast cancer. *Ann Oncol* 2010; 21 (Suppl 7): vii334-8.

Malanga M, Czubaty A, Girstun A, Staron K, Althaus FR. Poly(ADP-ribose) binds to the splicing factor ASF/SF2 and regulates its phosphorylation by DNA topoisomerase I. *J Biol Chem.* 2008 Jul 18;283(29):19991-8.

Mandel P, Okazaki H, Niedergang C. Purification and properties of calf thymus poly adenosine diphosphate ribose polymerase. *FEBS Lett.* 1977 Dec 15;84(2):331-6.

Mao Z, Hine C, Tian X, Van Meter M, Au M, Vaidya A, Seluanov A, Gorbunova V. SIRT6 promotes DNA repair under stress by activating PARP1. *Science.* 2011 Jun 17;332(6036):1443-6.

Marchio A, Meddeb M, Pineau P, Danglot G, Tiollais P, Bernheim A. Recurrent chromosomal abnormalities in hepatocellular carcinoma detected by comparative genomic hybridization. *Genes Chromosomes Cancer* 1997; 18:59-65.

Mazen A, Menissier-de Murcia J, Molinete M, Simonin F, Gradwohl G, Poirier G, de Murcia G. Poly(ADP-ribose)polymerase: a novel finger protein. *Nucleic Acids Res.* 1989 Jun 26;17(12):4689-98

Martin N, Schwamborn K, Schreiber V, Werner A, Guillier C, Zhang XD, Bischof O, Seeler JS, Dejean A. PARP-1 transcriptional activity is regulated by sumoylation upon heat shock. *EMBO J.* 2009 Nov 18;28(22):3534-48.

Mascolo M, Ilardi G, Romano MF, Celetti A, Siano M, Romano S, Luise C, Merolla F, Rocco A, Vecchione ML, De Rosa G, Staibano, S. Overexpression of chromatin assembly factor-1 p60, poly(ADP-ribose) polymerase 1 and nestin predicts metastasizing behaviour of oral cancer. *Histopathology*. 2012, 61 (6), 1089–1105

Masutani M, Fujimori H. Poly(ADP-ribosyl)ation in carcinogenesis. *Mol Aspects Med.* 2013 Dec; 34(6):1202-16.

Masutani M, Nakagama H, Sugimura T. Poly(ADP-ribosyl)ation in relation to cancer and autoimmune disease. *Cell Mol Life Sci.* 2005 Apr; 62(7-8):769-83.

McCabe N, Lord CJ, Tutt AN, et al. BRCA2-deficient CAPAN-1 cells are extremely sensitive to the inhibition of Poly (ADP-Ribose) polymerase: an issue of potency. *Cancer Biol Ther* 2005; 4: 934-6.

Mehrotra PV, Ahel D, Ryan DP, Weston R, Wiechens N, Kraehenbuehl R, Owen-Hughes T, Ahel I. DNArepair factor APLF is a histone chaperone. *Mol.Cell* 2011, 41, 46–55.

Mendoza-Alvarez H1, Alvarez-Gonzalez R. Poly(ADP-ribose) polymerase is a catalytic dimer and the automodification reaction is intermolecular. *J Biol Chem*. 1993 Oct 25;268(30):22575-80.

Ménissier-de Murcia J, Molinete M, Gradwohl G, Simonin F, de Murcia G. Zinc-binding domain of poly(ADP-ribose)polymerase participates in the recognition of single strand breaks on DNA. *J Mol Biol.* 1989 Nov 5; 210(1):229-33.

Michelman-Ribeiro A, Mazza D, Rosales T, Stasevich TJ, Boukari H, Rishi V, Vinson C, Knutson JR, McNally JG. Direct measurement of association and dissociation rates of DNA binding in live cells by fluorescence correlation spectroscopy. *Biophys J*. 2009 Jul 8; 97 (1):337-46.

Min W, Bruhn C, Grigaravicius P, Zhou ZW, Li F, Krüger A, Siddeek B, Greulich KO, Popp O, Meisezahl C, Calkhoven CF, Bürkle A, Xu X, Wang ZQ. Poly(ADP-ribose) binding to Chk1 at stalled replication forks is required for S-phase checkpoint activation. *Nat Commun. 2013*; 4:2993.

Minton A.P. How can biochemical reactions within cells differ from those in test tubes? Journal of *Cell Science*, 2006, 119, 2863-2869

Min W, Cortes U, Herceg Z, Tong WM, Wang ZQ. Deletion of the nuclear isoform of poly(ADP-ribose) glycohydrolase (PARG) reveals its function in DNA repair, genomic stability and tumorigenesis. *Carcinogenesis*. 2010 Dec; 31(12):2058-65.

Miwa M, Sugimura T. Splitting of the ribose-ribose linkage of poly(adenosine diphosphate-robose) by a calf thymus extract. J Biol Chem. 1971 Oct 25; 246(20):6362-4.

Mukhopadhyay A, Curtin N, Plummer R, Edmondson RJ. PARP inhibitors and epithelial ovarian cancer: an approach to targeted chemotherapy and personalised medicine. *BJOG*. 2011 Mar; 118(4):429-32.

Mueller-Dieckmann Rosenthal C, Kernstock S, Lisurek M, von Kries JP, Haag F, Weiss MS, Koch-Nolte F. The structure of human ADP ribosyl hydrolase 3 (ARH3) provides insights into the reversibility of protein ADP-ribosylation. *Proc Natl Acad Sci U S A* 2006, 103(41): 15026–15031.

Muñoz-Gámez JA1, Rodríguez-Vargas JM, Quiles-Pérez R, Aguilar-Quesada R, Martín-Oliva D, de Murcia G, Menissier de Murcia J, Almendros A, Ruiz de Almodóvar M, Oliver FJ. PARP-1 is involved in autophagy induced by DNA damage. *Autophagy*. 2009 Jan; 5(1):61-74. Epub 2009 Jan 27.

Murai J, Zhang Y, Morris J, Ji J, Takeda S, Doroshow JH, Pommier Y. Rationale for poly(ADP-ribose) polymerase (PARP) inhibitors in combination therapy with camptothecins or temozolomide based on PARP trapping versus catalytic inhibition. *J Pharmacol Exp Ther.* 2014 Jun; 349(3):408-16

Murai J, Huang SY, Das BB, Renaud A, Zhang Y, Doroshow JH, Ji J, Takeda S, Pommier Y. Trapping of PARP1 and PARP2 by Clinical PARP Inhibitors. *Cancer Res.* 2012 Nov 1;72(21):5588-99.

Müller KP, Erdel F, Caudron-Herger M, Marth C, Fodor BD, Richter M, Scaranaro M, Beaudouin J, Wachsmuth M, Rippe K. Multiscale analysis of dynamics and interactions of heterochromatin protein 1 by fluorescence fluctuation microscopy. *Biophys J.* 2009 Dec 2;97(11):2876-85.

Niere M, Mashimo M, Agledal L, Dolle C, Kasamatsu A, Kato J,Moss J, Ziegler M. ADP-ribosylhydrolase 3 (ARH3), not poly(ADPribose) glycohydrolase (PARG) isoforms, is responsible for degradation of mitochondrial matrix-associated poly(ADP-ribose). *J Biol Chem* 2012, 287(20):16088–16102.

Nishizuka Y, Ueda K, Nakazawa O, Hayaishi M. Studies on the polymer of adenosine diphosphate ribose. I. Enzymic formation from nicotinamide adenine dinuclotide in mammalian nuclei. *J. Biol. Chem.* 1967, 242:3164–3171.

Nishikimi M, Ogasawara K, Kameshita I, Taniguchi T, Shizuta Y. Poly(ADP-ribose) synthetase. The DNA binding domain and the automodification domain. *J Biol Chem.* 1982 Jun 10; 257(11):6102-5.

O'Donnell A1, Yang SH, Sharrocks AD. PARP1 orchestrates variant histone exchange in signal-mediated transcriptional activation. *EMBO Rep.* 2013 Dec;14(12):1084-91.

Okano S, Kanno S, NakajimaS, YasuiA. Cellular responses and repair of single-strand breaks introduced by UV damage endonuclease in mammalian cells. *J BiolChem* (2000) 275(42):32635–41.

Oliver FJ, Ménissier-de Murcia J, Nacci C, Decker P, Andriantsitohaina R, Muller S, de la Rubia G, Stoclet JC, de Murcia G. Resistance to endotoxic shock as a consequence of defective NF-kappaB activation in poly (ADP-ribose) polymerase-1 deficient mice. *EMBO J.* 1999 Aug 16;18(16):4446-54.

Ono T, Kasamatsu A, Oka S & Moss J. The 39-kDa poly(ADP-ribose) glycohydrolase ARH3 hydrolyzes O-acetyl-ADP-ribose, a product of the Sir2 family of acetyl-histone deacetylases. *Proc Natl Acad Sci USA* 2006, 103, 16687–16691.

Pan XF, Xie Y, Loh M, Yang SJ, Wen YY, Tian Z, Huang H, Lan H, Chen F, Soong R, Yang CX. Polymorphisms of XRCC1 and ADPRT genes and risk of noncardia gastric cancer in a Chinese population: a case-control study. *Asian Pac J Cancer Prev.* 2012;13(11):5637-42.

Panzeter,P.L.,Realini,C.A.,Althaus,F.R. Noncovalent interactions of poly(adenosine diphosphateribose) with histones. *Biochemistry* 1992, 31, 1379–1385

Patterson GH, Lippincott-Schwartz J. A photoactivatable GFP for selective photolabeling of proteins and cells. *Science*. 2002 Sep 13;297(5588):1873-7.

Phair RD, Gorski SA, Misteli T. Measurement of dynamic protein binding to chromatin in vivo, using photobleaching microscopy. *Methods Enzymol.* 2004;375:393-414.

Pavri R, Lewis B, Kim TK, Dilworth FJ, Erdjument-Bromage H, Tempst P, de Murcia G, Evans R, Chambon P, Reinberg D. PARP-1 determines specificity in a retinoid signaling pathway via direct modulation of mediator. *Mol Cell.* 2005 Apr 1;18(1):83-96.

Peng Gao, David W. Hoffman, Hung-wen Liu, Zhihua Tao. Domain C of Human Poly(ADP-ribose) Polymerase-1 Is Important for Enzyme Activity and Contains a Novel Zinc-Ribbon Motif. 2008 *Biochemistry* 2008, 47, 5804–5813

Pehrson, J. R. & Fried, V. A. MacroH2A, a core histone containing a large nonhistone region. *Science* 257, 1398–1400 (1992)

Petesch SJ, Lis JT. Activator-induced spread of poly(ADP-ribose) polymerase promotes nucleosome loss at Hsp70. *Mol Cell.* 2012 Jan 13;45(1):64-74

Piao L, Kang D, Suzuki T, Masuda A, Dohmae N, Nakamura Y, Hamamoto R.. The histone methyltransferase SMYD2 methylates PARP1 and promotes poly(ADP-ribosyl)ation activity in cancer cells. *Neoplasia.* 2014 Mar; 16(3):257-64, 264.e2

Pion, E., Bombarda, E., Stiegler, P., Ullmann, G. M., Mely, Y., de Murcia, G. & Gerard, D. (2003). Poly(ADP-ribose) polymerase-1 dimerizes at a 5′ recessed DNA end in vitro: a fluorescence study. *Biochemistry*, 42, 12409–12417.

Pion E, Bombarda E, Stiegler P, Ullmann GM, Mély Y, de Murcia G, Gérard D. Poly(ADP-ribose) polymerase-1 dimerizes at a 5' recessed DNA end in vitro: a fluorescence study. *Biochemistry*. 2003 Oct 28;42(42):12409-17.

Pinnola, A., Naumova, N., Shah, M., and Tulin, A. V. (2007) Nucleosomal core histones mediate dynamic regulation of poly(ADP-ribose) polymerase 1 protein binding to chromatin and induction of its enzymatic activity. *J. Biol. Chem*. 282, 32511–32519.

Pleschke JM, Kleczkowska HE, Strohm M, Althaus FR. Poly(ADP-ribose) binds to specific domains in DNA damage checkpoint proteins. *J Biol Chem*. 2000 Dec 29; 275(52):40974-80.

Poirier G.G., de Murcia G., Jongstra-Bilen J., Niedergang C., Mandel,P. (1982).Poly(ADP-ribosyl)ation of polynucleosomes causes relaxation of chromatin structure. *Proc. Natl. Acad. Sci. U.S.A.* 79, 3423–3427

Purnell MR, Whish WJ. Novel inhibitors of poly(ADP-ribose) synthetase. *Biochem J.* 1980 Mar 1;185(3):775-7.

Pyriochou A, Olah G, Deitch EA, Szabó C, Papapetropoulos A. Inhibition of angiogenesis by the poly(ADP-ribose) polymerase inhibitor PJ-34. *Int J Mol Med*. 2008 Jul; 22(1):113-8.

Qin LX, Tang ZY, Sham JS, Ma ZC, Ye SL, Zhou XD, et al. The association of chromosome 8p deletion and tumor metastasis in human hepatocellular carcinoma. *Cancer Res* 1999; 59:5662-5665.

Quararhni K, Hadj-Slimane R, Ait-Si-Ali S, Robin P, Mietton F, Harel-Bellan A, Dimitrov S, Hamiche A. The histone variant mH2A1.1 interferes with transcription by down-regulating PARP-1 enzymatic activity. *Genes Dev*. 2006 Dec 1; 20 (23):3324-36.

Rajamohan SB, Pillai VB, Gupta M, Sundaresan NR, Birukov KG, Samant S, Hottiger MO, Gupta MP. . SIRT1 promotes cell survival under stress by deacetylation-dependent deactivation of poly(ADP-ribose) polymerase 1. *Mol Cell Biol*. 2009 Aug; 29 (15):4116-29.

Rakyan VK, Down TA, Balding DJ, Beck S. Epigenome-wide association studies for common human diseases. *Nat Rev Genet*. 2011, Jul 12;12(8):529-41.

Reeder, R. H., K. Ueda, T. Honjo, Y. Nishizuka, and O. Hayaishi. 1967. Studies on the polymer of adenosine diphosphate ribose. II. Characterization of the polymer. *J. Biol. Chem*. 242:3172–3179.

Reid G, Hübner MR, Métivier R, Brand H, Denger S, Manu D, Beaudouin J, Ellenberg J, Gannon F. Cyclic, proteasome-mediated turnover of unliganded and liganded ERalpha on responsive promoters is an integral feature of estrogen signaling. *Mol Cell.* 2003 Mar; 11(3):695-707.

Rodríguez-Vargas JM, Ruiz-Magaña MJ, Ruiz-Ruiz C, Majuelos-Melguizo J, Peralta-Leal A, Rodríguez MI, Muñoz-Gámez JA, de Almodóvar MR, Siles E, Rivas AL, Jäättela M, Oliver FJ. ROS-induced DNA damage and PARP-1 are required for optimal induction of starvation-induced autophagy. *Cell Res*. 2012 Jul; 22(7):1181-98.

Roukos V, Misteli T. The biogenesis of chromosome translocations. *Nat Cell Biol*. 2014 Apr;16 (4):293-300.

Rosas-Acosta, G, Russell, WK, Deyrieux A, Russell DH, Wilson VG. A universal strategy for proteomic studies of SUMO and other ubiquitin-like modifiers. *Mol. Cell. Proteomics* 2005, 4, 56–72.

Rosen EM, Pishvaian MJ. Targeting the BRCA1/2 tumor suppressors. *Curr Drug Targets*. 2014 Jan; 15(1):17-31.

Rosenthal F, Feijs KL, Frugier E, Bonalli M, Forst AH, Imhof R, Winkler HC, Fischer D, Caflisch A, Hassa PO. Macrodomain-containing proteins are new mono-ADP-ribosylhydrolases. *Nat Struct Mol Biol* 2012, 20, 502–507.

Schuster-Böckler B, Lehner B. Chromatin organization is a major influence on regional mutation rates in human cancer cells. *Nature*. 2012 Aug 23;488(7412):504-7.

Schiewer MJ, Goodwin JF, Han S, Brenner JC, Augello MA, Dean JL, Liu F, Planck JL, Ravindranathan P, Chinnaiyan AM, McCue P, Gomella LG, Raj GV, Dicker AP, Brody JR,

Pascal JM, Centenera MM, Butler LM, Tilley WD, Feng FY, Knudsen KE. Dual roles of PARP-1 promote cancer growth and progression. *Cancer Discov.* 2012 Dec;2(12):1134-49.

Schreiber V, Molinete M, Boeuf H, de Murcia G, Ménissier-de Murcia J. The human poly(ADP-ribose) polymerase nuclear localization signal is a bipartite element functionally separate from DNA binding and catalytic activity. *EMBO J.* 1992 Sep;11(9):3263-9.

Semighini, C. P., Savoldi, M., Goldman, G. H., and Harris, S. D. Functional characterization of the putative Aspergillus nidulans poly(ADP-ribose) polymerase homolog PrpA. *Genetics* 2006, 173, 87–98.

Simonin F, Ménissier-de Murcia J, Poch O, Muller S, Gradwohl G, Molinete M, Penning C, Keith G, de Murcia G. Expression and site-directed mutagenesis of the catalytic domain of human poly(ADP-ribose)polymerase in Escherichia coli. Lysine 893 is critical for activity. *J Biol Chem.* 1990 Nov 5;265(31):19249-56.

Slattery E, Dignam JD, Matsui T, Roeder RG. Purification and analysis of a factor which suppresses nick-induced transcription by RNA polymerase II and its identity with poly(ADP-ribose) polymerase. *J Biol Chem*. 1983 May 10;258(9):5955-9.

Soriano GF, Virág L, Jagtap P, Szabó E, Mabley JG, Liaudet L, Marton A, Hoyt DG, Murthy KG, Salzman AL, Southan GJ, Szabó C. Diabetic endothelial dysfunction: the role of poly(ADP-ribose) polymerase activation. *Nat Med*. 2001 Jan; 7(1):108-13.

Soriano FG, Liaudet L, Szabó E, Virág L, Mabley JG, Pacher P, Szabó C. Resistance to acute septic peritonitis in poly(ADP-ribose) polymerase-1-deficient mice. *Shock.* 2002 Apr;17(4):286-92.

Sharifi R, Morra R, Appel CD, Tallis M, Chioza B, Jankevicius G, Simpson MA, Matic I, Ozkan E, Golia B, Schellenberg MJ, Weston R, Williams JG, Rossi MN, Galehdari H, Krahn J, Wan A, Trembath RC, Crosby AH, Ahel D, Hay R, Ladurner AG, Timinszky G, Williams RS, Ahel I. Deficiency of terminal ADP-ribose protein glycohydrolase TARG1/C6orf130 in neurodegenerative disease. *EMBO J.* 2013 May 2;32(9):1225-37

Sharp ZD, Mancini MG, Hinojos CA, Dai F, Berno V, Szafran AT, Smith KP, Lele TP, Ingber DE, Mancini MA. Estrogen-receptor-alpha exchange and chromatin dynamics are ligand- and domain-dependent. *J Cell Sci*. 2006 Oct 1;119(Pt 19):4101-16. Epub 2006 Sep 12.

Sugimura, T., S. Fujimura, S. Hasegawa, and Y. Kawamura. 1967. Polymerization of the adenosine 5-diphosphate ribose moiety of NAD by rat liver nuclear enzyme. *Biochim. Biophys. Acta* 138:438–441.

Soldatenkov VA1, Smulson M. Poly(ADP-ribose) polymerase in DNA damage-response pathway: implications for radiation oncology. *Int J Cancer.* 2000 Apr 20; 90(2):59-67.

Slade D, Dunstan MS, Barkauskaite E, Weston R, Lafite P, Dixon N, Ahel M, Leys D, Ahel I (2011) The structure and catalytic mechanism of a poly(ADP-ribose) glycohydrolase. *Nature* 477(7366):616–620

Steffen JD, Tholey RM, Langelier MF, Planck JL, Schiewer MJ, Lal S, Bildzukewicz NA, Yeo CJ, Knudsen KE, Brody JR, Pascal JM. Targeting PARP-1 allosteric regulation offers therapeutic potential against cancer. *Cancer Res.* 2014 Jan 1;74 (1):31-7.

Tanaka, Y.; Koide, S. S.; Yoshihara, K.; Kamiya, T. Poly (ADP-ribose) synthetase is phosphorylated by protein kinase C in vitro. *Biochem. Biophys. Res. Commun*. 1987, 148 (2), 709–17.

Tanaka, M., Miwa, M., Hayashi, K., Kubota, K., Matsushima, T., 1977. Separation of oligo(adenosine diphosphate ribose) fractions with various chain lengths and terminal structures. *Biochemistry* 16, 1485–1489

Tao Z1, Gao P, Hoffman DW, Liu HW. Domain C of human poly(ADP-ribose) polymerase-1 is important for enzyme activity and contains a novel zinc-ribbon motif. *Biochemistry*. 2008 May 27;47(21):5804-13

Tallis M, Morra R, Barkauskaite E, Ahel I. Poly(ADP-ribosyl)ation in regulation of chromatin structure and the DNA damage response. *Chromosoma.* 2014 Mar;123(1-2):79-90.

Tentori L, Lacal PM, Muzi A, Dorio AS, Leonetti C, Scarsella M, Ruffini F, Xu W, Min W, Stoppacciaro A, Colarossi C, Wang ZQ, Zhang J, Graziani G. Poly(ADP-ribose) polymerase (PARP) inhibition or PARP-1 gene deletion reduces angiogenesis. *Eur J Cancer.* 2007 Sep;43(14):2124-33. Epub 2007 Aug 21.

Tewari M, Quan LT, O'Rourke K, Desnoyers S, Zeng Z, Beidler DR, Poirier GG, Salvesen GS, Dixit VM. Yama/CPP32 beta, a mammalian homolog of CED-3, is a CrmA-inhibitable protease that cleaves the death substrate poly(ADP-ribose) polymerase. *Cell.* 1995 Jun 2;81(5):801-9.

Thibodeau J, Potvin F, Kirkland JB, Poirier G. Expression in Escherichia coli of the 36 kDa domain of poly(ADP-ribose) polymerase and investigation of its DNA binding properties. *Biochim Biophys Acta*. 1993 Apr 21;1163(1):49-53.

Till, S., Ladurner, A. G. Sensing NAD metabolites through macro domains. *Front. Biosci*. 14, 3246–3258 (2009).

Timinszky G, Till S, Hassa PO, Hothorn M, Kustatscher G, Nijmeijer B, Colombelli J, Altmeyer M, Stelzer EH, Scheffzek K, Hottiger MO, Ladurner AG. A macrodomain-containing histone rearranges chromatin upon sensing PARP1 activation. *Nat Struct Mol Biol* (2009) 16(9): 923–929

Tian F, Xu F, Zhang ZY, Ge JP, Wei ZF, Xu XF, Cheng W: Expression of CHD1L in bladder cancer and its influence on prognosis and survival. *Tumour Biol* 2013, 34(6):3687–90.

Trucco C, Flatter E, Fribourg S, de Murcia G, Ménissier-de Murcia J. Mutations in the amino-terminal domain of the human poly(ADP-ribose) polymerase that affect its catalytic activity but not its DNA binding capacity. *FEBS Lett.* 1996 Dec 16; 399(3):313-6.

Tucker J, Bennett N, Brassington C, Durant S, Hassall G, Holdgate G, McAlister M, Nissink W, Truman C & Watson M (2012) Structures of the human poly (ADP-ribose) glycohydrolase

catalytic domain confirm catalytic mechanism and explain inhibition by ADP-HPD derivatives. *PLoS ONE* 7, e50889.

Thomas CJ, Kotova E, Andrake M, Adolf-Bryfogle J, Glaser R, Regnard C, Tulin AV. Kinase-mediated changes in nucleosome conformation trigger chromatin decondensation via poly(ADP-ribosyl)ation. *Mol Cell*. 2014 Mar 6;53(5):831-42

Tulin A, Spradling A. Chromatin loosening by poly(ADP)-ribose polymerase (PARP) at Drosophila puff loci. *Science*. 2003 Jan 24;299(5606):560-2.

Tulin A, Stewart D, Spradling AC. The Drosophila heterochromatic gene encoding poly(ADP-ribose) polymerase (PARP) is required to modulate chromatin structure during development. *Genes Dev*. 2002 Aug 15;16 (16):2108-19.

Uchida K, Morita T, Sato T, Ogura T, Yamashita R, Noguchi S, Suzuki H, Nyunoya H, Miwa M, and Sugimura T. *Biochem. Biophys. Res. Commun*. 1987, 148,617-622.

Ueda K, Oka J, Naruniya S,Miyakawa N, Hayaishi O (1972) Poly ADPribose glycohydrolase from rat liver nuclei, a novel enzyme degrading the polymer. *Biochem Biophys Res Commun* 46(2): 516–523.

Vertegaal AC, Ogg SC, Jaffray E, Rodriguez MS, Hay RT, Andersen JS, Mann M, Lamond AI. A proteomic study of SUMO-2 target proteins. *J. Biol. Chem*. 2004, 279, 33,791–33,798

Vyas S, Chesarone-Cataldo M, Todorova T, Huang YH, Chang P. A systematic analysis of the PARP protein family identifies new functions critical for cell physiology. *Nat Commun*. 2013; 4:2240.

Wacker D, Donald D, Ehsan H, Balagamwala, Hope K, Zhang T, Kraus LW. The DNA Binding and Catalytic Domains of Poly(ADP-Ribose) Polymerase 1 Cooperate in the Regulation of Chromatin Structure and Transcription *Mol. Cell. Biol*. 2007, 27(21):7475.

Wachsmuth M, Weidemann T, Muller G, Hoffmann-Rohrer W, Knoch TA. Analyzing intracellular binding and diffusion with continuous fluorescence photobleaching. *Biophys. J*. 2003, 84:3353–3363.

Wachsmuth M, Caudron-Herger M, Rippe K. Genome organization: balancing stability and plasticity. *Biochim Biophys Acta.* 2008 Nov; 1783(11):2061-79.

Wachsmuth M, Waldeck W, Langowski J. Anomalous diffusion of fluorescent probes inside living cell nuclei investigated by spatially-resolved fluorescence correlation spectroscopy. *J Mol Biol.* 2000 May 12; 298(4):677-89.

Wahlberg E, Karlberg T, Kouznetsova E, Markova N, Macchiarulo A, Thorsell AG, Pol E, Frostell Å, Ekblad T, Öncü D, Kull B, Robertson GM, Pellicciari R, Schüler H, Weigelt J. Family-wide chemical profiling and structural analysis of PARP and tankyrase inhibitors. *Nat Biotechnol.* 2012 Feb 19; 30(3):283-8.

Walker JW, Jijon HB, Madsen KL. AMP-activated protein kinase is a positive regulator of poly(ADP-ribose) polymerase. *Biochem. Biophys. Res. Commun*. 2006, 342 (1), 336–41.

Wang T, Simbulan-Rosenthal CM, Smulson ME, Chock PB, and Yang DC. Polyubiquitylation of PARP-1 through ubiquitin K48 is modulated by activated DNA, NAD+, and dipeptides. *J Cell Biochem* 2008, 104, 318–328

Wang Z, Michaud GA, Cheng Z, Zhang Y, Hinds TR, Fan E, Cong F, Xu W. Recognition of the iso-ADP-ribose moiety in poly(ADP-ribose) by WWE domains suggests a general mechanism for poly(ADP-ribosyl)ation-dependent ubiquitination. *Genes Dev*. 2012 Feb 1; 26(3):235-40.

Wang XG, Wang ZQ, Tong WM, Shen Y. PARP1 Val762Ala polymorphism reduces enzymatic activity. *Biochem Biophys Res Commun*. 2007 Mar 2;354(1):122-6. Epub 2006 Dec 29.

Wang M, Wu W, Wu W, Rosidi B, Zhang L, Wang H, Iliakis G. .PARP-1 and Ku compete for repair of DNA double strand breaks by distinct NHEJ pathways. *Nucleic Acids Res*. 2006; 34(21):6170-82

Wielckens, K., R. Bredehorst, and H. Hilz. Quantification of protein bound ADP-ribosyl and (ADP-ribosyl)n residues. *Methods Enzymol.* 1984, 106:472–482.

Wielckens, K., E. George, T. Pless, and H. Hilz. Stimulation of poly(ADP-ribosyl)ation during Ehrlich ascites tumor cell "starvation" and suppression of concomitant DNA fragmentation by benzamide. *J. Biol.Chem.* 1983, 258:4098–4104.

Williamson LM1, Lees-Miller SP. Estrogen receptor α-mediated transcription induces cell cycle-dependent DNA double-strand breaks. *Carcinogenesis*. 2011 Mar;32(3):279-85.

Witte JS. Genome-wide association studies and beyond. *Annu Rev Public Health.* 2010, 31:9-20 4.

Wong N, Lai P, Lee SW, Fan S, Pang E, Liew CT, et al. Assessment of genetic changes in hepatocellular carcinoma by comparative genomic hybridization analysis: relationship to disease stage, tumor size, and cirrhosis. *Am J Pathol* 1999, 154:37-43.

Wright RH, Castellano G, Bonet J, Le Dily F, Font-Mateu J, Ballaré C, Nacht AS, Soronellas D, Oliva B, Beato M. CDK2-dependent activation of PARP-1 is required for hormonal gene regulation in breast cancer cells. Genes Dev. 2012 Sep 1;26 (17):1972-83.

Yamanaka H, Penning CA, Willis EH, Wasson DB, Carson DA. Characterization of human poly(ADP-ribose) polymerase with autoantibodies. *J Biol Chem* 1988, 263(8):3879–3883

Yamagami, T., Miwa, A., Takasawa, S., Yamamoto, H., Okamoto, H. Induction of rat pancreatic B-cell tumors by the combined administration of streptozotocin or alloxan and poly(adenosine diphosphate ribose) synthetase inhibitors. *Cancer Res.* 1985, 45 (4), 1845–1849.

Ying S, Hamdy FC, Helleday T. Mre11-dependent degradation of stalled DNA replication forks is prevented by BRCA2 and PARP1. *Cancer Res*. 2012 Jun 1;72(11):2814-21.

Yu X, Minter-Dykhouse K, Malureanu L, Zhao WM, Zhang D, Merkle CJ, Ward IM, Saya H, Fang G, van Deursen J, Chen J. Chfr is required for tumor suppression and Aurora A regulation. *Nat Genet.* 2005 Apr;37(4)

Yu SW, Andrabi SA, Wang H, Kim NS, Poirier GG, Dawson TM, Dawson VL. Apoptosis-inducing factor mediates poly(ADP-ribose) (PAR) polymer-induced cell death. *Proc Natl Acad Sci U S A*. 2006 Nov 28; 103(48):18314-9.

Zahradka P, Ebisuzaki K. Poly(ADP-ribose) polymerase is a zinc metalloenzyme. Eur J Biochem. 1984 Aug 1;142(3):503-9.

Zhang M, Qureshi AA, Guo Q, Han J. Genetic variation in DNA repair pathway genes and melanoma risk. *DNA Repair*. 2011, 10 (1), 111–116.

Zhang X, Miao X, Liang G, Hao B, Wang Y, Tan W, Li Y, Guo Y, He F, Wei Q, Lin D. Polymorphisms in DNA base excision repair genes ADPRT and XRCC1 and risk of lung cancer. *Cancer Res*. 2005, 65 (3), 722–726.

Zhang S, Lin Y, Kim Y, Hande MP, Liu ZG, Shen HM. c-Jun N-terminal kinase mediates hydrogen peroxide-induced cell death via sustained poly(ADP-ribose) polymerase-1 activation. *Cell Death Differ*. 2007, 14 (5), 1001–10.

Zhang F, Chen Y, Li M, Yu X. The oligonucleotide/oligosaccharide-binding fold motif is a poly(ADP-ribose)-binding domain that mediates DNA damage response. *Proc Natl Acad Sci U S A*. 2014 May 20;111(20):7278-83.

a Zhang F, Wang Y, Wang L, Luo X, Huang K, Wang C, Du M, Liu F, Luo T, Huang D, Huang K. Poly(ADP-ribose) polymerase 1 is a key regulator of estrogen receptor α-dependent gene transcription. *J Biol Chem*. 2013 Apr 19;288(16):11348-57.

b Zhang Y, Wang J, Ding M, Yu Y. Site-specific characterization of the Asp- and Glu-ADP-ribosylated proteome. *Nat Methods*. 2013 Oct; 10(10):981-4

Zilio N, Williamson CT, Eustermann S, Shah R, West SC, Neuhaus D, Ulrich HD. DNA-dependent SUMO modification of PARP-1. DNA Repair (Amst). 2013 Sep;12(9):761-73.

Zobeck KL, Buckley MS, Zipfel WR, Lis JT. Recruitment timing and dynamics of transcription factors at the Hsp70 loci in living cells. *Mol Cell*. 2010 Dec 22;40(6):965-75.

9 Abbreviations

Abbreviation	Full name
A	adenine, a nucleotide
aa	amino acid
Ab	antibody
3AB	3-aminobenzamide
ALC1	amplified in liver cancer 1
APS	ammonium persulfate
BER	base excision repair
bp	base pair
BSA	bovine serum albumin
C	cytosin, a nucleotide
CB	Cycle/Burst (count)
C-terminus	carboxy-terminus of a peptide
ChIP	chromatin immune-precipitation
Da	Dalton; atomic mass unit, used here for the mass of peptides and proteins; 1 Da = $1.66*10\text{-}24$ g
H_2O	water
DF	Duty Factor (%)
DMEM	Dulbecco's modified Eagle medium – named after Renato Dulbecco
DMSO	dimethyl sulfoxide
DNA	deoxyribonucleic acid
dNTP	deoxyribonucleotide triphosphate
EB	elution buffer
EDTA	ethylenediamine tetraacetic acid
FRAP	fluorescence recovery after photobleaching
G guanine,	a purine base

G418	geneticin; aminoglycoside antibiotic, resistance through neo gene; here used as marker for eukaryotic cell culture selection
GFP	gfp green fluorescent protein
Gln	glutamine
Glu	glutamate, glutamic acid
GO	GeneOntology
HeLa	Henriette Lacks; HeLa cells are an immortal human cell line derived from cervical cancer of this person
HEPES	4-(2-hydroxyethyl)-1-piperazineethanesulphonic acid
HR	homologous recombination
IF	immunofluorescence
IgG	immunoglobulin G
IP	immunoprecipitation
Kan	kanamycin
KD	knockdown
NAD^+	nicotinamide adenine dinucleotide
MeOH	methanol
MS	mass spectrometry
MW	molecular weight, in Da or kDa
NER	nucleotide excision repair
NMR	nuclear magnetic resonance
NP-40	Nonidet P40
N-terminus	amino-terminus of a peptide
o/N	overnight
OptiMEM	modification of MEM, for reduced serum supplementation
PAGE	polyacrylamide gel electrophoresis
PBS-	phosphate buffered saline

PFA	para-formaldehyde
Puromycin	aminoglycoside antibiotic; resistance through pac gene; here used as selection marker in eukaryotic cell culture
PJ34	Acetamide, N-(5,6-dihydro-6-oxo-2-phenanthridinyl)-2-(dimethylamino)-, hydrochloride (1:1)
PTM	post-translational modification
PIP	Peak Incident Power (Watt)
PVDF	polyvinylidene fluoride; material of WB membranes
RNA	ribonucleic acid
ROI	region of interest
rpm	revolutions per minute
RT	room temperature
SDS	sodium dodecyl sulphate
SEM	standard error of the mean
siRNA	short interfering RNA
TE	Tris-EDTA
TEMED	N,N,N',N'-Tetramethylethylene-1,2-diamine
Tris	tris(hydroxymethyl)aminoethane
TSS	transcription start site
YFP	yellow fluorescent protein

10 List of Figures and Tables

11 *Curriculum Vitae*

Marek Kozlowski

Current telephone - 0049-151-124-91114
Current address - Hans-Grässel-Weg 12, 81375 Munich
kozlowskim@yahoo.com

EDUCATION

2010-2014	**Ph.D. candidate** (Dr. rer. nat., Doktorgrades der Naturwissenschaften)
	• International **Max Planck Research School** for Molecular and Cellular Life Sciences: From Biology to Medicine (Martinsried, Germany)
	• **Ludwig Maximilian University** of Munich, Butenandt Institute of Physiological Chemistry (Munich, Germany)
	• **European Molecular Biology Laboratory**, Genome Biology Unit (Heidelberg, Germany)
2000-2005	**M.Sc. (Eng),** Master of Engineering in Biotechnology
	• **Warsaw University** of Life Sciences, Interfaculty Studies in Biotechnology (Warsaw, Poland)
	Thesis: MMS mutagenesis and MFD repair in *Escherichia coli alkb* mutants (with Prof. Dr. Elżbieta Grzesiuk)

RESEARCH EXPERIENCE

2007-2010	**Harvard Medical School** and **Children`s Hospital** (Boston, U.S.A.) Department of Medicine and Program in Genomics (The Manton Center for Orphan Disease Research) (with Prof. Dr. Alan Beggs) Research Technologist (2009- 2010), Research Assistant II (2008-2009), Research Assistant I (2007-2008)
2006-2007	**ITOCHU** Deutschland GmbH (Lodz, Poland) and **AJINOMOTO** Eurolysine S.A.S. (Paris, France). Research and Development Department, Product Development Officer
2003-2005	**Polish Academy of Sciences** (Warsaw, Poland) Institute of Biochemistry and Biophysics, Department of Molecular Biology Trainee, (with Prof. Dr. Elzbieta Grzesiuk)

HONORS (recent only)

- Finalist of Merck Serono Innovation Cup 2013 (Team Oncology member – "A novel therapeutic for pancreatic cancer" (Darmstadt, 2013)

- Recipient of Protein Production Platform P-CUBE fellowship, European Community's Seventh Framework Programme (FP7/2007-2013) - grant agreement no. 227764 (P-CUBE), Principal Investigator: Marek Kozlowski (Heidelberg, 2011)

PUBLICATIONS

Ali AEA, Timinszky G, R Arribas-Bosacoma, **Kozlowski M**, Hassa PO, Hassler M, Ladurner AG, Pearl LH, and Oliver AW. The zinc-finger domains of PARP1 cooperate to recognize DNA strand breaks. ***Nat Struct & Mol Bio*** 2012 June 10 [PMID:22683995]

Beggs AH, Böhm J, Snead E, **Kozlowski M**, Maurer M, Minor K, Childers MK, Taylor SM, Hitte C, Mickelson JR, Guo LT, Mizisin AP, Buj-Bello A, Tiret L, Laporte J, Shelton GD. MTM1 mutation associated with X-linked myotubular myopathy in Labrador Retrievers. ***Proc Natl Acad Sci U S A***. 2010 Aug3. [PMID: 20682747]

Wrzesiński M, Nieminuszczy J, Sikora A, Mielecki D, Chojnacka A**, Kozlowski M**, Krwawicz J, Grzesiuk E. Contribution of transcription-coupled DNA repair to MMS-induced mutagenesis in E. coli strains deficient in functional AlkB protein. ***Mutat Res.*** 2010 Jun 1;688(1-2):19-27.[PMID: 20178806]

Melchior D, Le Bellego L, Relandeau C, **Kozlowski M**; Tryptophan in Young Pigs: A Key Nutrient for Growth and Feed Intake – ***Ajinomoto Eurolysine Information*** No 28, November, 2006 (**non peer reviewed*)

PROFESSIONAL AFFILIATIONS

2013-	The EpiGeneSys Network of Excellence (Training Advisory Board Member)
2011-2012	INTERACT Scientific Committee -The Munich Life Science Symposium for Young Scientists (Munich, 2012)
2010-	ADEQUATION Germany – nonprofit organization (Heidelberg)
2009-2010	Association for Women in Science
2008-2010	American Society of Human Genetics
2008-2010	World Muscle Society
2007-2010	MIT European Club (Massachusetts Institute of Technology) Organizational Committee -13th European Career Fair at MIT (Cambridge 2009)

RESEARCH PRESENTATIONS (local, national and international- selected)

"Functions of ALC1 in transcription and regulation of PARP1 activity", Max Planck Institute 16th IMPRS Seminar, Munich, July 2014 (**poster**)

"The chromatin remodeler ALC1 modulates PARP1's activity", Butenandt Institute of Physiological Chemistry, March, 2014 (**talk**)

"Nucleosome modification and remodeling mediated by human PARP1's ignaling", SFB11064 grant application process, Munich, February, 2013 **(poster)**

"Mechanism of PARP1`s binding to DNA *in vivo*, and its functions in ALC1 regulated transcription", Butenandt Institute of Physiological Chemistry, Munich, February, 2012 (**talk**)

"The mechanism of PARP1's binding to DNA in living cells", Spetses Summer School - Chromatin and Systems Biology and 11th IMPRS Seminar, September and December 2011, respectively (**poster**)

"Dissecting binding mechanism of PARP1 to DNA *in vivo*, through FCS and FRAP", PARP symposium, Zurich, May 2011 (**talk**)

"Towards the binding mechanism of PARP1 to DNA in living cells", EMBL, Genome Biology Unit Seminar, Heidelberg, March 2011 (**talk**)

"Developmental defects in mtmr1 deficient zebrafish embryos", Friedrich Miescher Institute, Basel, January 2010 (**talk**)

"Knock down of two *mtmr1* paralogs cause broad developmental defects in zebrafish", The Ottawa Conference on New Directions in Biology and Disease of Skeletal Muscle, Ottawa, May 2010 (**poster**)

"Identification of X-Linked Myotubular Myopathy in Labrador retrievers", The American Society of Human Genetics, 57th Annual Meeting, Honolulu, October, 2009 (**poster**)

"A missense mutation in *MTM1* gene causes X-Linked Myotubular Myopathy in Labrador retrievers ", 14th World Muscle Society Congress, Geneva, September, 2009 (**poster**)

"Knockdown of myotubularin gene in differentiating C2C12 cells is associated with upregulation of doublecortin, a microtubule associated protein", The Third New Directions in Skeletal Muscle Biology Meeting, New Orleans, May, 2008 (**poster**)

TEACHING RESPONSIBILITIES

2012, 2013 • Teaching assistant (Biochemistry course for students of Faculty of Medicine, LMU)

2012, 2013 • Training of Teresa Burell (Research Technician, Ladurner lab, LMU)

2010 • Training of Mervin Zhao (Cornell University) summer internship (Beggs lab, Harvard)

- Epi-genomics of Common Diseases, Welcome Trust, Hinxton, Cambridge, 2013

- 3rd Munich Biomarker Conference, Munich, 2013

- Data visualization with R, Max Planck Institute, Munich, 2013

- Getting Funded, Max Planck Institute, Munich, 2013

- Data analysis with R, Max Planck Institute, Munich, 2012

- Towards Next Generation Sequencing Data Integration, EMBL Advanced Courses, Heidelberg, 2012

- Introduction to Statistics with R, Max Planck Institute, Munich, 2012

- Scientific Writing, Max Planck Institute, Munich, 2011

- Time and Project Management, Max Planck Institute, 2011

- Team work and leadership, Max Planck Institute, 2011

- Basics in FRET Imaging, Advanced Light Microscopy Facility, EMBL, 2011

- Scientific Writing, Max Planck Institute, Munich, 2011

- Time and Project Management, Max Planck Institute, Munich 2011

- Team work and leadership, Max Planck Institute, Munich, 2011

- Basics in FRET Imaging, Advanced Light Microscopy Facility, EMBL, 2011

- Basics in Confocal Microscopy, Advanced Light Microscopy Facility, EMBL, 2011

- Basics in Light Microscopy, Advanced Light Microscopy Facility, EMBL, 2011

12 Acknowledgements

Foremost, I would like to thank Prof. Dr. Andreas Ladurner for an opportunity to work on very exciting research projects in his laboratory (first at EMBL, then at LMU). Throughout the years I developed multiple scientific skills, which will stay with me forever. For this experience, discussions and your support I am saying thank you very much!

I would like to thank Dr. Gyula Timinszky for scientific discussions and support! It has been interesting to see how we both evolved during that time.

I would like to thank Dr. Markus Hassler, Dr. Carla Margulies, Teresa Burrell, Bianca Nijmejer, Sandra Essen, Dr. Aurelio Nardozza, Barbara Golia, Dr. Tamas Schauer, Ava Handley, and Hari Singh for discussions and technical help. I sincerely thank all the members of the Ladurner laboratory and Physiological Chemistry Department (Ramon, Christiane, Paula, Heiko, Kai, Julia, Simone, Rupa, Ulrike and others) for a nice working atmosphere. Also, I would like to thank Christine Werner for taking care of all the administration obligations.

My special thanks go to Dr. Anton Eberharter and Dr. Corey Laverty for critical reading of my thesis manuscript.

I am very grateful to Dr. Malte Wachsmuth (EMBL, Heidelberg) for discussions regarding experimental and theoretical part of FCS and FRAP. Also, I was would like to thank Dr. Christian Tischer, Dr. Stefan Terjung and Dr. Yury Belyaev for the technical support at the Advanced Light Microscopy Facility at EMBL.

It has been a privilege to become a member, and to take advantage, of the generous International Max Planck Research School for Molecular and Cellular Life Sciences at the Max Planck Institute of Biochemistry. I would like to thank Dr. Hans Joerg Schaeffer, Dr. Ingrid Wolf and Maximiliane Reif for the fantastic environment and enriching program of classes that they created within the program.

I would like to thank my Thesis Advisory Committee Members, Prof. Dr. Peter Becker, Dr. Johannes Söding and Dr. Carla Margulies for their critical and strategic view of my research goals and progress during the Ph.D. work.